



**HAL**  
open science

## Novel Inhibitory Site Revealed by XAP044 Mode of Action on the Metabotropic Glutamate 7 Receptor Venus Flytrap Domain

Nunzia Cristiano, Alexandre Cabayé, Isabelle Brabet, Ralf Glatthar, Amelie Tora, Cyril Goudet, Hugues-Olivier Bertrand, Anne Goupil-Lamy, Peter Flor, Jean-Philippe Pin, et al.

► **To cite this version:**

Nunzia Cristiano, Alexandre Cabayé, Isabelle Brabet, Ralf Glatthar, Amelie Tora, et al.. Novel Inhibitory Site Revealed by XAP044 Mode of Action on the Metabotropic Glutamate 7 Receptor Venus Flytrap Domain. *Journal of Medicinal Chemistry*, inPress, 67 (14), pp.11662-11687. 10.1021/acs.jmedchem.3c01924 . hal-04569147

**HAL Id: hal-04569147**

**<https://hal.science/hal-04569147v1>**

Submitted on 6 May 2024

**HAL** is a multi-disciplinary open access archive for the deposit and dissemination of scientific research documents, whether they are published or not. The documents may come from teaching and research institutions in France or abroad, or from public or private research centers.

L'archive ouverte pluridisciplinaire **HAL**, est destinée au dépôt et à la diffusion de documents scientifiques de niveau recherche, publiés ou non, émanant des établissements d'enseignement et de recherche français ou étrangers, des laboratoires publics ou privés.

# A novel inhibitory site revealed by XAP044 mode of action on metabotropic glutamate 7 receptor Venus flytrap domain

*Nunzia Cristiano<sup>a,g,#</sup>; Alexandre Cabayé<sup>a,b,#</sup>; Isabelle Brabet<sup>c</sup>; Ralf Glatthar<sup>d</sup>; Amelie Tora<sup>c</sup>, Cyril Goudet<sup>c</sup>; Hugues-Olivier Bertrand<sup>b</sup>; Anne Goupil-Lamy<sup>b</sup>; Peter J. Flor<sup>e</sup>; Jean-Philippe Pin<sup>c</sup>; Isabelle McCort-Tranchepain<sup>a</sup>, Francine C. Acher<sup>a,f,\*</sup>*

<sup>a</sup> Laboratoire de Chimie et Biochimie Pharmacologiques et Toxicologiques, Université Paris Cité, CNRS UMR 8601, 75006 Paris, France

<sup>b</sup> BIOVIA Dassault Systèmes, F-78140, Vélizy-Villacoublay Cedex, France

<sup>c</sup> Institute of Functional Genomics, University of Montpellier, CNRS, Inserm, 34094 Montpellier, France

<sup>d</sup> Novartis Biomedical Research, CH-4002 Basel, Switzerland

<sup>e</sup> Laboratory of Molecular and Cellular Neurobiology, Faculty of Biology and Preclinical Medicine, University of Regensburg, 93053 Regensburg, Germany

<sup>f</sup> Saints-Pères Paris Institute for the Neurosciences, Université Paris Cité, CNRS UMR 8003, 75006 Paris, France

<sup>g</sup> Present address: French National Agency for the Safety of Medicines and Health Products, 93200 Saint-Denis, France

# N.C. and A.C. contributed equally

\*Corresponding author: Francine C. Acher, E-mail: francine.acher@parisdecartes.fr

KEYWORDS: metabotropic glutamate receptor; non-competitive antagonist; negative allosteric modulator; selectivity; docking.

## **ABSTRACT**

Metabotropic glutamate (mGlu) receptors play a key role in modulating most synapses in the brain. The mGlu7 receptors inhibit pre-synaptic neurotransmitter release, and offer therapeutic possibilities for post-traumatic stress disorders or epilepsy. Screening campaigns provided mGlu7 specific allosteric modulators as the inhibitor XAP044 (Gee et al. J. Biol. Chem. 2014). In contrast to other mGlu receptor allosteric modulators, XAP044 does not bind in the transmembrane domain but to the extracellular domain of mGlu7 receptor and not at the orthosteric site. Here we identified the mode of action of XAP044, combining synthesis of derivatives, modeling and docking experiments and mutagenesis. We propose a unique mode of action of these inhibitors, preventing the closure of the Venus flytrap agonist binding domain. While acting as a non-competitive antagonist of L-AP4, XAP044 and derivatives, act as apparent competitive antagonists of LSP4-2022. These data revealed more potent XAP044 analogs and new possibilities to target mGluRs.

## **INTRODUCTION**

Glutamate is the major excitatory neurotransmitter in the central nervous system (CNS). Together with GABA the major inhibitory neurotransmitter, they govern synaptic transmission at most vertebrate synapses. Numerous CNS pathologies result from a disturbance of that process. Notably, glutamate dysregulation has been identified in ischemia, epilepsy, neurodegenerative diseases such as Parkinson's disease, psychiatric disorders such as schizophrenia, mood disorders such as depression, addictive behavior and chronic pain.<sup>1</sup> Accordingly, glutamate receptors have been identified as major therapeutic targets. Glutamate activates two types of receptors: ionotropic (iGlu) and metabotropic glutamate (mGlu) receptors. The iGlu receptors are ligand-gated ion channels that secure the fast synaptic transmission. Their essential role makes them challenging targets to be regulated with drugs, although a few drugs targeting these receptors are on the market, such as ketamine and NMDA receptor blocker, for depression<sup>2</sup>. On the other hand, the mGlu receptors modulate many synapses and are thus optimal targets for drug discovery.<sup>3</sup> Despite intense research,

no drugs targeting mGluRs are yet on the market<sup>4</sup>, however some clinical trials are still on going.<sup>5</sup> The 8 genes encoding mGlu receptor subunits have been identified and classified in three groups according to their sequence identity, transduction mechanism and pharmacological profile.<sup>6</sup> Group I includes mGlu1 and mGlu5 receptors, group II, mGlu2 and mGlu3 receptors; and group III, mGlu4, 6, 7 and 8 receptors. Group I receptors are mostly located in the postsynaptic compartment and activate phospholipase C (PLC). They are selectively activated by **3,5-DHPG** and **quisqualate** (**Chart 1**). Group II receptors are predominantly presynaptic and inhibit adenylyl cyclase (AC). **LY354740** and analogs are among their most potent and specific agonists (**Chart 1**). Similarly, group III receptors are also mostly presynaptic, inhibit AC and are selectively activated by **L-AP4**, a phosphonate analog of glutamate (**Chart 1**). Activation of presynaptic receptors reduces the release of glutamate or other neurotransmitters, which may be beneficial in excitotoxicity related disorders. All mGlu receptors are activated by micromolar concentrations of glutamate except mGlu7 receptor that is activated by millimolar concentrations. Despite this surprising low affinity for glutamate, this mGlu receptor is essential for normal brain development, as best illustrated by the deficit observed in KO animals<sup>7</sup> and the loss of function mutations in the mGlu7 encoding gene (GRM7).<sup>8</sup> In many cases mGlu7 activators or PAMs are expected to have beneficial effects such as in epilepsy, cognition or neurodevelopmental disorders including idiopathic autism, attention deficit hyperactivity disorder and Rett syndrome. However, inhibition of mGlu7 is also expected to decrease mood disorders including anxiety and depression, or stress disorders including post-traumatic stress disorders.<sup>9</sup> The development of highly selective mGlu7 compounds is therefore of much interest. A few known selective mGlu7 receptor ligands have been identified and are displayed in **Chart 1**. **LSP4-2022** and its analog **LSP2-9166** are the only orthosteric agonist that exhibit micromolar activities at mGlu7 receptor.<sup>10</sup> Although **LY341495** is a competitive antagonist of all mGlu receptors, it is the most potent mGlu7 competitive antagonist.<sup>10</sup> Subtype selectivity has been recently reached with allosteric modulators: **VU6027459**<sup>11</sup> and its derivative **VU6046980**<sup>12</sup> as PAMs, **AMN082**<sup>13</sup> and **CVN636**<sup>14</sup> as allosteric agonists and **MMPIP**<sup>15</sup>, **ADX71743**<sup>16</sup> and **XAP044**<sup>17</sup> as NAMs (**Chart 1**). **AMN082** has been

widely used in spite of its rapid metabolism and off target effects.<sup>18</sup> In contrast to other modulators, **XAP044** was shown not to bind in the transmembrane domain but to the extracellular domain of mGlu7 receptor<sup>17</sup> and yet not at the orthosteric site suggesting a new mechanism of action for an mGlu7 receptor NAM.

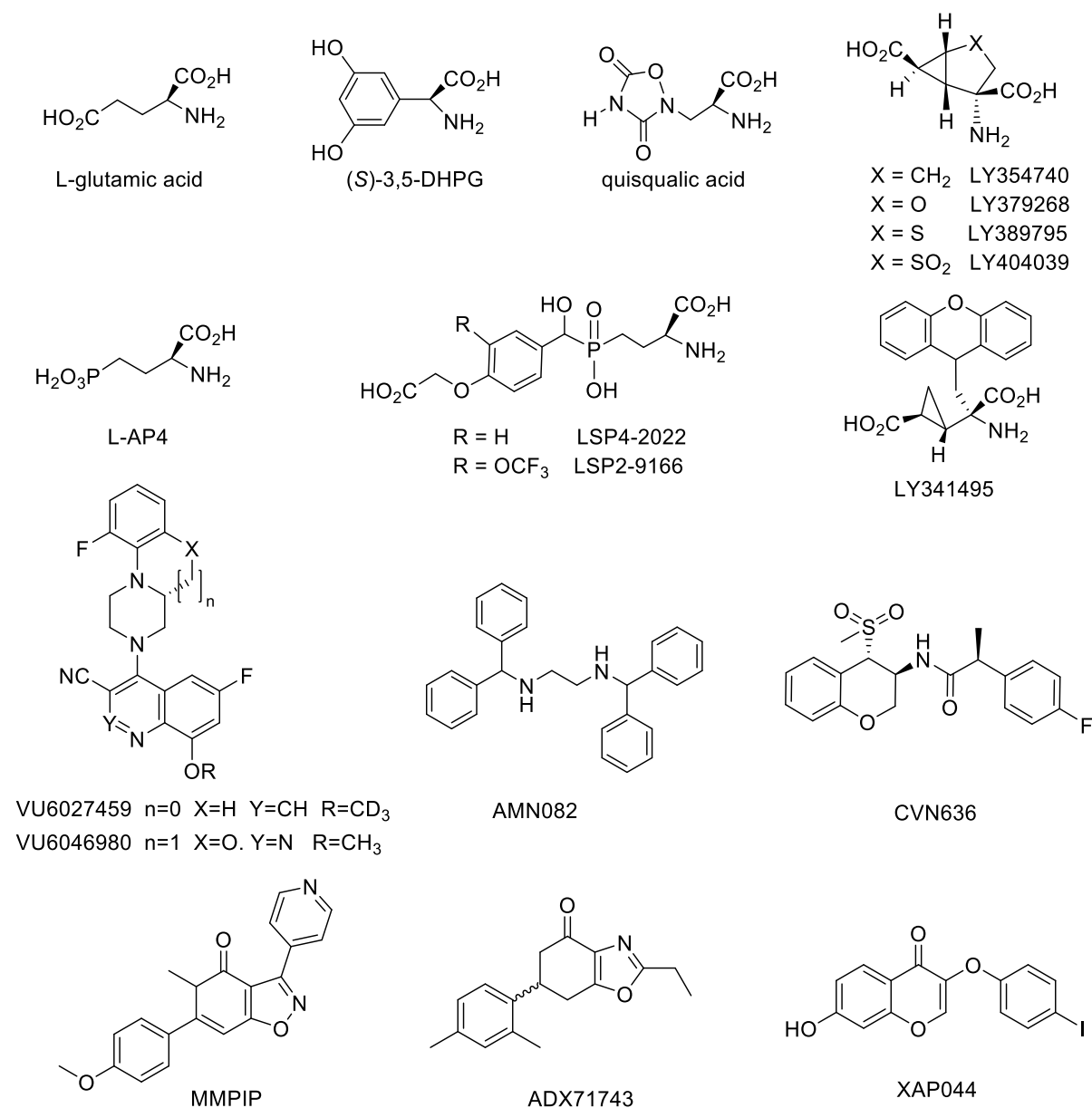


**Chart 1.** Chemical structures of most common mGlu receptor agonists and mGlu7 ligands.

The purpose of the present article was to identify the binding site and the mode of action of **XAP044**. We first developed a series of analogs to provide information on the bioactive conformation of **XAP044** and the role of its chemical groups. Then, we carried out a molecular modeling study of its binding to mGlu7 receptor, providing a possible inhibitory mechanism which was confirmed by pharmacological assays and mutagenesis. This study reports a new possible binding site for mGlu NAMs that is not located in the hydrophobic central region of the transmembrane domain. Such an information highlights new possibilities to develop antagonists with less hydrophobicity, and, thus, fewer possible off target actions.

## RESULTS

### Ligand Design and Structure - Activity Relationship.

To gain insight into the molecular determinants of **XAP044**, we designed both constrained and opening derivatives (**Figure 1**).

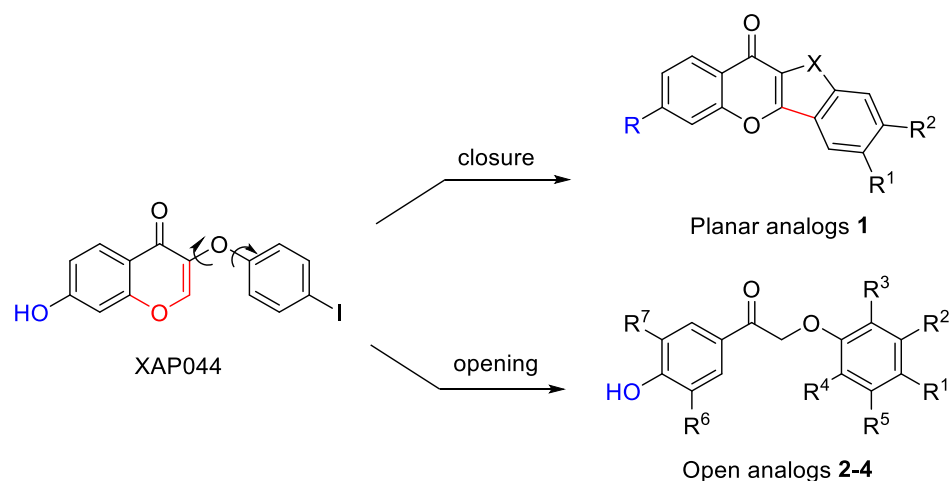
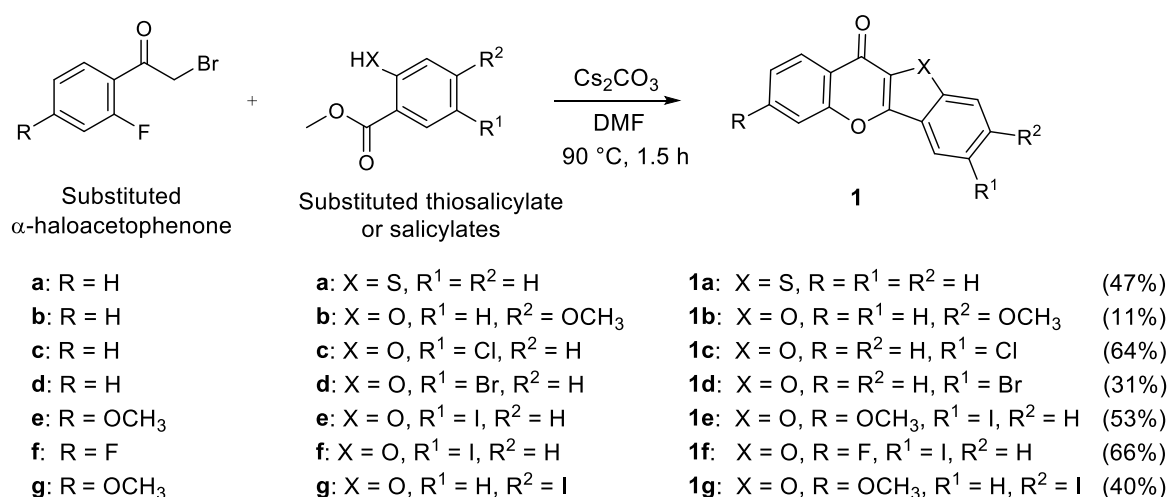


**Figure 1.** Two types of XAP044 derivatives for SAR. For R and R<sup>1-7</sup> see **Scheme 1** and **Figure 2**.

#### *Constrained derivatives of XAP044*

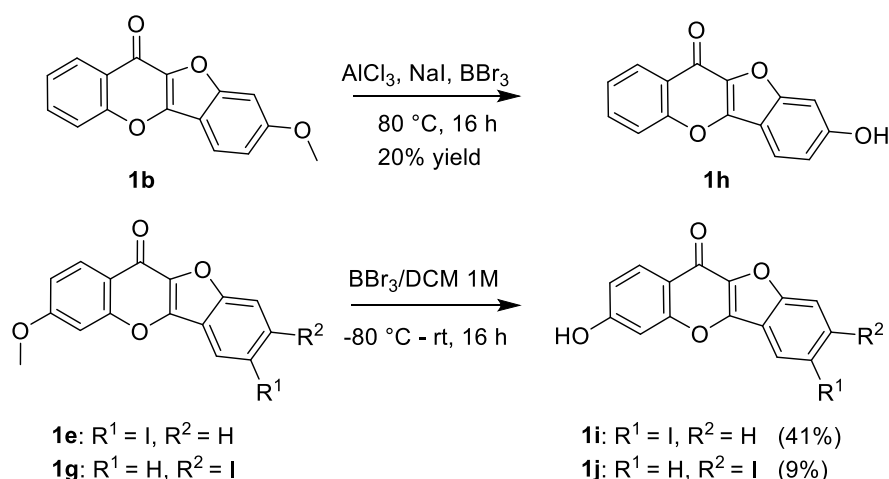
**XAP044** is a substituted chromone entity with two rotatable bonds that orient the two aromatic groups. To probe its possible planar conformation, we prepared constrained derivatives **1a-j** bearing

various substituents in similar positions as in **XAP044** (**Scheme 1**). The constrained analogs were synthesized in one step by a reaction described by Miller *et al.* (**Scheme 1**).<sup>19</sup> In this reaction, the methoxy group in position 8 (**1b**) stabilizes an intermediate, which may slow down the cyclisation or lead to side products, thereby explaining the lower yield for this compound. Yields were not optimized.



**Scheme 1.** Synthesis of constrained **XAP044** derivatives **1a-g**. Yields are indicated in brackets.

Compounds **1b**, **1e**, **1g** bear a methoxy group that protects a free hydroxyl. Deprotection was performed using Lewis acids: AlCl<sub>3</sub>/NaI/BBr<sub>3</sub> to afford **1h** or BBr<sub>3</sub> alone to obtain **1i** and **1j** (**Scheme 2**).

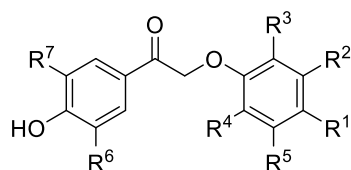


**Scheme 2.** Deprotection of methoxy substituents in **1b**, **1e** and **1g**. Yields vary according to the purification method used (see experimental section).



## Open-ring derivatives of XAP044

To define the minimal structure of **XAP044** and probe out of plane orientations of the two aromatic rings, we designed several open-ring derivatives in which the chomenone is chopped (**Figure 2**). The series of **2a-z** was designed to investigate the SAR of the iodophenyl part of **XAP044**, and the analogs **3**, and **4a,b** for the phenol part (**Figure 2**).



**2a-z:**  $R^6 = R^7 = H$ , for  $R^{1-5}$  see Table 1

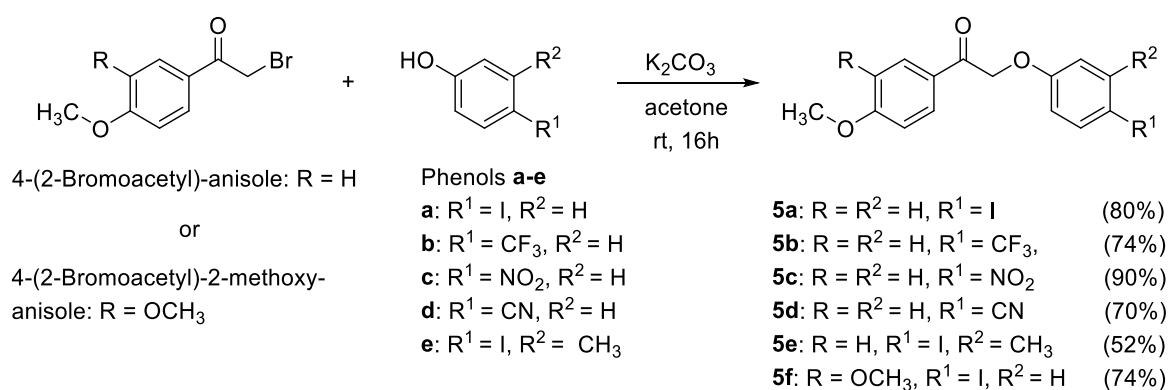
**3:**  $R^6 = OH$ ,  $R^7 = H$ ,  $R^1 = Br$ ,  $R^3 = F$ ,  $R^2 = R^4 = R^5 = H$

**4a:**  $R^6 = F$ ,  $R^7 = H$ ,  $R^1 = Br$ ,  $R^3 = F$ ,  $R^2 = R^4 = R^5 = H$

**4b:**  $R^6 = R^7 = F$ ,  $R^1 = Br$ ,  $R^3 = F$ ,  $R^2 = R^4 = R^5 = H$

**Figure 2.** Open derivatives of **XAP044**: **2a-z**, **3**, **4a** and **4b**.

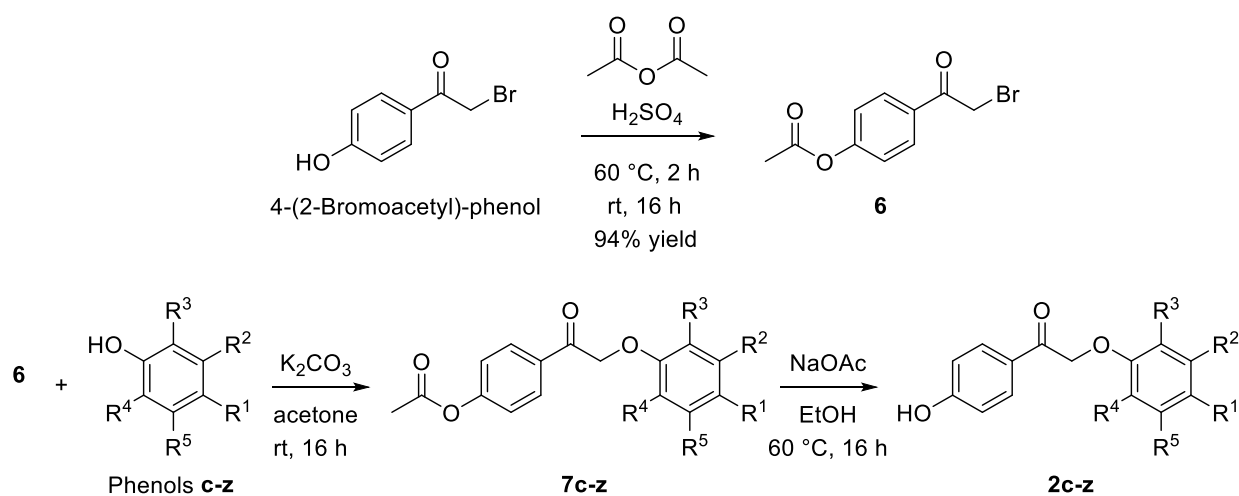
The phenol group of the open-ring **XAP044** derivatives requires protection along the syntheses and deprotection in a final step. It was first protected by a methyl group and compounds **5a-f** were easily obtained by nucleophilic substitution of 4-(2-bromoacetyl)-anisole by various phenols in the presence of potassium carbonate in acetone at room temperature (**Scheme3**).



**Scheme 3.** Synthesis of methoxy protected derivatives **5a-f**. Yields are indicated in brackets.

Demethylation of the methoxy protected analogs **5** using  $BBr_3$  in 1 M DCM was investigated with product **5a**. However, these conditions were found to be unsuitable because  $BBr_3$  also coordinates to

the oxygen atoms of the carbonyl group and the phenoxy of the molecule, ultimately leading to degradation. We therefore moved to ethyl carbonate which was introduced onto 4-(2-bromoacetyl)-phenol using ethyl chloroformate and potassium carbonate in ethyl acetate. Coupling to phenols as described in **Scheme 3** proceeded smoothly but basic deprotection by heating in aqueous KOH led to degradation and unidentified products. Finally, acetylation of the phenoxy reagents proved to be best (**Scheme 4**). Acetylation of 4-(2-bromoacetyl)-phenol was achieved using acetic anhydride and sulphuric acid to afford **6** in an excellent yield (**Scheme 4**). The synthesis of acetylated analogs **7c-z** was easily achieved by nucleophilic substitution of **6** by various phenols in the presence of potassium carbonate in acetone at room temperature (**Table 1**). Yields are variable according to the reactivity of the phenols and increased compared to the same coupling without the phenol protection *e.g.* **2a,b**. Deacetylation was performed by sodium acetate in ethanol providing **2c-z** which were either purified by chromatography or crystallized or used as crude materials (see experimental section).



**Scheme 4.** Synthesis of **2c-z** derivatives. For  $R^1$  to  $R^5$  see **Table 1**.

**Table 1.** Substituted phenols **a-z** used for the synthesis of **7c-z** and **2a-z**.

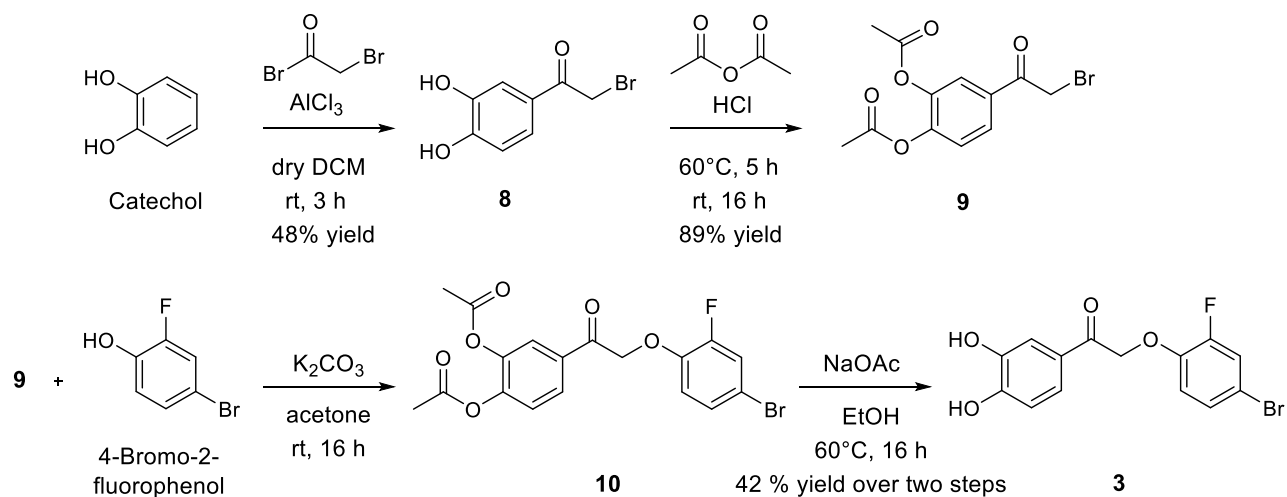
Phenoxy substituents						
	$R^1$	$R^2$	$R^3$	$R^4$	$R^5$	<b>2a-z yields</b>
<b>a</b>	H	H	H	H	H	18% <sup>a</sup>
<b>b</b>	CF <sub>3</sub>	H	H	H	H	19% <sup>a</sup>

<b>c</b>	NO <sub>2</sub>	H	H	H	H	48%
<b>d</b>	CN	H	H	H	H	66%
<b>e</b>	I	CH <sub>3</sub>	H	H	H	71%
<b>f</b>	I	H	CH <sub>3</sub>	H	H	34%
<b>g</b>	Cl	H	Cl	H	H	62%
<b>h</b>	CH <sub>3</sub>	H	H	H	H	57%
<b>i</b>	OCH <sub>3</sub>	H	H	H	H	58%
<b>j</b>	OCH <sub>3</sub>	OCH <sub>3</sub>	H	H	H	37%
<b>k</b>	Br	H	H	H	H	45%
<b>l</b>	Cl	H	H	H	H	61%
<b>m</b>	Br	H	Br	H	H	74%
<b>n</b>	Br	H	Cl	H	H	89%
<b>o</b>	CHO	F	H	H	H	31%
<b>p</b>	NO <sub>2</sub>	NO <sub>2</sub>	H	H	H	34%
<b>q</b>	CN	F	H	H	F	87%
<b>r</b>	Br	H	F	F	H	46%
<b>s</b>	H	I	H	H	H	50%
<b>t</b>	F	H	F	H	H	72%
<b>u</b>	SONH <sub>2</sub>	H	H	H	H	33%
<b>v</b>	Br	H	Cl	Cl	H	50%
<b>w</b>	Br	H	F	H	H	35%
<b>x</b>	H	OH	H	H	H	25%
<b>y</b>	OH	H	H	H	H	7%
<b>z</b>	CO <sub>2</sub> H	H	H	H	H	9%

<sup>a</sup> Derivative **2a** and **2b** were prepared from 2-bromo-1-(4-hydroxyphenyl)ethan-1-one and the corresponding substituted phenols in the presence of sodium methylate in THF.

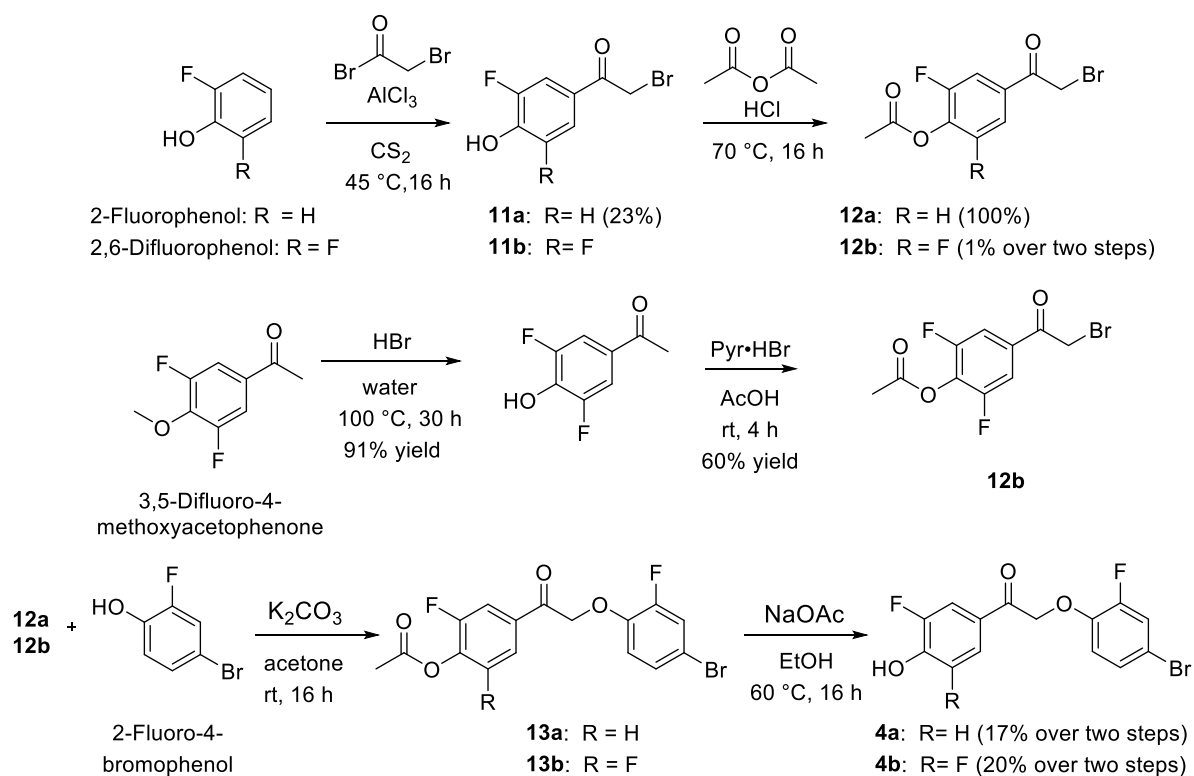
Since compound **2w** was most active in a first series of assays (**Table 2**), substituents of **2w** (R<sup>1</sup> = Br, R<sup>3</sup> = F) were kept in the next series where phenol substituents were introduced (**3**, **4a** and **4b**).

The synthesis of the dihydroxy analog **3** (**Scheme 5**) started with a Friedel-Crafts acylation of catechol and 2-bromoacetyl bromide, followed by acetylation of both hydroxyl groups using acetic anhydride. The resulting intermediate **9** was then converted to **10** in a nucleophilic substitution reaction with the corresponding phenol and followed by subsequent de-acetylation of both hydroxyl-groups to the target molecule **3**.



**Scheme 5.** Synthesis of dihydroxy open analog **3**.

To evaluate the pharmacological impact of the acidity of phenolic ligands, fluorine substituents *ortho* to the phenol group were introduced in open analogs **4a** and **4b**. Whereas 4-(2-bromoacetyl)-2-fluorophenol **11a** could be synthesized by a Friedel-Craft reaction similarly to **8**, the corresponding reaction to **11b** using the more deactivated 2,6-difluorophenol resulted in a significantly lower conversion (**Scheme 6**). Thus, **11b** was prepared from 3,5-difluoro-4-methoxyacetophenone by demethylation in aqueous HBr followed by  $\alpha$ -bromination of the acetyl group using pyridine hydrobromide in acetic acid (**Scheme 6**). Subsequent acetylation of **11a,b** was performed using acetic anhydride in concentrated HCl followed by nucleophilic substitution with 2-fluoro-4-bromophenol to **13a,b** and deprotection of the phenol, afforded the open analogs **4a** and **4b** (**Scheme 6**).



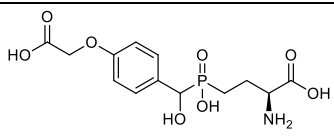
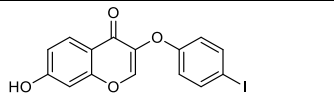
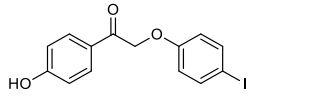
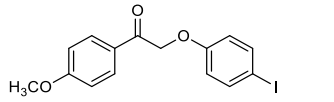
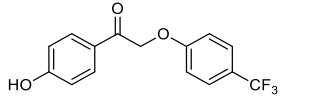
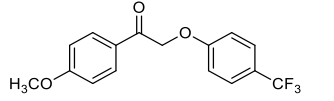
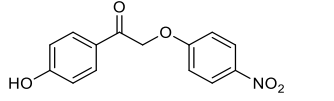
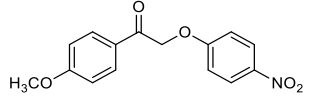
**Scheme 6.** Synthesis of open analogs **4a** and **4b**.

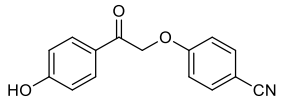
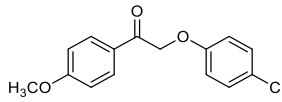
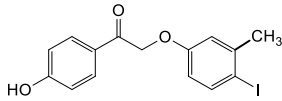
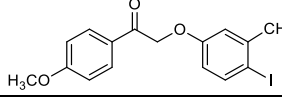
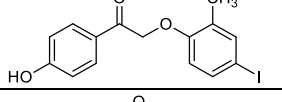
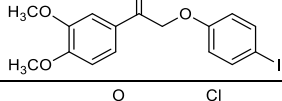
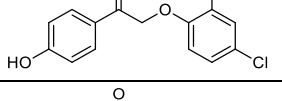
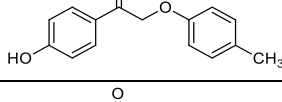
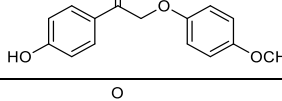
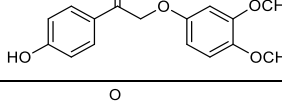
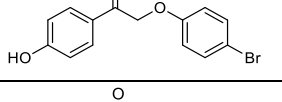
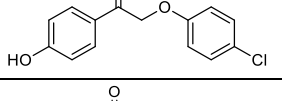
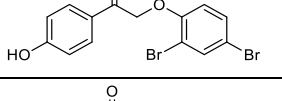
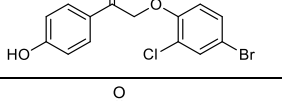
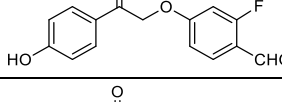
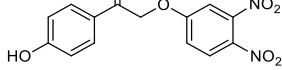
### Pharmacological evaluation

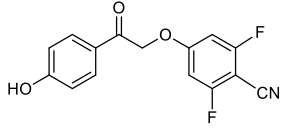
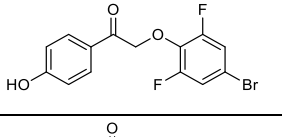
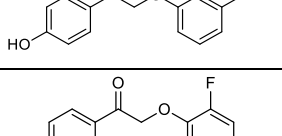
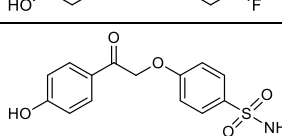
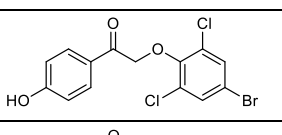
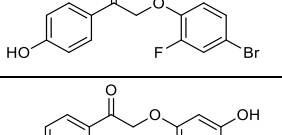
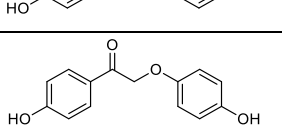
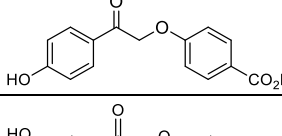
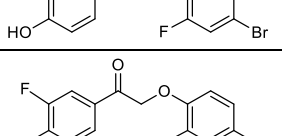
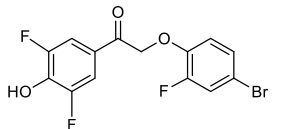
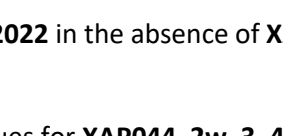
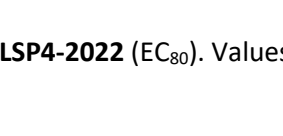

Compounds **1a-j**, **2a-z**, **3**, **4a** and **4b**, **5a-d**, were first evaluated at a single dose of 30  $\mu\text{M}$  or 100  $\mu\text{M}$  for their ability to inhibit mGlu7 receptor activation induced by the agonist LSP4-2022 at a single dose of 30  $\mu\text{M}$  in an IP-One functional assay. The inhibitory action of **XAP044** and its derivatives was examined by their capacity to decrease the potency of the agonist **LSP4-2022**. The potency of LSP4-2022 in the absence ( $\text{pEC}_{50}$  Ctrl) and in the presence of **XAP044** derivative ( $\text{pEC}_{50}$ ) were measured and the ratio  $\text{pEC}_{50}/\text{pEC}_{50}$  Ctrl (**Table 2**) were calculated. A ratio of 1 reveals an inactive derivative of **XAP044**. The lower the ratio, the more efficient is the derivative.

The whole series of constrained analogs **1a-j** showed no significant inhibition (data not shown). These data suggest that **XAP044** is binding to mGlu7 receptor in a non-planar conformation. We then tested the open analogs **5a-d**, **2a-y**, **3**, **4a** and **4b**. The results are shown in **Table 2**. Typical concentration-response curves obtained with the best compounds are shown in **Figure 3**.

**Table 2.** Ability of open **XAP044** analogs to inhibit **LSP4-2022** effect. The full concentration effect of **LSP4-2022** in stimulating the IP1 production in cells co-expressing mGlu7 and Gqi9 was performed in the absence and in the presence of the indicated compounds, and both the pEC<sub>50</sub> and maximal effect relative to that of **LSP4-2022** alone were determined. The ratio of the pEC<sub>50</sub> measured in the presence of the compound, over that measured in the absence (pEC<sub>50</sub>/pEC<sub>50</sub>Ctrl) are shown. Values are means ± sem of n independent experiments performed in triplicates. If only two experiments were performed, the values measured in each experiment are shown. Statistical significance determined using a paired T-test is as follow: \* p<0.05, \*\* p<0.01, \*\*\* p<0.001, \*\*\*\* p<0.0001, ns non-significant.

Compounds	Compound structures	LSP4-2022 potency in the presence of 30 μM or 100 μM of XAP044 derivatives			n
		pEC <sub>50</sub> ± sem	pEC <sub>50</sub> /pEC <sub>50</sub> Ctrl ± sem	Max ± sem %	
<b>LSP4-2022<sup>a</sup></b>		<b>4.71 ± 0.03</b>	<b>1.00 ± 0.00</b>	<b>100</b>	39
<b>+ XAP044</b>		<b>3.87 ± 0.06 ****</b>	<b>0.82 ± 0.01</b>	<b>97.5 ± 1.4 ns</b>	19
		<b>3.95 ± 0.05****</b>	<b>0.84 ± 0.01</b>	<b>96.4 ± 1.5 ns</b>	8
<b>+ 2a</b>		<b>3.38 ± 0.04****</b>	<b>0.83 ± 0.01</b>	<b>98.3 ± 3.3 ns</b>	10
<b>+ 5a</b>		4.58 ; 4.45	0.98, 0.97	93.6 ; 109	2
<b>+ 2b</b>		<b>4.12 ± 0.03 ns</b>	<b>0.91 ± 0.02</b>	<b>101.0 ± 5.7 ns</b>	3
<b>+ 5b</b>		4.71 ; 4.45	1.01, 0.97	96.6 ; 107	2
<b>+ 2c</b>		<b>3.94 ± 0.06*</b>	<b>0.87 ± 0.02</b>	<b>98.5 ± 1.5 ns</b>	4
<b>+ 5c</b>		4.35 ; 4.45	0.96, 0.95	85.2 ; 100	2

<b>+ 2d</b>		<b>4.02 ± 0.03**</b>	<b>0.89 ± 0.02</b>	<b>92.6 ± 2.4 ns</b>	4
<b>+ 5d</b>		4.44 ; 4.40	0.95, 0.96	89.4 ; 100	2
<b>+ 2e</b>		4.51 ; 4.39	0.97, 0.96	100 ; 97.5	2
<b>+ 5e</b>		4.61 ; 4.43	0.99, 0.97	95.9 ; 103	2
<b>+ 2f</b>		4.77 ; 4.45	1.03, 0.97	98.6 ; 98.3	2
<b>+ 5f</b>		4.95 ; 4.80	1.06, 1.05	80.4 ; 101	2
<b>+ 2g</b>		4.37 ; 4.29	0.94, 0.94	94.3 ; 92.3	2
<b>+ 2h</b>		4.65 ; 4.39	1.00, 0.96	95.4 ; 110	2
<b>+ 2i</b>		4.68 ; 4.40	1.01, 0.96	97.6 ; 104	2
<b>+ 2j</b>		<b>4.46 ± 0.03 ns</b>	<b>0.99 ± 0.00</b>	<b>96.0 ± 3.1 ns</b>	4
<b>+ 2k</b>		<b>3.62 ± 0.02***</b>	<b>0.81 ± 0.01</b>	<b>99.2 ± 5.7 ns</b>	5
<b>+ 2l</b>		<b>3.74 ± 0.03****</b>	<b>0.83 ± 0.01</b>	<b>98.5 ± 4.3 ns</b>	5
<b>+ 2m</b>		<b>4.32 ± 0.08 ns</b>	<b>0.97 ± 0.02</b>	<b>96.1 ± 1.9 ns</b>	6
<b>+ 2n</b>		<b>4.23 ± 0.07 ns</b>	<b>0.95 ± 0.02</b>	<b>93.3 ± 4.8 ns</b>	6
<b>+ 2o</b>		<b>4.46 ± 0.08 ns</b>	<b>1.00 ± 0.02</b>	<b>106 ± 5.1 ns</b>	6
<b>+ 2p</b>		<b>4.47 ± 0.03 ns</b>	<b>1.00 ± 0.01</b>	<b>101 ± 3.2 ns</b>	6

<b>+ 2q</b>		$4.59 \pm 0.02$ ns	$1.03 \pm 0.01$	$94.2 \pm 5.0$ ns	3
<b>+ 2r</b>		$3.76 \pm 0.05^{**}$	$0.85 \pm 0.03$	$94.6 \pm 7.8$ ns	8
<b>+ 2s</b>		$4.35 \pm 0.09$ ns	$1.02 \pm 0.03$	$101.8 \pm 9.3$ ns	4
<b>+ 2t</b>		$4.44 \pm 0.06$ ns	$1.04 \pm 0.03$	$100.0 \pm 6.9$ ns	4
<b>+ 2u</b>		$4.53 \pm 0.03$ ns	$1.06 \pm 0.03$	$89.2 \pm 4.2$ ns	4
<b>+ 2v</b>		$4.92 \pm 0.05$ ns	$1.01 \pm 0.01$	$101.4 \pm 4.7$ ns	3
<b>+ 2w</b>		$3.54 \pm 0.05^{****}$	$0.76 \pm 0.01$	$87.3 \pm 9.4$ ns	10
<b>+ 2x</b>		$4.83 \pm 0.05$ ns	$1.03 \pm 0.01$	$96.8 \pm 10.9$ ns	3
<b>+ 2y</b>		$4.95 \pm 0.05$ ns	$1.06 \pm 0.01$	$88.1 \pm 11.23$ ns	3
<b>+2z</b>		$5.0 \pm 0.08^*$	$1.07 \pm 0.01$	$98.6 \pm 2.80$ ns	3
<b>+ 3</b>		$3.47 \pm 0.05^{****}$	$0.76 \pm 0.01$	$90.3 \pm 12.1$ ns	6
<b>+ 4a</b>		< 3	< 0.6		5
<b>+ 4b</b>		< 3	< 0.6		2

<sup>a</sup> Effect of **LSP4-2022** in the absence of **XAP044** derivative.

**Table 3.** IC<sub>50</sub> values for **XAP044**, **2w**, **3**, **4a** and **4b**, as determined for their inhibitory action of the effect of 30 μM **LSP4-2022** (EC<sub>80</sub>). Values are means ± sem of n independent experiments performed



in triplicates. Statistical significance of the pIC<sub>50</sub> compared to that of **XAP044** determined using an unpaired T-test is as follow: \* p<0.05, ns non-specific. In this series of experiments the pEC<sub>50</sub> of **LSP4-2022** was 4.76 ± 0.06 (n = 7).

Inhibition of 30µM LSP4-2022 effect by XAP044 derivatives			
Compounds	IC <sub>50</sub> (µM) mean ± sem	pIC <sub>50</sub> mean ± sem	n
<b>XAP044</b> <sup>a</sup>	4.33 ± 1.16	5.40 ± 0.12	3
<b>2w</b>	2.60 ± 0.82	5.65 ± 0.14 ns	4
<b>3</b>	3.44 ± 0.62	5.48 ± 0.07 ns	3
<b>4a</b>	0.95 ± 0.25	6.07 ± 0.13*	4
<b>4b</b>	1.25 ± 0.37	5.94 ± 0.12*	3

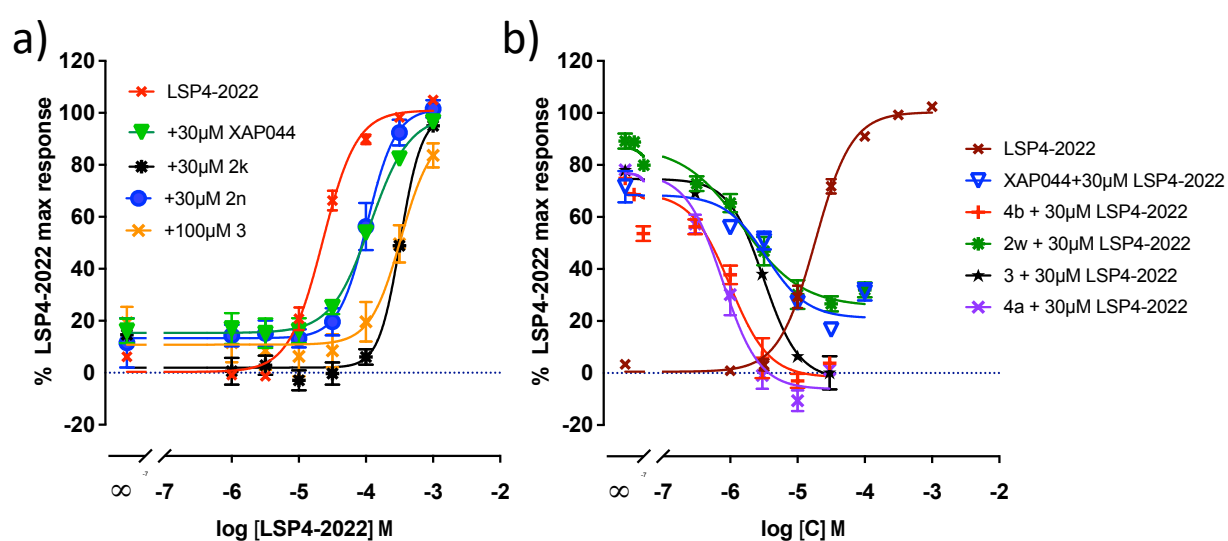


**Figure 3:** Inhibitory effect of **XAP044** derivatives on **LSP4-2022** activation of mGlu7 measured through the IP One assay. a) Effect of **XAP044**, compound **2k**, **2n** and **3** at 30 or 100µM on the effect of increasing concentrations of **LSP4-2022**. b) Effect of increasing concentrations of **XAP044**, **4b**, **2w**, **3** and **4a** compounds on the IP1 production produced by 30µM **LSP4-2022**. In a) and b) data are shown as the percentage of the maximal effect of **LSP4-2022** over basal, and are means ± sem of 3 independent experiments performed in triplicates.

The first observation is a similar mGlu7 receptor inhibition by **XAP044** and **2a** revealing that the chromone structure is not required allowing easier synthesis of its open equipotent analog. Next, we note that methylation of the phenol is detrimental for potency: compare **2a** with **5a**, **3** with **5f**, **2c** with **5c**, **2d** with **5d** revealing the importance of a free hydroxyl group. Introducing *ortho* substituents to this phenol such as hydroxyl or fluorine is beneficial as in **3**, **4a** and **4b**. Adding *ortho* fluorine increases the phenol acidity. Indeed, calculated pKa's of 4-acetylphenols<sup>20</sup> show a decrease from 7.8 with no substituents to 6.8 with one *ortho* fluorine and to 6.0 with two *ortho* fluorine atoms. More acidic phenols are stronger H-bond donor<sup>21</sup>, consequently the increased potency reveals that such an interaction occurs between **XAP044** and its analogs and mGlu7 receptor. Adding a second hydroxyl *ortho* to the phenol does not increase its acidity but provides possible additional H-bonds that may stabilize the complex.

On the *para*-iodophenoxy side, the iodine may be replaced by a few other polarizable substituents: nitro in **2c**, cyano in **2d**, and other halides as bromine in **2k**, chlorine in **2l** but not by hydrophobic or bulky groups such as methyl in **2h**, trifluoromethyl in **2b**, methoxy in **2i**, sulfonamide in **2u**, and negatively charged groups as carboxylate in **2z**. Thus, a polar negatively charged surface is anticipated around this *para* position. *Ortho* substitution of the phenoxy is limited to fluorine attesting of a restricted environment of this moiety.

Among the tested analogs, **2w**, **3**, **4a** and **4b** are the most efficient inhibitors even more potent than **XAP044**. They were thus, further characterized by analyzing their ability to inhibit an EC<sub>80</sub> concentration of **LSP4-2022** (**Figure 3b**). Their IC<sub>50</sub>'s at inhibiting 30 μM **LSP4-2022** are shown in **Table 3** and confirm that compounds **4a** and **4b** are statistically more potent than **XAP044**. Of note a full inhibition of the LSP4-2022 effect could not be obtained with the highest concentrations of **XAP044** and **2w**. This could be due to a partial effect (and then allosteric effect) of these molecules, or alternatively to the difficulty in reaching the expected concentrations of these compounds due to solubility issues. The summary of the SAR is displayed in **Figure 4**. These determinants were helpful for the docking of **XAP044** (see the modeling section).

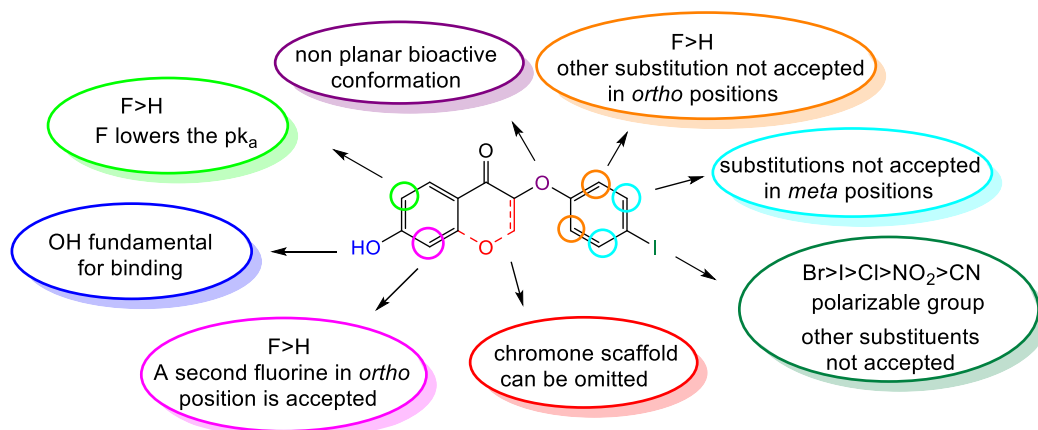


**Figure 4.** Compilation of **XAP044** SAR.

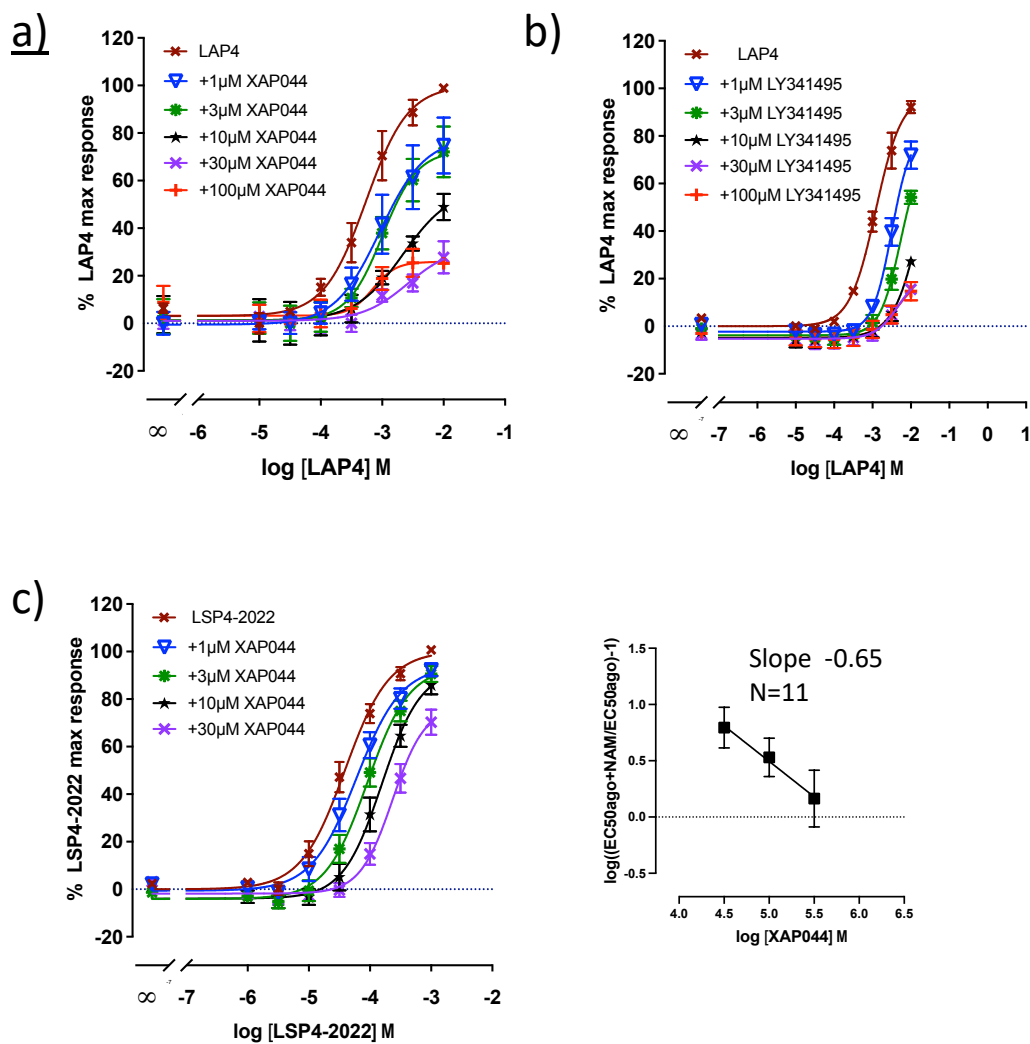
### **Competition between LSP4-2022 and XAP044 and its derivatives.**

Pharmacological properties of **XAP044** are also crucial to help defining its binding mode. We thus characterized the type of inhibition carried out by **XAP044** and compared it with that of **LY341495** (**Figure 5**).

As shown in **Figure 5a**, **XAP044** displays a non-competitive antagonist profile of **L-AP4** activation at mGlu7 receptor, with a clear decrease in the maximal **L-AP4** effect. This is quite different from what is observed with **LY341495**, despite the difficulty in reaching the max limit for the full interpretation of these data (**Figure 5b**). However, there is a clear difference between the inhibitory actions of **XAP044** and **LY341495** on the **L-AP4** effect. In contrast, **XAP044** looks like a competitive antagonist of **LSP4-2022** (**Figure 5b**) as is **LY341495** (**Figure 5c**), although the difficulty in reaching a clear conclusion is occluded by the impossibility to reach saturations of the maximal effect, as higher concentrations could not be tested. However, the inhibitory effect of **XAP044** on **LSP4-2022** is clearly different from that observed on the **L-AP4** effect, but similar to that obtained with increasing concentrations of the competitive antagonist **LY341495**. A possible competitive mode of action of both **XAP044** and **LY341495** on the **LSP4-2022**, is coherent with the Schild analysis (**Figure 5c,d**), although the slopes are still low. The need for high concentrations of both the competitor and the agonist limits the correct analysis of the data, and may provide a possible explanation for the low

slope values. Such results are expected for the two glutamate derivatives (**LSP4-2022** and **LY341495**) but not for **XAP044** as it is not expected to bind at the **L-AP4**/glutamate site. An additional observation is also informative, **XAP044** does not inhibit [<sup>3</sup>H]-**LY341495** binding while **LY341495** does, consistent with **XAP044** not being able to bind to the glutamate binding site (**Figure 6**). Of interest, **XAP044** increased the binding of [<sup>3</sup>H]-**LY341495** (**Figure 6**), consistent with its ability to stabilize the inactive state of the receptor, possibly increasing the **LY341495** affinity, though more work is needed to confirm this interpretation.

Thus, **XAP044** appears to be similar to the competitive antagonist **LY341495** in inhibiting **LSP4-2022** effect, even though they do not bind to the same site.



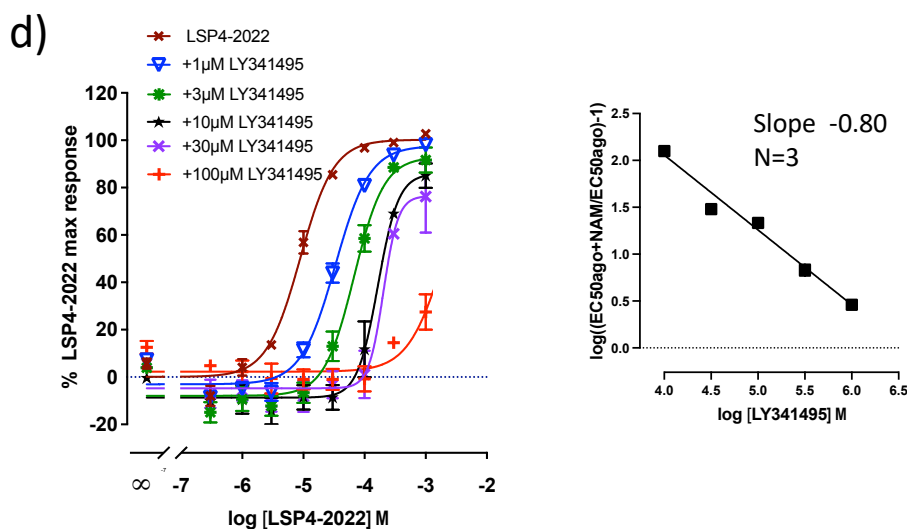


**Figure 5.** Competitive or non-competitive nature of the inhibition by mGlu7 inhibitor depending on the agonist used. a) Effect of increasing concentration of **XAP044** on the **L-AP4** potency at mGlu7. b) Effect of increasing concentration of **LY341495** on the **L-AP4** potency at mGlu7. c) and d) Effect of **XAP044** and **LY341495**, respectively, on the potency of **LSP4-2022**. Schild representation of the observed shift in the agonist concentration response curves is shown in both panel c) and d). Data are means  $\pm$  sem of 3 to 11 experiments performed in triplicates.

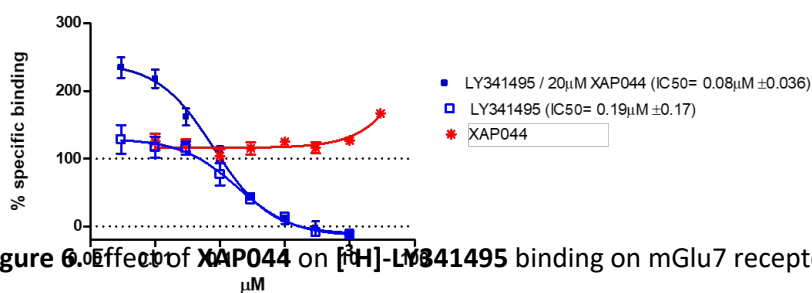
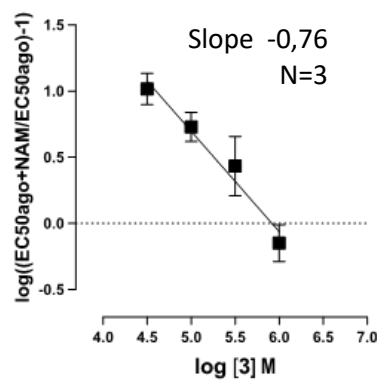
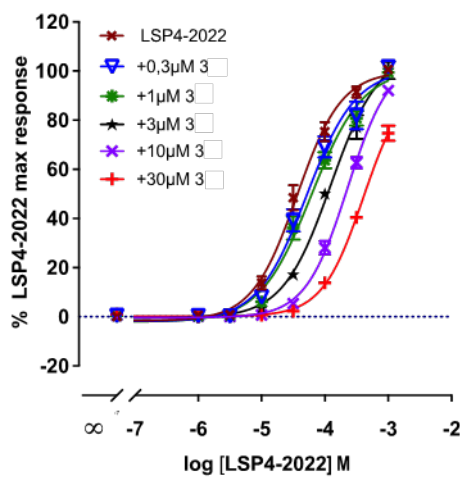


**Figure 6.** Effect of **XAP044** on [<sup>3</sup>H]-**LY341495** binding on mGlu7 receptor. [<sup>3</sup>H]-**LY341495** binding on CHO cells expressing rat mGlu7 was determined in the presence of increasing concentrations of **XAP044**, or **LY341495** alone or with 20 μM **XAP044**. Values are means  $\pm$  sem of triplicate determinations from a typical experiment.

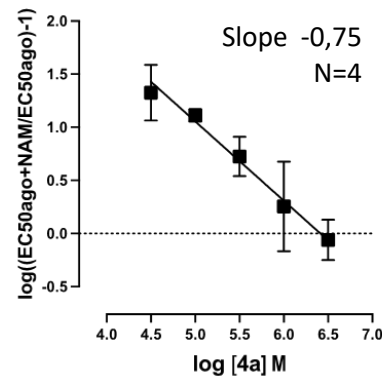
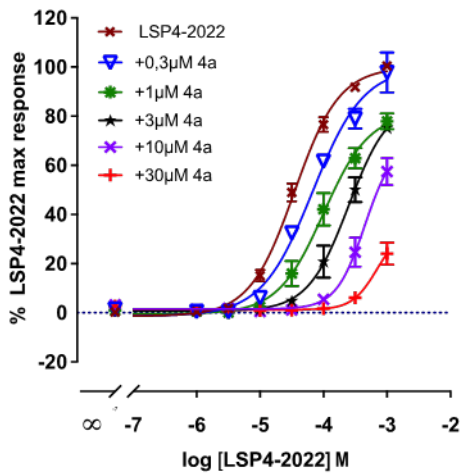
The mode of action of the three most potent derivatives of **XAP044** in inhibiting the agonist effect of **LSP4-2022** were then also examined (**Figure 7**). In addition to an increased potency, they show a better solubility. Similar to **XAP044**, **3**, **4a** and **4b** appear to mainly shift the concentration response

curve of **LSP4-2022** to the right, similar to a competitive inhibition. The Schild slopes were all higher than 0.75, consistent with a competitive nature of the antagonism, although it was not possible to reach saturation at the high concentrations of antagonists that had to be used in such an analysis. These results suggest a binding of these **XAP044** analogs and **XAP044** to overlapping sites on mGlu7 receptor extracellular domain.

3



4a



4b

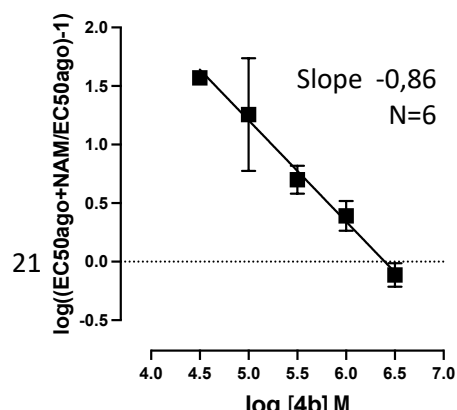
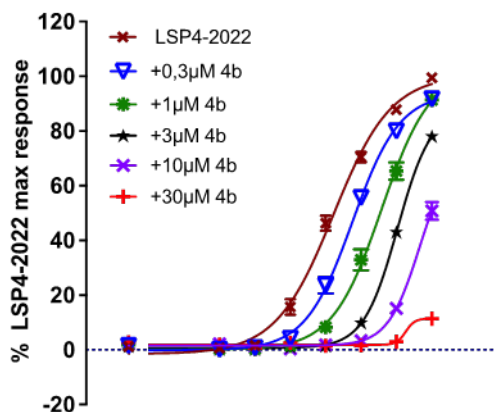


**Figure 7.** Effect of various concentrations of **3**, **4a** and **4b** on the agonist response mediated by increasing concentrations of **LSP4-2022** on mGlu7 receptor. The Schild representations are indicated on the right. Data are means  $\pm$  sem of 3 to 6 independent experiments performed in triplicates.

### **Molecular Modeling for XAP044 binding mode identification**

The mGlu7 receptor belongs to class C G-protein coupled receptors (GPCRs). In addition to the 7-helix transmembrane domain (7TM) common to all GPCRs, these receptors possess a large extracellular domain folding in two lobes linked by a flexible hinge and connected to the 7TM by a cysteine rich domain (CRD). The orthosteric binding site is located in the cleft between the two lobes, which close in the active state.<sup>22</sup> By analogy with the carnivorous plant, this domain has been named the Venus FlyTrap domain (VFT). Moreover, these receptors are obligatory dimers that oscillate between a resting and an active state (**Figure 8**).<sup>23</sup> Agonists such as glutamate, **L-AP4** and **LSP4-2022** bind to the upper lobe of the VFT in the Resting<sub>open-open</sub> (Roo) state and are trapped between the two lobes, which close in a rigid body movement to the Active<sub>closed-closed</sub> (Acc) state (**Figure 8**). The closing of the two VFTs leads to a rotation of the protomers relative to each other, allowing the 7TM domains to interact in an active conformation.<sup>24</sup>

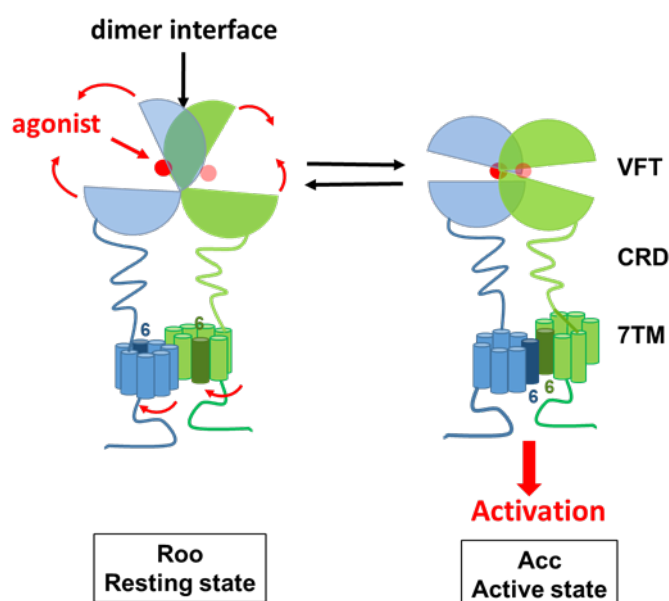


**Figure 8.** Schematic structure of an mGlu receptor dimer and the equilibrium between resting and active conformations. Both VFTs are open in the resting state (Resting open-open) and closed in the active state (Active closed-closed).

In order to interpret the **XAP044** inhibitory mechanism, we required the 3D-structures of the Roo and the Acc states of the mGlu7 receptor VFT domain.<sup>17</sup> At the time of the study, three X-Ray structures of mGlu7 receptor open VFT were available (PDB ID 2E4Z<sup>25</sup>, 3MQ4<sup>26</sup>, 5C5C<sup>27</sup>, **Table S1**). We selected 2E4Z template because it had the lowest number of missing residues and an intermediate value of the opening angle of the VFT, falling within the range of mGlu1, 2, 3 receptor angles when bound to various antagonists (**Table S2**). The long  $\alpha 2$ - $\beta 6$  missing loop (consisting of 18 missing residues) was rebuilt by homology modeling using a loop refined from the mGlu5 receptor 6N52 structure (**Table S3**), (see SI and alignment in **Figure S1**), followed by refinement steps in Discovery Studio.<sup>28</sup> This template was selected because of its smallest amount of missing residues in this loop at the time (14 missing residues). For the  $\beta 10$ - $\alpha 7$  loop, we used the 6BSZ mGlu8 receptor template<sup>29</sup> (**Table S4**). Finally, for the other short missing loops (less than 5 missing residues), we simply performed a short minimization after inserting them (see experimental section).

Next, we built the mGlu7 Acc 3D-model. We used the above Roo model where we cut the hinge and superimposed each lobe to those of the Acc 6BT5 mGlu8 structure. Then we grafted the mGlu8 3



hinge segments (that are conserved but one residue, **Figure S1**), for reconnecting the two lobes and minimized these segments. We note that the closing angle of the mGlu8 VFT (**Table S2**) is similar to the homologous one in the mGlu4 structure (later released in the PDB). The long  $\alpha$ 2- $\beta$ 6 missing loop was rebuilt in a similar fashion as in the Roo model (**Table S5**).

The Acc model was used to dock the agonists **L-AP4** and **LSP4-2022**, while the Roo model was employed for the antagonist **XAP044** and its analogs. Only one VFT is displayed in the figures.

#### **LSP4-2022** docking to the closed mGlu7 receptor VFT

**L-AP4** was docked at the mGlu7 receptor glutamate binding site (**Figure S2**). **LSP4-2022** was docked similarly to **L-AP4** for its proximal part and at chloride site 2 for its distal part (**Figure 9a and b**), consistent with previous descriptions at mGlu4 receptor<sup>10, 30</sup> (**Figure S3**). Docking experiments were performed using GOLD<sup>31</sup> as implemented in Discovery Studio.<sup>28</sup> Some interaction constraints were applied to maintain the glutamate-like part bound as **L-AP4**, as previously described.<sup>10, 30</sup> The stability of the system was assessed by molecular dynamics (see experimental section). The distal part of **LSP4-2022** binds to a set of residues of mGlu7 receptor (K60, S160, S229 (backbone), Q258, **Figure 9b**) similar to those in the analogous docking at mGlu4 receptor<sup>10, 30</sup> (**Figure S3**).

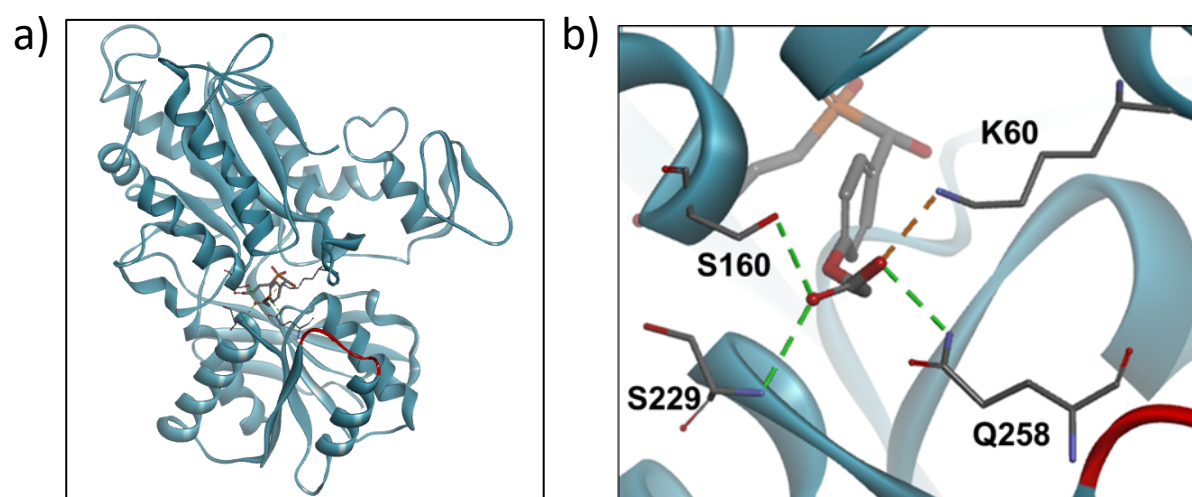


**Figure 9.** Docking of **LSP4-2022** at the glutamate and chloride 2 sites of mGlu7 receptor.<sup>10, 30, 32</sup> a) VFT view where the backbone ribbon is colored in gray-blue and loop  $\beta$ 10- $\alpha$ 7 in red (atom colors: C gray,

O red, N blue, P orange, H omitted for clarity; H bonds and salt bridge, green and brown dashed lines). **b)** Expanded view of the **LSP4-2022** distal part interactions. Only residues binding the distal carboxylate are displayed.

#### *Validation of LSP4-2022 docking*

The binding of the distal carboxylic group of **LSP4-2022** at mGlu7 receptor was evaluated through mutation of the set of binding residues and subsequent functional assays. Data are reported in **Table 4**. Altogether, mutations of residues K60 and S160 from lobe 1 have the greatest impact on **LSP4-2022** potency (similar observations were made for homologous mGlu4 receptor residues, **Table 4**). However, these mutations also affect **L-AP4** activation, likely by disturbing chloride 2 site as described in Tora et al.<sup>32</sup> Binding to Q258 from lobe 2 appears to be less critical, but swapping the entire loop  $\beta$ 10- $\alpha$ 7 between mGlu4 (R258-A262) and mGlu7 (Q258-T263) (see alignment in **Figure S1**) underscores the importance of that loop. Earlier, D. Hampson demonstrated an increase of mGlu7 receptor activity when introducing mGlu4 residues in that loop.<sup>33</sup> Indeed, as he proposed, because this loop is two residues longer in mGlu7 receptor, it protrudes from lobe 2 in the VFT cleft preventing optimal closure as in mGlu4. We hypothesize that when **LSP4-2022** interacts with Q258, loop  $\beta$ 10- $\alpha$ 7 adopts a fold that prevents protrusion, thereby explaining the increased activation compared to **L-AP4**.

**Table 4.** Mutation of distal residues interacting with **L-AP4** and **LSP4-2022** docked at mGlu4 and mGlu7 receptors. Values are means  $\pm$  sem of (n) independent experiments performed in triplicates.

	EC <sub>50</sub> ( $\mu$ M)			EC <sub>50</sub> ( $\mu$ M)	
	L-AP4	LSP4-2022		L-AP4	LSP4-2022
<b>mGlu4</b>			<b>mGlu7</b>		
WT	0.343 $\pm$ 0.09 (6)	0.833 $\pm$ 0.23 (12)	WT	> 100 (6)	21.2 $\pm$ 1.49 (39)
R60A	1.16 $\pm$ 0.36 (5)	9.07 $\pm$ 0.12 (3)	K60A	1980 $\pm$ 475 (2)	178 $\pm$ 37 (5)
	-	-	K60A+S160A	<sup>a</sup>	> 300 (3)
K74A	0.23 $\pm$ 0.07 (3)	0.0245 $\pm$ 0.008 (3)	N74A	> 100 (3)	32.0 $\pm$ 6.94 (4)
	-	-	N74K	10.5 $\pm$ 1.9 (3)	47.0 $\pm$ 6.52 (5)
S160A	2.66 $\pm$ 0.9 (8)	26.2 $\pm$ 7.32 (7)	S160A	<sup>a</sup>	> 300 (3)
S160D	12.3 $\pm$ 9.16 (8)	18.5 $\pm$ 7.05 (10)	-	-	-
R258A	1.87 $\pm$ 0.67(7)	4.91 $\pm$ 2 (7)	Q258A	<sup>a</sup>	18.2 $\pm$ 6.25 (3)

R258Q+D262+R263	11.1 ± 3.89 (7)	7.00 ± 2.52 (7)	Q258R-D262-R263	> 100 (5)	13.9 ± 1.33 (5)
loop β10-α7 of mGlu7	0.505 ± 0.017 (3)	3.68 ± 0.25 (3)	loop β10-α7 of mGlu4	45.0 ± 8.5 (6)	2.18 ± 0.24 (3)
	-	-	N74K+loop4	<sup>a</sup>	2.56 ± 0.51 (4)
	-	-	S229A	182 ± 11.5 (2)	14.5 ± 1.8 (14)
	-	-	K233A	<sup>a</sup>	87.7 ± 11.3 (7)
	-	-	K233S	<sup>a</sup>	40.9 ± 10.1 (9)
	-	-	K233D	<sup>a</sup>	155 ± 13.9 (4)
	-	-	S237A	<sup>a</sup>	18.3 ± 5.68 (3)
N286A	<sup>-a</sup>	1.79 ± 0.36 (3)	N288A	<sup>a</sup>	49.3 ± 16 (3)
	-	-	D314A	> 1000 (2)	> 1000 (5)

<sup>a</sup> Not tested.

#### **XAP044** binding to an open form of the mGlu7 receptor VFT

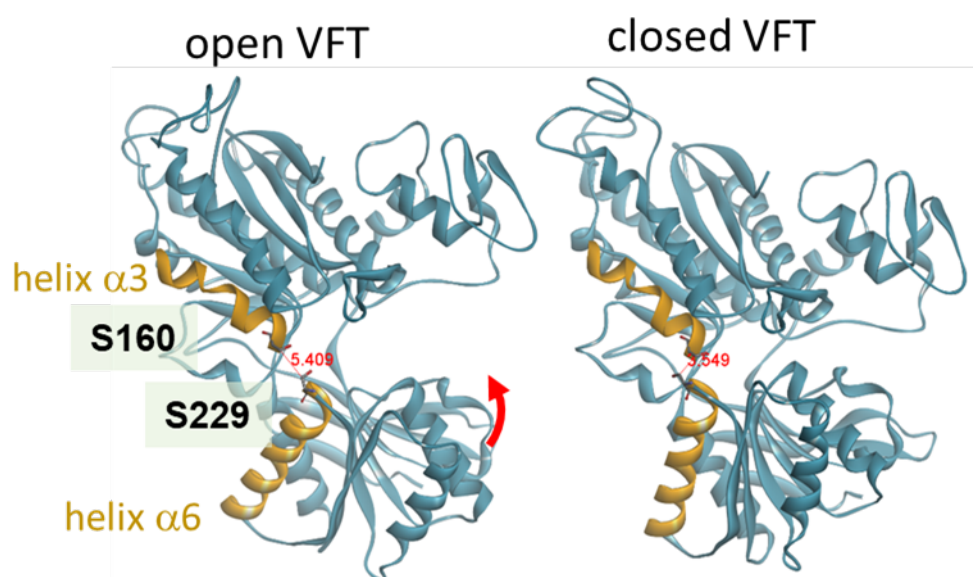
Since **XAP044** binds to the VFT and inhibits the homodimer activation, we envisaged two possible mechanisms. Either XAP044 prevents the closure of the VFT or it blocks the dimer transition from the resting orientation to the active orientation (**Figure S4**).

We first investigated the VFT closure hypothesis. A careful examination of the two models reveals that the rigid body movement of the lobes brings the bottom part of the α3 helix closer to the top part of the α6 helix (**Figure 10**). The two closest residues are S160 and S229. The distance of their Cβ varies from 5.40 Å in Roo to 3.55 Å in Acc (**Figure 10**). We hypothesized that **XAP044** could be operating as a wedge that blocks the movement of the lobes by interacting with these serine residues. Indeed, the S229A mutation abolishes the inhibitory effect of **XAP044** (see **Table S7**) without affecting the **LSP4-2022** binding (**Table 4**). On the other hand, S160 has been identified as part of a chloride site,<sup>32</sup> and its mGlu4 homolog is predicted to bind to the distal carboxylate of **LSP4-2022**<sup>30</sup> similarly to the mGlu7 docking (see above and **Figure 9**). Not surprisingly, the S160A mutation drastically reduces the **LSP4-2022** activation of mGlu7 receptor (**Table 4**).

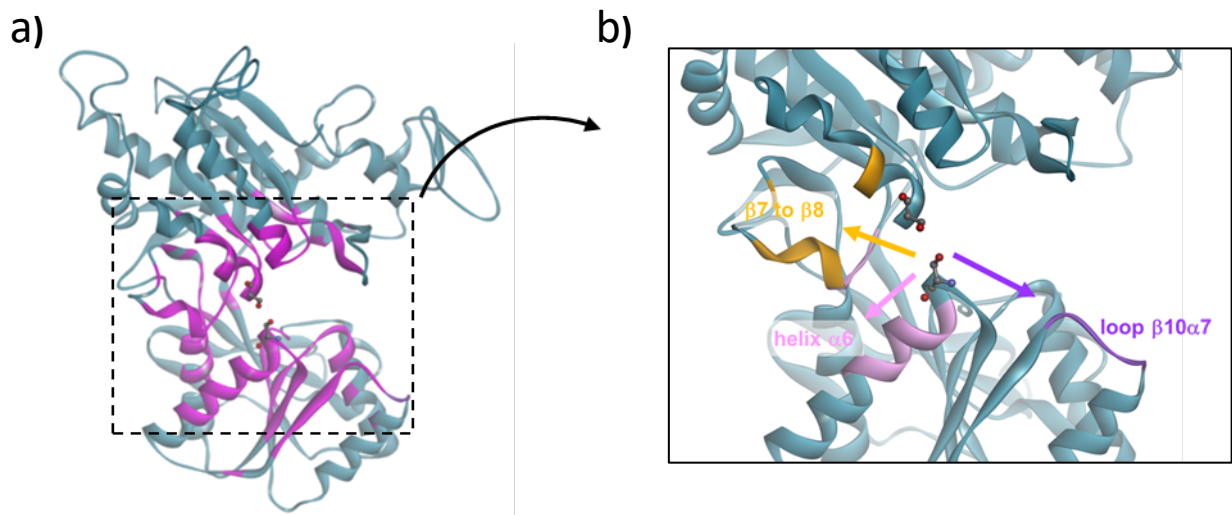
Given that **XAP044**, in its most extended conformation, has a length of 13.6 Å, we opted to explore potential binding sites within a maximum distance of 15 Å from S229 in the open VFT model (**Figure 11a**). Furthermore, selective residues within this zone were identified. Considering the selectivity of **XAP044** for the mGlu7 receptor over other mGlu receptor subtypes<sup>17</sup>, only three orientations around S229 were possible for **XAP044** to bind to these residues (**Figure 11b**) (see alignment in **Figure S1**).

The first option was for **XAP044** to interact with loop β10-α7. This particular loop is partly

responsible for the weak activation of mGlu7 receptor.<sup>33</sup> The second option was to orient **XAP044** towards the portion between  $\beta 7$  and  $\beta 8$  because of selective D189/R190 residues. In the third option, **XAP044** would bind along the  $\alpha 6$  helix because of the mGlu7 selective residues K233 and S237 (**Figure 11b**). Each of the 3 options was tested by docking experiments of **XAP044**. Given the essential role of S229 in **XAP044** activity (see above and **Table S7**), we imposed an interaction with its side chain. Additionally, some residues were set flexible: S226, S229, Q258, N288, E20, D291 for option 1, S160, I163, E185, R191, Y192, K233 for option 2 and S160, E185, S229, K233, E236, S237 for option 3. All dockings yielding satisfactory scores positioned **XAP044** with its phenol making H-bonds with S160 and S229, consistent with the SAR data (see above).

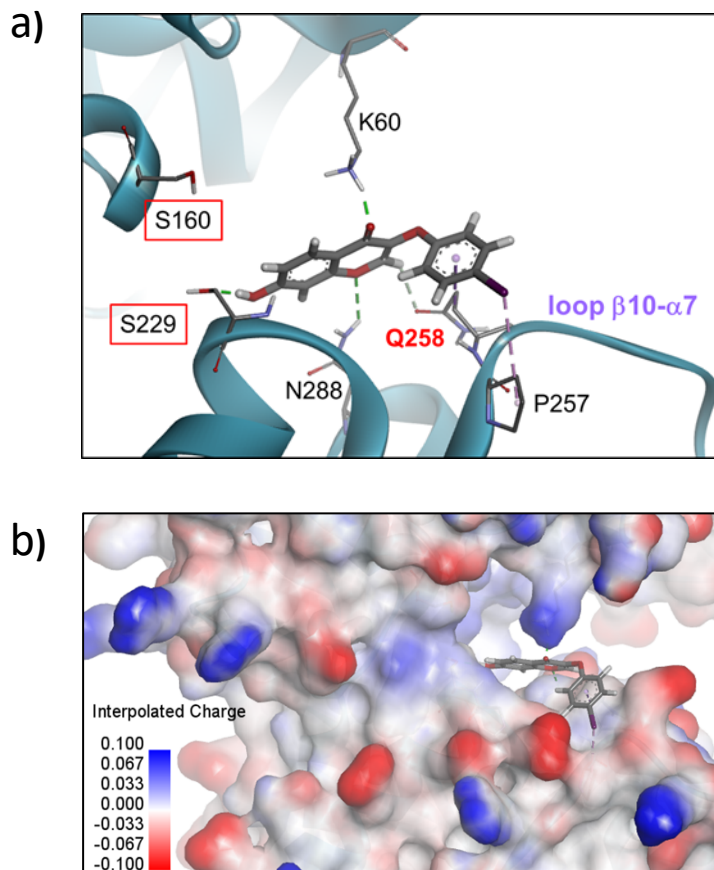


**Figure 10.** 3D-structures of open (left) and closed (right) VFT domain of mGlu7 receptor. Helices  $\alpha 3$  and  $\alpha 6$  are colored in gold. S160 and S229 side chains and distances between their respective C $\beta$  are displayed.



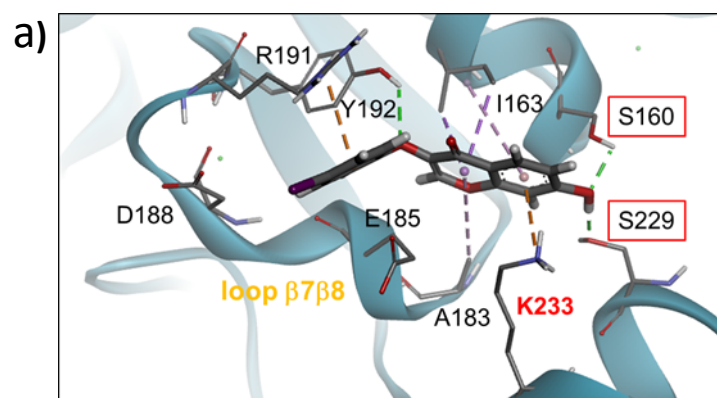
**Figure 11.** a) Open mGlu7 receptor VFT model: ribbon of residues at less than 15 Å from S229 is colored in magenta. b) Three possible orientations for **XAP044** to bind to S229.

In option 1, **XAP044** was expected to interact with loop β10-α7 (Figure 12). However, swapping that loop with the one of mGlu4 receptor had no effect on the activity of **XAP044**, so we abandoned this site before running any MD simulations (Table S7).



**Figure 12.** Docking of **XAP044** in option 1 (contact with loop  $\beta$ 10- $\alpha$ 7). **a)** Backbone ribbon and side chain display of residues interacting with **XAP044**. Q258 (red) is a selective residue from loop  $\beta$ 10 $\alpha$ 7. S160 and 229 are framed in red. Only polar hydrogens of side chains are displayed. Interactions are shown as dashed lines: green for H-bonds, brown for salt bridges, mauve for hydrophobic interactions. Atom colors C gray, O red, N blue. **b)** Receptor solvent accessible surface displayed by interpolated charge surface, showing the position of **XAP044** at the hinge of the VFT.

With respect to option 2 orientation, the pose exhibiting the best score (using CHEMPLP scoring function)<sup>34</sup> is depicted in **Figure 13**. Molecular characteristics of this docking are in agreement with the SAR data: 1) H-bond with S160 and S229, 2) hydrophobic contacts with I163, A183, R191, Y192 in an out of plane conformation, 3) a negatively charged environment of the iodophenyl *para* substituent due to E 185 and D188, 4) a restricted environment around the iodophenyl, 5) mGlu7 selectivity because of K233 specific interaction. Yet, when running a 5 ns molecular dynamics simulations, the ligand was unable to remain bound to this site even with constraints. Consequently, this potential binding of **XAP044** was ruled out.



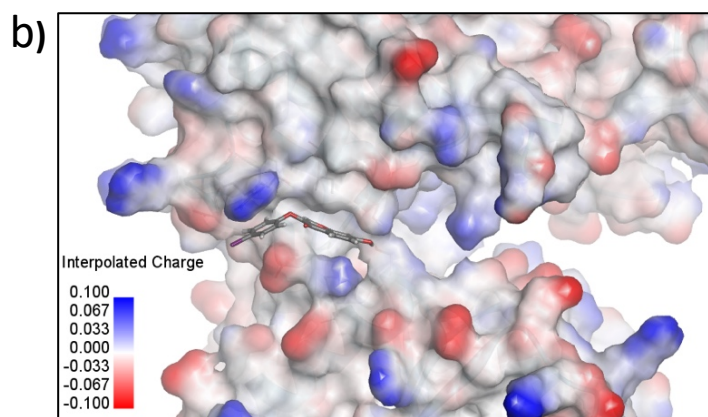


**Figure 13.** Docking of **XAP044** in option 2 (contact with segment  $\beta 7$  to  $\beta 8$ ). a) Backbone ribbon and side chain display around segment  $\beta 7$  to  $\beta 8$ . b) Receptor solvent accessible surface displayed by interpolated charge surface, showing the position of **XAP044** at the hinge of the VFT. Color code as in **Figures 9** and **12**.

Docking in the third orientation along the  $\alpha 6$  helix looked promising (**Figure 14**). As for option 2, molecular characteristics of this docking are in agreement with the SAR data: 1) H-bonds with S160 and S229, 2) hydrophobic contacts with A183, P184, K233 in an out of plane conformation, 3) halogen bonds<sup>35</sup> with S237, Q240, 4) a restricted environment around the iodophenyl, 5) mGlu7 selectivity because of K233 and S237 interactions. The complex remained stable in a 5 ns molecular dynamics simulation. We thus retained this binding mode of **XAP044** to mGlu7 receptor VFT domain. Next, we proceeded to the validation of this model.

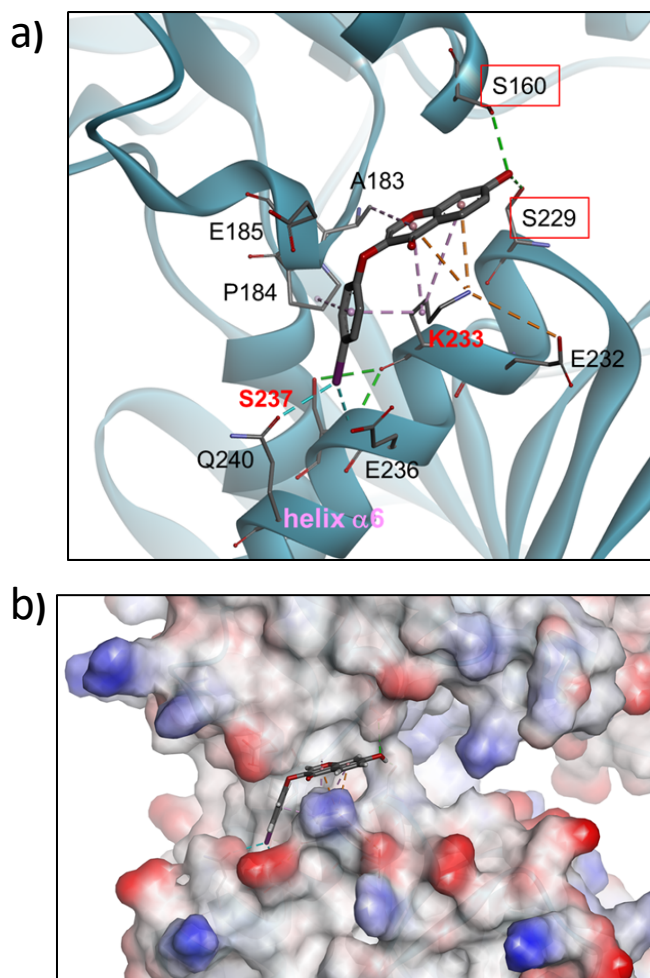


**Figure 14.** Docking of **XAP044** in option 3 (contact with  $\alpha 6$  helix). **a)** Backbone ribbon and side chain display along  $\alpha 6$  helix. **b)** Receptor solvent accessible surface displayed by interpolated charge surface, showing the position of **XAP044** at the hinge of the VFT operating as a wedge. Hydrogens are omitted for clarity. Color code as in **Figures 9** and **12**.

We first carried out virtual mutations of K233 into the 19 other amino acids to assess their effect on the binding energy. We found that K233A mutation is the first destabilizing mutation in the binding energy ranking followed by K233S, while K233D is the most destabilizing for a charged residue (**Table S6**).

*Validation of **XAP044** docking at mGlu7 receptor VFT*



Experimental validations were performed in HEK cells expressing mGlu7 receptor mutants. In functional assays (IP One readout), we measured how much the mutations affected the EC<sub>50</sub> of **LSP4-2022** in the presence of **XAP044**. K233 was mutated to Ala, Ser and Asp while S237 to Ala. Results are reported in **Table 5** and **Table S7**. The higher the ratio the lower the inhibition meaning an effective mutation. All three mutations of K233 reduced the inhibition by **XAP044** indicating a loss of interactions with this selective residue. On the other hand, mutation of S237, the other selective residue in the  $\alpha 6$  helix, resulted in no change probably because the loss of a weak interaction had a minor effect on the total binding energy.

**Table 5.** Effect of mGlu7 receptor mutations on the inhibitory effect of **XAP044** on **LSP4-2022** induced activity. Values are means  $\pm$  sem of pEC<sub>50</sub> of **LSP4-2022** alone, or in the presence of 100  $\mu$ M **XAP044**. Values are means of n independent experiments performed in triplicates. Statistical difference between the pEC<sub>50</sub> with and without **XAP044** was determined by paired T-test, \*\*\*  $p < 0.001$ ; \*\*  $p < 0.01$ ; *n.s.* not significant.

LSP4-2022 pEC <sub>50</sub>						
mGlu7	WT	S229A	K233A	K233S	K233D	S237A
control	4.67 $\pm$ 0.03	4.96 $\pm$ 0.10	4.06 $\pm$ 0.08	4.39 $\pm$ 0.10	3.83 $\pm$ 0.03	4.74 $\pm$ 0.15
+ XAP044	3.76 $\pm$ 0.06	4.99 $\pm$ 0.09	3.58 $\pm$ 0.06	4.25 $\pm$ 0.15	3.56 $\pm$ 0.04	3.70 $\pm$ 0.10
ratio	<b>0.83</b> $\pm$ 0.06	<b>1.02</b> $\pm$ 0.02	<b>0.88</b> $\pm$ 0.01	<b>0.93</b> $\pm$ 0.04	<b>0.93</b> $\pm$ 0.01	<b>0.78</b> $\pm$ 0.01
<i>n</i>	18	4	7	3	3	3
<i>paired T-test</i>	***	<i>n.s.</i>	***	<i>n.s.</i>	**	**

These results confirm the interaction of **XAP044** with S229 and K233 which supports its binding in orientation 3 along the  $\alpha 6$  helix (**Figure 14**).

#### *XAP044 derivatives 3, 4a, 4b binding to mGlu7 receptor VFT in an open conformation*

We have shown that **3, 4a, 4b**, the open analogs of **XAP044** act as competitive antagonists of **LSP4-2022** activation (**Figure 7**) similarly to **XAP044**. This led us to hypothesize that they adopt the same binding mode to mGlu7 receptor as described above (**Figure 14**). To validate this hypothesis, we

examined whether the interactions of **3** and **4a** with S229 would be reduced or abolished by the S229A mutation (**Table 6**). Comparison of the ratio of pEC<sub>50</sub> of **LSP4-2022** with and without antagonist in the WT and S229A mutant (**Table 6**) confirmed a similar binding for **XAP044** and the open analogs.

**Table 6.** Mutation S229A abolishes the antagonist effect of **XAP044**, **3**, **4a** on **LSP4-2022** activation of mGlu7 receptor. Comparison with WT. Values are means ± sem of n independent experiments performed in triplicates.

mGlu7 WT					mGlu7 S229A			
evaluated compounds	Conc. (μM)	EC <sub>50</sub> μM (n)	pEC <sub>50</sub>	pEC <sub>50</sub> 2022 + antago / pEC <sub>50</sub> 2022 in the same assay	Conc. (μM)	EC <sub>50</sub> μM (n)	pEC <sub>50</sub>	pEC <sub>50</sub> 2022 + antago / pEC <sub>50</sub> 2022 in the same assay
<sup>a</sup> <b>LSP4-2022</b>		20.3 ± 1.6 (6)	4.7	<b>1.0</b>		15.2 ± 1.79 (13)	4.86	<b>1.0</b>
<sup>a</sup> + <b>XAP044</b>	1	31.4 ± 2.7 (6)	4.5	<b>0.96</b>	-	-	-	-
<sup>a</sup> + <b>XAP044</b>	3	43.4 ± 6.9 (6)	4.4	<b>0.94</b>	-	-	-	-
<sup>a</sup> + <b>XAP044</b>	10	66.2 ± 10.8 (6)	4.3	<b>0.91</b>	10	25.0 ± 1.44 (3)	4.60	<b>0.96</b>
<sup>a</sup> + <b>XAP044</b>	30	138 ± 18.0 (6)	3.9	<b>0.83</b>	30	49.5 ± 9.74 (3)	4.32	<b>0.90</b>
<sup>a</sup> + <b>XAP044</b>					100	10.9 ± 2.36 (4)	4.99	<b>1.0</b>
<sup>a</sup> + <b>3</b>	3	38.3 ± 4.9 (3)	4.42	<b>0.91</b>				
<sup>a</sup> + <b>3</b>	10	76.9 ± 6.2 (3)	4.12	<b>0.85</b>	10	38.2 ± 1.98 (3)	4.42	<b>0.91</b>
<sup>a</sup> + <b>3</b>	30	146 ± 11.3 (5)	3.84	<b>0.79</b>	30	35.7 ± 8.89 (5)	4.53	<b>0.93</b>
					100	27.0 ± 7.78 (3)	4.60	<b>0.95</b>
<sup>a</sup> + <b>4a</b>	3	107 ± 26.5 (4)	4.01	<b>0.82</b>	3	6.88 (1)	5.16	<b>1</b>
<sup>a</sup> + <b>4a</b>	10	325 ± 75.3 (4)	3.53	<b>0.72</b>	10	9.91 (1)	5	<b>0.97</b>
<sup>a</sup> + <b>4a</b>	30	1190 ± 257 (4)	2.9	<b>0.59</b>	30	21.7 ± 3.83 (3)	4.68	<b>0.91</b>
					100	60.7 ± 18.3 (3)	4.25	<b>0.82</b>

<sup>a</sup> Concentration response curve of LSP4-2022

We thus docked **3** and **4a** (**Figure 15**) as described in orientation 3 above. As for **XAP044**, H-bonds with S160 and S229 secure the binding of the ligands as a wedge between the 2 lobes and hydrophobic contacts with A183, P184 and K233 anchor them along the α6 helix. We anticipate a similar binding mode for **4b**.

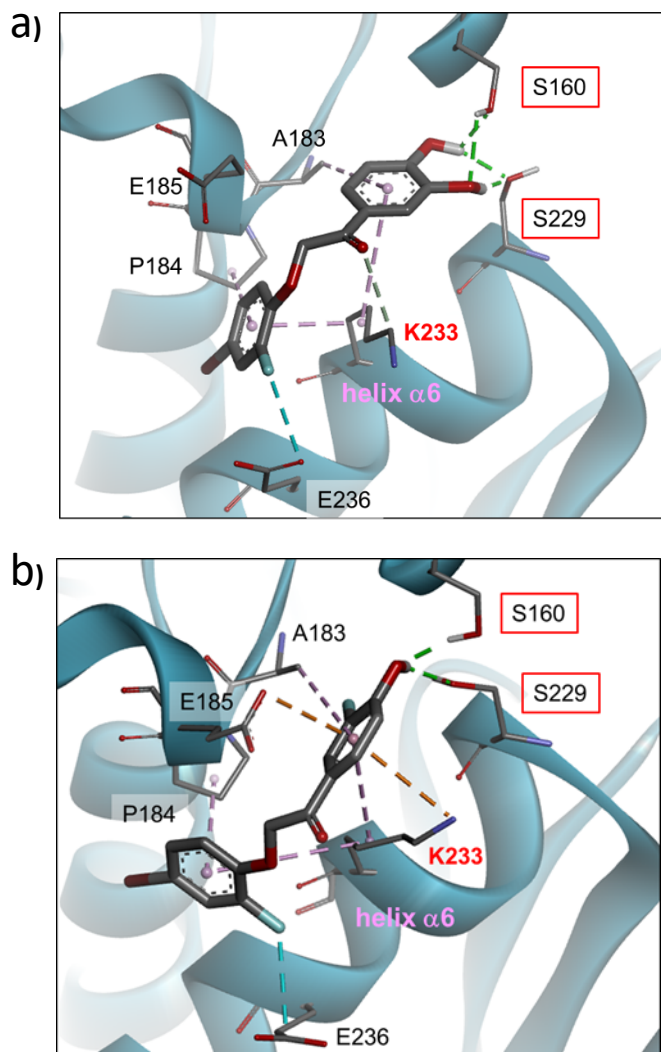
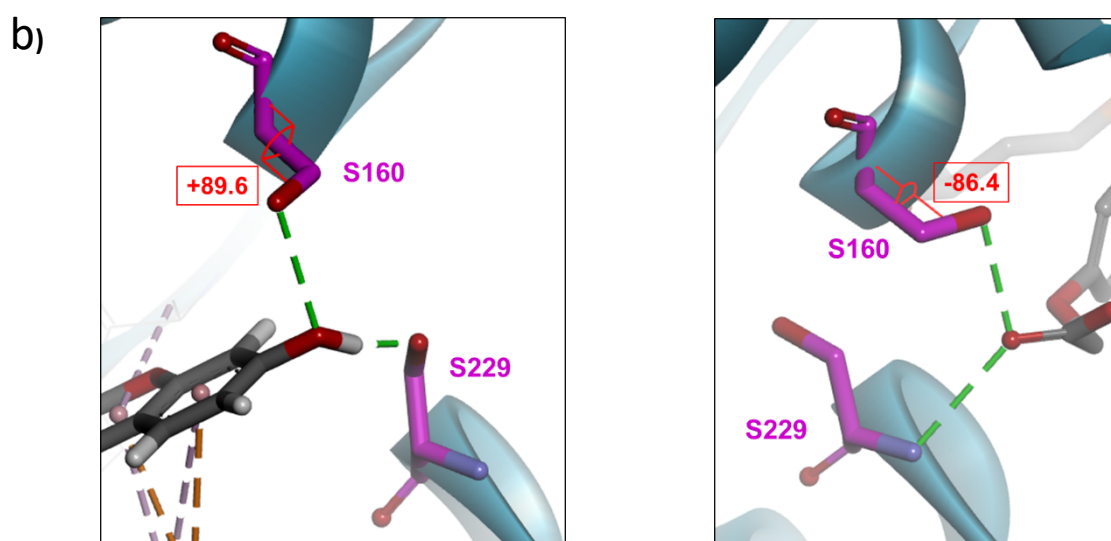
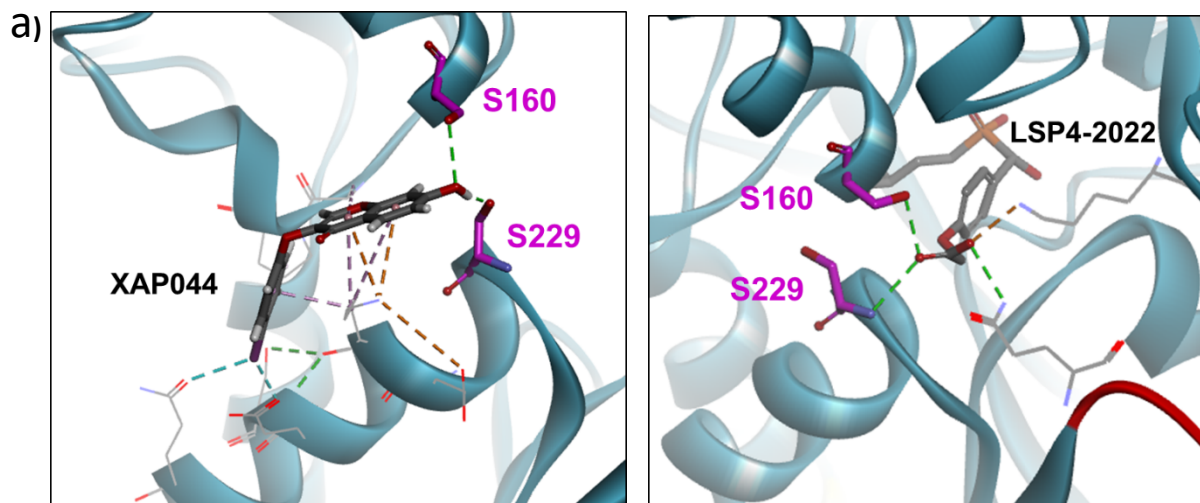


**Figure 15.** Docking of **3** (a) and **4a** (b) in a similar orientation as **XAP044** along  $\alpha 6$  helix. Protons are not displayed for clarity besides hydroxyl ones of ligands and side chains of S160 and S229. Color code as in **Figures 9** and **12**.

*Interpretation of the competition between LSP4-2022 and XAP044.*

A careful examination of the dockings of **LSP4-2022** and **XAP044** at the mGlu7 receptor VFT reveals that they both bind to S160 through an H-bond. In order to share its proton with the carboxylate of **LSP4-2022** or the phenol oxygen of **XAP044**, S160 side chain must adopt two different conformations (**Figure 16**). As a result, the two ligands cannot bind simultaneously to the receptor which may explain their apparent competitive behavior.



**XAP044** docked at mGlu7 receptor open VFT    **LSP4-2022** docked at mGlu7 receptor closed VFT

**Figure 16.** a) Binding of **XAP044** (in open VFT, left) and **LSP4-2022** (in closed VFT, right) to S160 (magenta) and S229 (magenta) of mGlu7 receptor. b) Expanded view of S160 and S229 side chains. The 2 torsion angles of S160 side chain [C (from backbone CO)-C $\alpha$ -C $\beta$ -O (from OH)] when bound to **XAP044** or **LSP4-2022** are displayed: +89.6° and -86.4° respectively. Hydrogen of S160 and S229 are not displayed for clarity. Color code as in **Figures 9** and **12**.

## DISCUSSION AND CONCLUSION

The discovery of mGlu7 homodimer ligands has been hampered by its difficult activation, despite its value as a therapeutic target in several CNS diseases.<sup>9,36</sup> Yet, screening campaigns have yielded some allosteric modulators,<sup>37</sup> including **XAP044** discovered by scientists at Novartis.<sup>17</sup> They showed that **XAP044** is an mGlu7 receptor antagonist with the particularity that it does not bind to the receptor transmembrane domain as most other mGluR modulators, but to the extracellular domain. However, its binding site and inhibitory mode of action have remained elusive. To address these questions, we initiated a SAR study followed by pharmacological investigations that would guide the molecular modeling.

Initially, we demonstrated that **XAP044** is not planar and adopts a bent conformation. Furthermore, its 3-phenoxy-chromone structure can be reduced to a phenoxyacetophenone. On the phenyl side, a *para*-hydroxyl group is mandatory. Substituents that increase its acidity (*e.g.* fluorine) or the H-bond capacity (*e.g.* additional OH), prove most favorable. On the phenoxy side, there should be a polarizable substituent in the *para*-position and one or two fluorines in *ortho*. This SAR study led to the identification of three derivatives **3**, **4a** and **4b** that are up to four fold more potent than **XAP044** for **4a** (Figure 2, Table 3).

Analyzing the type of mGlu7 receptor inhibition by **XAP044**, revealed it acts as a non-competitive inhibitor of **L-AP4** activation, as expected. Its binding at a different site as the strict glutamate binding site is supported by its inability to displace bound [<sup>3</sup>H]-**LY341405**. Surprisingly, its inhibition mode was found different against **LSP4-2022** action on mGlu7. Although the data were not sufficient to firmly conclude on a direct competition due to the limitation of the highest compound concentration that could be used, still the inhibition mode resemble a competitive inhibition. Such a proposal is further supported by the analysis of the mode of action of the more potent and more soluble **XAP044** derivatives. Since we have proposed how the two agonists are binding to the mGlu7 receptor VFT domain (Figures S2 and 9), these findings were crucial for **XAP044** docking at this domain. Indeed, they showed that **XAP044** cannot bind at the glutamate site but does interact at a

site overlapping that occupied by the distal part of **LSP4-2022**, a site occupied neither by glutamate, **L-AP4** nor **LY341495**.

The distal part of **LSP4-2022** interacts at a site close to the flexible hinge of the VFT, so we hypothesized that **XAP044** and its derivatives may block the closing of the VFT by acting as a wedge between the two lobes at this hinge site. Residues S160 (lobe 1) and S229 (lobe 2) from each lobe, become the closest upon VFT closure leading to mGlu7 receptor activation. Knowing that **XAP044** is mGlu7 selective, we identified three possible binding orientation around S229 (**Figure 11**). The first orientation towards loop  $\beta_{10}$ - $\alpha_7$  was invalidated by mutagenesis/functional assays whereas the second to loop  $\beta_7$ - $\alpha_8$  was ruled out by molecular dynamics. The third orientation was validated by MD's and mutations of critical residues (**Figure 14** and **Table 5**). In this binding mode, **XAP044** lines  $\alpha_6$  helix in a bent conformation and subtype selectivity is attributed to K233 interaction. The free phenol interacts with S160 and S229 through H-bonds (**Figure 14**, **16** and **17**). This network prevents the full closure of the VFT that brings closer the two serines as observed upon agonist binding (**Figure 17**). Interestingly **XAP044** and **LSP4-2022** share the binding to the same side chain of S160 but this cannot not be concomitant (**Figure 17**). Thus, this situation explains the possibility for **XAP044** and its derivatives to compete with **LSP4-2022**, preventing its agonist action.

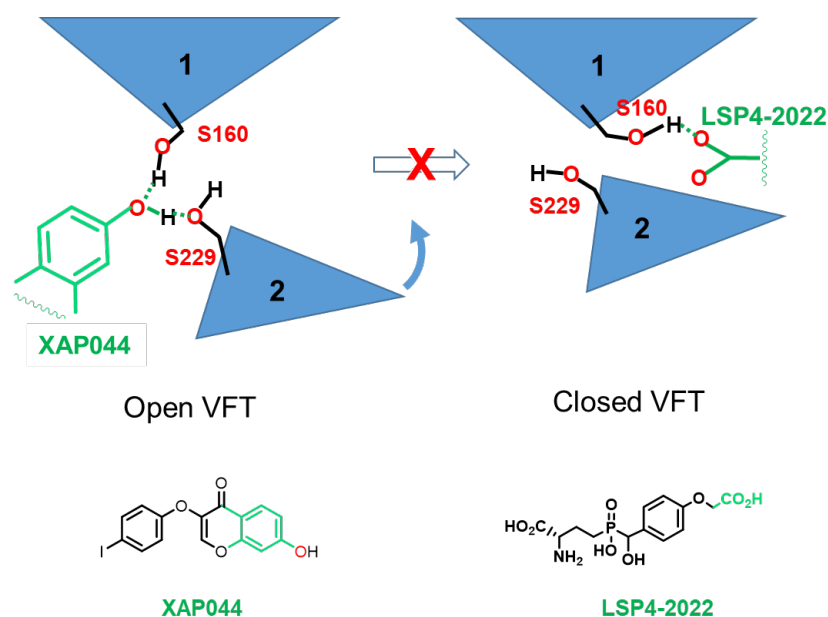


**Figure 17.** Cartoon of the proposed blocking of the mGlu7 receptor VFT closing by **XAP044** and analogs. The two lobes are represented as blue triangles, 1 upper N-ter lobe, 2 lower lobe.

In the present study, we describe a series of **XAP044** analogs with increased potency as mGlu7 receptor inhibitors for some of them. Additionally, we elucidated **XAP044** binding mode to the VFT domain and explained its blocking mechanism.

## EXPERIMENTAL SECTION

### Chemistry

#### *General.*

All chemicals and solvents were purchased from commercial suppliers (Sigma, Alpha Aesar, Acros, FluoroChem....) and used as received. Anhydrous solvents were purchased from Sigma. Dry tetrahydrofuran (THF) and dichloromethane ( $\text{CH}_2\text{Cl}_2$ ) were obtained by distillation. All reactions were carried out under argon atmosphere with anhydrous solvent and were monitored by thinlayer chromatography (TLC) with silica gel Merck 60 F254, on aluminium sheets. Manual flash column chromatography was performed with VWR silica gel 60 (40–63  $\mu\text{m}$ ). Automated flash chromatography was performed with an Isolera One Biotage apparatus with detectors at 254 nm and 280 nm, using Büchi FlashPure silica. Solvent systems were given according to (s/s: v/v).  $^1\text{H}$  (500.16 MHz),  $^{13}\text{C}$  (125.78 MHz), and  $^{19}\text{F}$  (470.57 MHz) NMR spectra were recorded on an Avance II 500 Bruker spectrometer. Chemical shifts ( $\delta$ , ppm) are given with reference to deuterated solvents for  $^1\text{H}$  and  $^{13}\text{C}$  NMR respectively,  $\text{CDCl}_3$ : 7.24, 77.23;  $\text{DMSO}-d_6$ : 2.50, 39.51. Signal multiplicity is described as follows: s (singlet), d (doublet), t (triplet), q (quartet), m (multiplet). Broad signals are described as br. Coupling constants ( $J$ ) are given in Hz.

Molecule numbering is only related to atom assignment, which was established on the basis of  $^{13}\text{C}$  using  $^1\text{H}$  decoupled spectra as well as COSY, HSQC and HMBC.

IR spectra were obtained with a Perkin-Elmer Spectrum One FT-IR spectrometer equipped with a MIRacleTM single reflection horizontal ATR unit (zirconium-selenium crystal). Mass spectra (MS) were recorded with a LCQadvantage (ThermoFinnigan) mass spectrometer with positive ( $\text{ESI}^+$ ) or negative ( $\text{ESI}^-$ ) electrospray ionization (ionization tension 4.5 kV, injection temperature 240 °C).

HPLC-MS analyses were performed on a Thermo Finnigan LCQ Advantage Instrument as described above, equipped for HPLC with a Phenomenex RP Polar column (50 mm x 2.1 mm, 2.6  $\mu\text{m}$ ). Products were eluted with the following gradient using solvent A ( $\text{H}_2\text{O}/\text{HCO}_2\text{H}$ : 100/0.1), solvent B



(MeCN/HCO<sub>2</sub>H: 100/0.1): 100% A linear increase from 0 to 100% B for 20 min, 100% B from 20 to 30 min, 100% B linear increase from 0 to 100% A from 30 to 40 min. The purity of the tested compounds was established by analytical HPLC-MS and was at least 95%.

#### *General procedures*

**General procedure A:** Salicylate or thiosalicylate (1 eq),  $\alpha$ -haloacetophenone (1 eq) and Cs<sub>2</sub>CO<sub>3</sub> (1.7 eq) in DMF (0.06 M) were heated at 90 °C for 1.5 h. The reaction mixture was poured into water and extracted with CH<sub>2</sub>Cl<sub>2</sub> (3x), washed with brine (2x), dried over MgSO<sub>4</sub>, filtered, and evaporated *in vacuo* to obtain the crude product that was triturated with MeOH to yield the desired product.

**General procedure B:** 11*H*-Benzofuro[3,2-*b*]chromen-11-one derivative (1 eq) and 1 M BBr<sub>3</sub> in CH<sub>2</sub>Cl<sub>2</sub> (0.06 M) was stirred at –80 °C then at room temperature overnight. The reaction mixture was evaporated under *vacuo* and the resulted solid washed with saturated NaHCO<sub>3</sub> solution (2x). The crude residue was purified by trituration or by column chromatography on silica gel to yield the desired product.

**General procedure C:** The phenol derivative (1 eq) and K<sub>2</sub>CO<sub>3</sub> (1.1 eq) were stirred at room temperature in acetone (0.16 M) for 1 h. Then 2-bromo-1-(4-methoxyphenyl)ethan-1-one (1 eq) or compound **6** (1 eq) or **9** (1 eq) was added to the mixture and stirred overnight. The suspension was then filtered and the filtrate evaporated *in vacuo*. The solid was dissolved in EtOAc, washed with 5% aqueous NaOH (2x) then water (2x). The organic phase was dried over Na<sub>2</sub>SO<sub>4</sub>, filtered, and evaporated *in vacuo*. The crude product was purified by recrystallization or by column chromatography on silica gel to yield the desired products.

**General procedure D:** To a solution of sodium methylate (1.46 eq) in anhydrous THF (0.17 M) was added the phenol derivative (1 eq) and the mixture was stirred at room temperature 6 h. 2-Bromo-1-(4-hydroxyphenyl)ethan-1-one (1 eq) was then added to the mixture and stirred overnight. The crude residue was purified by column chromatography on silica gel (Cyclohexane/EtOAc, 7:3) to yield the desired product.

**General procedure E:** Bromohydroxyphenylethanone (1 eq) in acetic anhydride and concentrated HCl were stirred at 60 °C for 2 h then at room temperature overnight. To the resulting mixture was added water at 0 °C and extracted with EtOAc (3x). The organic phases were washed with water and brine (2x), dried over MgSO<sub>4</sub> and concentrated *in vacuo*. The crude residue was purified to yield the desired product.

**General procedure F:** The phenoxyacetylphenyl acetate derivative (1 eq) in EtOH and NaOAc (10 eq) in water was stirred at reflux overnight. The resulting mixture was extracted with EtOAc (3x). The organic phase was washed with water and brine (2x), dried over MgSO<sub>4</sub> and concentrated *in vacuo*. The crude residue was purified by column chromatography on silica gel to yield the desired product.

**General procedure G:** To a solution of fluorophenol (1 eq) in CS<sub>2</sub> was added portion wise AlCl<sub>3</sub> (6 eq) and the reaction was stirred at room temperature for 10 min. Then 2-bromoacetyl bromide (1.3 eq) was added and the reaction mixture heated at reflux overnight. The reaction mixture was filtered, and extracted with EtOAc (3x), washed with 1 M aqueous HCl and brine (2x). Then dried with Na<sub>2</sub>SO<sub>4</sub>, filtered and evaporated *in vacuo*. The crude residue was purified to obtain the desired product.

**11H-Benzo[4,5]thieno[3,2-b]chromen-11-one (1a):** The general procedure A was followed using methyl thiosalicylate (0.24 mL, 1.72 mmol), 2-bromo-2'-fluoroacetophenone (0.24 mL, 1.72 mmol), Cs<sub>2</sub>CO<sub>3</sub> (0.955 g, 2.92 mmol) and DMF (30 mL) to get **1a** as a pink solid (0.205 g, 0.812 mmol) in 47% yield. R<sub>f</sub> = 0.80 (Cyclohexane/EtOAc : 7/3); <sup>1</sup>H NMR (500 MHz, CDCl<sub>3</sub>) δ: 8.32 (d, J<sub>H-1,H-2</sub> = 7.5 Hz, 1H, H-1), 8.08 (d, J<sub>H-8,H-9</sub> = 8.0 Hz, 1H, H-8), 7.83 (d, J<sub>H-11,H-10</sub> = 8.0 Hz, 1H, H-11), 7.69 (t, J<sub>H-3,H-2</sub> = J<sub>H-3,H-4</sub> = 7.5 Hz, 1H, H-3), 7.59 (d, J<sub>H-4,H-3</sub> = 8.5 Hz, 1H, H-4), 7.51 (t, J<sub>H-10,H-9</sub> = J<sub>H-10,H-11</sub> = 7.5 Hz, 1H, H-10), 7.45 (t, J<sub>H-9,H-8</sub> = J<sub>H-9,H-10</sub> = 7.5 Hz, 1H, H-9), 7.41 (t, J<sub>H-2,H-1</sub> = J<sub>H-2,H-3</sub> = 7.5 Hz, 1H, H-2); <sup>13</sup>C NMR (126 MHz, CDCl<sub>3</sub>) δ: 173.4 (C-14), 156.2 (C-5), 153.9 (C-6), 140.2 (C-12), 133.9 (C-3), 129.5 (C-7), 129.4 (C-10), 126.2 (C-1), 125.3, 125.1 (C-2, C-9), 123.9 (C-11), 122.9 (C-15), 122.6 (C-8), 121.0 (C-13), 118.2 (C-4); IR ν<sub>max</sub>/cm<sup>-1</sup>: 1638, 1618, 1606, 1560, 1526, 1481, 1459, 1415, 1334, 1311, 1246, 1217, 1178, 1135, 1098, 1064, 1018, 937, 876, 788, 745, 731, 688, 642; MS (ESI<sup>-</sup>) m/z: 251.03 [M - H]<sup>-</sup>; HRMS (ESI<sup>+</sup>) m/z: calcd for

[C<sub>15</sub>H<sub>8</sub>O<sub>2</sub>S + H]<sup>+</sup>: 253.0323, found 253.0312; HPLC-MS (ESI) m/z; (λ = 235 nm): Rt = 13.46 min;  
253.0312 [M + H]<sup>+</sup>.

**8-Methoxy-11H-benzofuro[3,2-b]chromen-11-one (1b)**: The general procedure A was followed using methyl 2-hydroxy-4-methoxybenzoate (0.313 g, 1.72 mmol), 2-bromo-2'-fluoroacetophenone (0.24 mL, 1.72 mmol), Cs<sub>2</sub>CO<sub>3</sub> (0.955 g, 2.92 mmol) and DMF (30 mL) to get **1b** as a white solid (0.050 g, 0.187 mmol) in 11% yield. R<sub>f</sub> = 0.65 (Cyclohexane/EtOAc, 7:3); <sup>1</sup>H NMR (500 MHz, CDCl<sub>3</sub>) δ: 8.42 (dd, J<sub>H-1,H-2</sub> = 8.0 Hz, J<sub>H-1,H-3</sub> = 1.5 Hz, 1H, H-1), 7.78 (d, J<sub>H-8,H-9</sub> = 9.0 Hz, 1H, H-8), 7.68 (dt, J<sub>H-3,H-2</sub> = J<sub>H-3,H-4</sub> = 8.5 Hz, J<sub>H-3,H-1</sub> = 1.5 Hz, 1H, H-3), 7.62 (d, J<sub>H-4,H-3</sub> = 8.5 Hz, 1H, H-4), 7.44 (t, J<sub>H-2,H-1</sub> = J<sub>H-2,H-3</sub> = 7.5 Hz, 1H, H-2), 7.06 (d, J<sub>H-11,H-9</sub> = 2.0 Hz, 1H, H-11), 7.01 (dd, J<sub>H-9,H-8</sub> = 8.5 Hz, J<sub>H-9,H-11</sub> = 2.0 Hz, 1H, H-9), 3.89 (s, 3H, OCH<sub>3</sub>); <sup>13</sup>C NMR (126 MHz, CDCl<sub>3</sub>) δ: 166.5 (C-14), 162.9 (C-10), 157.2 (C-12), 155.8 (C-5), 149.7 (C-q), 137.1 (C-q), 133.2 (C-3), 126.7 (C-1), 125.3 (C-q), 125.0 (C-2), 121.2 (C-8), 118.3 (C-4), 114.8 (C-9), 111.2 (C-7), 96.6 (C-11), 56.1 (OCH<sub>3</sub>); IR ν<sub>max</sub>/cm<sup>-1</sup>: 1663, 1620, 1471, 1449, 1433, 1417, 1337, 1278, 1233, 1193, 1165, 1148, 1106, 1016, 982, 946, 900, 833, 813, 787, 759, 696, 668, 654, 636; MS (ESI<sup>+</sup>) m/z: 267.06 [M + H]<sup>+</sup>; HRMS (ESI<sup>+</sup>) m/z: calcd for [C<sub>16</sub>H<sub>10</sub>O<sub>4</sub> + H]<sup>+</sup>: 267.0657, found 267.0648; HPLC-MS (ESI) m/z; (λ = 235 nm): Rt = 12.55 min; 267.0647 [M + H]<sup>+</sup>.

**7-Chloro-11H-benzofuro[3,2-b]chromen-11-one (1c)**: The general procedure A was followed using methyl-5-chloro-2-hydroxybenzoate (0.321 g, 1.72 mmol), 2-bromo-2'-fluoroacetophenone (0.24 mL, 1.72 mmol), Cs<sub>2</sub>CO<sub>3</sub> (0.955 g, 2.93 mmol) and DMF (30 mL) to get **1c** as an orange solid (0.297 g, 1.097 mmol) in 64% yield. R<sub>f</sub> = 0.86 (Cyclohexane/EtOAc, 7:3); <sup>1</sup>H NMR (500 MHz, CDCl<sub>3</sub>) δ: 8.45 (d, J<sub>H-1,H-2</sub> = 8.0 Hz, 1H, H-1), 7.96 (s, 1H, H-8), 7.75 (t, J<sub>H-3,H-2</sub> = J<sub>H-3,H-4</sub> = 8.0 Hz, 1H, H-3), 7.67 (d, J<sub>H-4,H-3</sub> = 8.0 Hz, 1H, H-4), 7.62 (d, J<sub>H-11,H-10</sub> = 8.5 Hz, 1H, H-11), 7.56 (d, J<sub>H-10,H-11</sub> = 8.5 Hz, 1H, H-10), 7.49 (t, J<sub>H-2,H-1</sub> = 7.5 Hz, 1H, H-2); <sup>13</sup>C NMR (126 MHz, CDCl<sub>3</sub>) δ: 167.5 (C-14), 156.1 (C-5), 153.5 (C-12), 148.2 (C-q), 138.6 (C-13), 134.0 (C-3), 131.0 (C-10), 130.3 (C-9), 126.9 (C-1), 125.3 (C-2), 120.3 (C-8), 119.5 (C-q), 118.6 (C-4), 114.9 (C-11); IR ν<sub>max</sub>/cm<sup>-1</sup>: 1671, 1609, 1489, 1466, 1420, 1318, 1279, 1197, 1117, 1057, 996, 930, 857, 813, 754, 714, 698, 671, 639, 629, 617; MS (ESI<sup>+</sup>) m/z: 271.01 [M + H]<sup>+</sup>; HRMS (ESI<sup>+</sup>)

m/z: calcd for  $[C_{15}H_7ClO_3 + H]^+$ : 271.0162, found 271.0162; HPLC-MS (ESI) m/z; ( $\lambda = 235$  nm): Rt = 13.59 min; 271.0162  $[M + H]^+$ .

**7-Bromo-11H-benzofuro[3,2-b]chromen-11-one (1d):** The general procedure A was followed using methyl-5-bromo-2-hydroxybenzoate (0.397 g, 1.72 mmol), 2-bromo-2'-fluoroacetophenone (0.24 mL, 1.72 mmol),  $Cs_2CO_3$  (0.955 g, 2.93 mmol) and DMF (30 mL) to get **1d** as a light orange solid (0.170 g, 0.539 mmol) in 31% yield. Rf = 0.58 (Cyclohexane/EtOAc, 7:3);  $^1H$  NMR (500 MHz,  $CDCl_3$ )  $\delta$ : 8.45 (d,  $J_{H-1,H-2} = 8.0$  Hz, 1H, H-1), 8.12 (d,  $J_{H-8,H-10} = 1.5$  Hz 1H, H-8), 7.75 (t,  $J_{H-3,H-2} = J_{H-3,H-4} = 7.5$  Hz, 1H, H-3), 7.70 (dd,  $J_{H-10,H-11} = 9.0$  Hz,  $J_{H-10,H-8} = 1.5$  Hz, 1H, H-10), 7.67 (d,  $J_{H-4,H-3} = 8.0$  Hz, 1H, H-4), 7.56 (d,  $J_{H-11,H-10} = 9.0$  Hz, 1H, H-11), 7.49 (t,  $J_{H-2,H-1} = 7.5$  Hz, 1H, H-2);  $^{13}C$  NMR (126 MHz,  $CDCl_3$ )  $\delta$ : 167.5 (C-14), 156.1 (C-5), 153.9 (C-12), 147.9 (C-q), 138.4 (C-13), 134.0 (C-3), 133.6 (C-10), 126.9 (C-1), 125.3 (C-2), 123.4 (C-8), 120.1 (C-9), 118.6 (C-4), 117.5 (C-7), 115.3 (C-11); IR  $\nu_{max}/cm^{-1}$ : 1674, 1605, 1485, 1458, 1318, 1274, 1193, 1119, 991, 926, 860, 827, 759, 694, 666, 637; HRMS (ESI $^+$ ) m/z: calcd for  $[C_{15}H_7BrO_3 + H]^+$ : 314.9657, found 314.9660; HPLC-MS (ESI) m/z; ( $\lambda = 235$  nm): Rt = 13.91 min; 314.9660  $[M + H]^+$ .

**7-Iodo-3-methoxy-11H-benzofuro[3,2-b]chromen-11-one (1e):** The general procedure A was followed using methyl-5-iodosalicylate (0.478 g, 1.72 mmol), 2-fluoro-4-methoxyphenacylbromide (0.425 g, 1.72 mmol),  $Cs_2CO_3$  (0.955 g, 2.93 mmol) and DMF (25 mL) to get **1e** as a yellow solid (0.355 g, 0.905 mmol) in 53% yield. Rf = 0.90 (Cyclohexane/EtOAc, 7:3);  $^1H$  NMR (500 MHz,  $CDCl_3$ )  $\delta$ : 8.33 (d,  $J_{H-1,H-2} = 8.0$  Hz, 1H, H-1), 8.28 (d,  $J_{H-8,H-10} = 2.0$  Hz, 1H, H-8), 7.85 (dd,  $J_{H-10,H-11} = 8.5$  Hz,  $J_{H-10,H-8} = 2.0$  Hz, 1H, H-10), 7.44 (d,  $J_{H-11,H-10} = 8.5$  Hz, 1H, H-11), 7.05 (brs, 1H, H-4), 7.04 (dd,  $J_{H-2,H-1} = 8.0$  Hz,  $J_{H-2,H-4} = 2.5$  Hz, 1H, H-2), 3.95 (s, 3H,  $CH_3$ );  $^{13}C$  NMR (126 MHz,  $CDCl_3$ )  $\delta$ : 167.2 (C-14), 164.4 (C-3), 157.9 (C-q), 154.3 (C-q), 147.1 (C-q), 138.8 (C-10), 138.1 (C-q), 129.3 (C-8), 128.1 (C-1), 120.8 (C-q), 119.1 (C-q), 115.6 (C-11), 114.3 (C-2), 101.2 (C-4), 87.4 (C-9), 56.2 (C-16); IR  $\nu_{max}/cm^{-1}$ : 1640, 1625, 1607, 1477, 1432, 1311, 1262, 1246, 1199, 1173, 1120, 1105, 1032, 991, 955, 919, 857, 839, 825, 766, 749, 693, 659, 651, 637, 630; HRMS (ESI $^+$ ) m/z: calcd for  $[C_{16}H_9IO_4 + H]^+$ : 392.9624, found 392.9609; HPLC-MS (ESI) m/z; ( $\lambda = 235$  nm): Rt = 14.54 min; 392.9609  $[M + H]^+$ .

**Fluoro-7-iodo-11H-benzofuro[3,2-b]chromen-11-one (1f):** The general procedure A was followed using methyl-5-iodosalicylate (0.478 g, 1.72 mmol), 2-chloro-2',4'-difluoroacetophenone (0.328 g, 1.72 mmol, 0.25 mL), Cs<sub>2</sub>CO<sub>3</sub> (0.955 g, 2.93 mmol) and DMF (25 mL) to get **1f** as an orange solid (0.221 g, 0.581 mmol) in 66% yield. R<sub>f</sub> = 0.91 (Cyclohexane/EtOAc, 7:3); <sup>1</sup>H NMR (500 MHz, CDCl<sub>3</sub>) δ: 8.46 (dd, *J*<sub>H-1,H-2</sub> = 8.5 Hz, *J*<sub>H-1,F</sub> = 6.0 Hz, 1H, H-1), 8.31 (d, *J*<sub>H-8,H-10</sub> = 2.0 Hz, 1H, H-8), 7.88 (dd, *J*<sub>H-10,H-11</sub> = 8.5 Hz, *J*<sub>H-10,H-8</sub> = 2.0 Hz, 1H, H-10), 7.45 (d, *J*<sub>H-11,H-10</sub> = 8.5 Hz, 1H, H-11), 7.35 (dd, *J*<sub>H-4,F</sub> = 8.5 Hz *J*<sub>H-4,H-2</sub> = 2.5 Hz, 1H, H-4), 7.22 (ddd, *J*<sub>H-2,F</sub> = 10.0 Hz, *J*<sub>H-2,H-1</sub> = 8.5 Hz, *J*<sub>H-2,H-4</sub> = 2.5 Hz, 1H, H-2); <sup>13</sup>C NMR (126 MHz, CDCl<sub>3</sub>) δ: 166.6 (C-14), 165.8 (d, *J*<sub>C-3,F</sub> = 256.4 Hz, C-3), 157.0 (d, *J*<sub>C-5,F</sub> = 13.6 Hz, C-5), 154.5 (C-12), 147.8 (C-q), 139.3 (C-10), 137.9 (C-13), 129.5 (C-8), 129.2 (d, *J* = 11.0 Hz, C-1), 122.2 (C-q), 120.5 (C-q), 115.6 (C-11), 114.2 (d, *J*<sub>C-2,F</sub> = 21.8 Hz, C-2), 105.4 (d, *J*<sub>C-4,F</sub> = 26.3 Hz, C-4), 87.7 (C-9); <sup>19</sup>F NMR (470 MHz, DMSO-*d*<sub>6</sub>) δ: -103.3 (dd, *J* = 15.5 Hz, *J* = 8.5 Hz); <sup>19</sup>F<sub>cpd</sub> NMR (470 MHz, DMSO-*d*<sub>6</sub>) δ: -103.3; IR ν<sub>max</sub>/cm<sup>-1</sup>: 1681, 1615, 1601, 1472, 1437, 1311, 1240, 1208, 1192, 1170, 1139, 1100, 991, 964, 852, 827, 763, 698, 658, 635, 618; HRMS (ESI<sup>+</sup>) *m/z*: calcd for [C<sub>15</sub>H<sub>6</sub>FIO<sub>3</sub> + H]<sup>+</sup>: 380.9424, found 380.9415; HPLC-MS (ESI) *m/z*; (λ = 235 nm): R<sub>t</sub> = 14.68 min; 380.9414 [M + H]<sup>+</sup>.

**8-Iodo-3-methoxy-5a,10a-dihydro-11H-benzofuro[3,2-b]chromen-11-one (1g):** The general procedure A was followed using methyl-2-hydroxy-4-iodobenzoate (0.400 g, 1.44 mmol), 2-bromo-2'-fluoro-4'-methoxyacetophenone (0.355 g, 1.44 mmol), Cs<sub>2</sub>CO<sub>3</sub> (0.769 g, 2.44 mmol) and DMF (30 mL) to get **1g** as a pink solid (0.226 g, 0.576 mmol) in 40% yield. R<sub>f</sub> = 0.54 (Cyclohexane/EtOAc, 7:3); <sup>1</sup>H NMR (500 MHz, CDCl<sub>3</sub>) δ: 8.34 (d, *J*<sub>H-1,H-2</sub> = 8.5 Hz, 1H, H-1), 8.05 (brd, *J*<sub>H-11,H-9</sub> = 1.5 Hz, 1H, H-11), 7.75 (dd, *J*<sub>H-9,H-8</sub> = 8.5 Hz, *J*<sub>H-9,H-11</sub> = 1.5 Hz, 1H, H-9), 7.66 (d, *J*<sub>H-8,H-9</sub> = 8.5 Hz, 1H, H-8), 7.06 (d, *J*<sub>H-4,H-2</sub> = 2.0 Hz, 1H, H-4), 7.04 (dd, *J*<sub>H-2,H-1</sub> = 8.5 Hz, *J*<sub>H-2,H-4</sub> = 2.0 Hz, 1H, H-2), 3.94 (s, 3H, OCH<sub>3</sub>); <sup>13</sup>C NMR (126 MHz, CDCl<sub>3</sub>) δ: 167.1 (C-14), 164.4 (C-q), 157.9 (C-q), 155.0 (C-q), 148.3 (C-q), 137.6 (C-13), 133.7 (C-9), 128.0 (C-1), 123.0 (C-11), 121.6 (C-8), 119.1 (C-q), 118.0 (C-q), 114.2 (C-2), 101.2 (C-4), 95.0 (C-10), 56.2 (C-16); IR ν<sub>max</sub>/cm<sup>-1</sup>: 1654, 1612, 1480, 1452, 1390, 1349, 1302, 1247, 1211, 1192, 1174, 1119, 1104, 980, 953, 916, 870, 847, 806, 765, 744; HRMS (ESI<sup>+</sup>) *m/z*: calcd for [C<sub>16</sub>H<sub>9</sub>IO<sub>4</sub> + H]<sup>+</sup>: 392.9624, found 392.9609; HPLC-MS (ESI) *m/z*; (λ = 235 nm): R<sub>t</sub> = 14.40 min; 392.9613 [M + H]<sup>+</sup>.

**8-Hydroxy-11H-benzofuro[3,2-b]chromen-11-one (1h):** 8-Methoxy-11H-benzofuro[3,2-b]chromen-11-one **1b** (0.300 g, 1.13 mmol, 1 eq), AlCl<sub>3</sub> (0.602 g, 4.52 mmol, 4 eq) and NaI (0.677 g, 4.52 mmol, 4 eq) were heated at 80 °C for 4 h. Then 1 M BBr<sub>3</sub> in CH<sub>2</sub>Cl<sub>2</sub> (0.26 mL, 2.26 mmol, 2 eq) was added to a temperature of 30 °C for 1 h and left at room temperature overnight. The reaction mixture was diluted with 5% aqueous solution of Na<sub>2</sub>S<sub>2</sub>O<sub>3</sub> (50 mL) and extracted with CH<sub>2</sub>Cl<sub>2</sub> (3×30 mL). Then dried over MgSO<sub>4</sub>, filtered and evaporated *in vacuo* to obtain the crude product (0.152 g). The crude residue was purified by column chromatography on silica gel (CH<sub>2</sub>Cl<sub>2</sub>/MeOH, 9:1) to recover **1h** as a white solid (0.057 g, 0.225 mmol) in 20% yield. R<sub>f</sub> = 0.25 (Cyclohexane/EtOAc, 7:3); <sup>1</sup>H NMR (500 MHz, DMSO-*d*<sub>6</sub>) δ: 10.69 (s, 1H, OH), 8.27 (d, *J*<sub>H-1,H-2</sub> = 8.0 Hz, 1H, H-1), 7.90 (d, *J*<sub>H-8,H-9</sub> = 8.0 Hz, 1H, H-8), 7.87–7.84 (m, 2H, H-3, H-4), 7.57 (m, 1H, H-2), 7.13 (s, 1H, H-11), 7.03 (d, *J*<sub>H-9,H-8</sub> = 8.0 Hz, 1H, H-9); <sup>13</sup>C NMR (126 MHz, DMSO-*d*<sub>6</sub>) δ: 164.8 (C-14), 161.3 (C-q), 156.5 (C-q), 155.0 (C-q), 149.4 (C-q), 135.7 (C-q), 133.5 (C-3), 125.5 (C-1), 125.1 (C-2), 124.6 (C-q), 121.4 (C-8), 118.4 (C-4), 115.0 (C-9), 109.0 (C-q), 98.6 (C-11); IR *v*<sub>max</sub>/cm<sup>-1</sup>: 3200, 1642, 1611, 1577, 1557, 1519, 1473, 1434, 1354, 1332, 1279, 1242, 1221, 1192, 1168, 1156, 1108, 992, 955, 907, 864, 838, 809, 786, 749, 698, 684, 668, 648, 626, 607; HRMS (ESI<sup>-</sup>) *m/z*: calcd for [C<sub>15</sub>H<sub>8</sub>O<sub>4</sub> – H]<sup>-</sup>: 251.0344, found 251.0340; HPLC-MS (ESI) *m/z*; (λ = 235 nm): R<sub>t</sub> = 10.66 min; 251.0339 [M – H]<sup>-</sup>.

**3-Hydroxy-7-iodo-11H-benzofuro[3,2-b]chromen-11-one (1i):** The general procedure B was followed using 7-iodo-3-methoxy-11H-benzofuro[3,2-b]chromen-11-one **1e** (0.390 g, 0.995 mmol, 1 eq), 1 M BBr<sub>3</sub> in CH<sub>2</sub>Cl<sub>2</sub> (16 mL, 91.8 mmol, 94 eq). Finally, acetone was used to solubilize some impurities to give **1i** as a white solid (0.160 g, 0.449 mmol) in 41% yield. R<sub>f</sub> = 0.45 (Cyclohexane/EtOAc 7:3); <sup>1</sup>H NMR (500 MHz, DMSO-*d*<sub>6</sub>) δ: 11.02 (s, 1H, OH), 8.41 (d, *J*<sub>H-8,H-10</sub> = 1.5 Hz, 1H, H-8), 8.09 (d, *J*<sub>H-1,H-2</sub> = 9.0 Hz, 1H, H-1), 7.97 (dd, *J*<sub>H-10,H-11</sub> = 9.0 Hz, *J*<sub>H-10,H-8</sub> = 1.5 Hz 1H, H-10), 7.70 (d, *J*<sub>H-11,H-10</sub> = 7.5 Hz, 1H, H-11), 7.05 (d, *J*<sub>H-4,H-2</sub> = 2.0 Hz 1H, H-4), 7.00 (dd, *J*<sub>H-2,H-1</sub> = 9.0 Hz, *J*<sub>H-2,H-4</sub> = 2.0 Hz 1H, H-2); <sup>13</sup>C NMR (126 MHz, DMSO-*d*<sub>6</sub>) δ: 165.7 (C-14), 162.9 (C-3), 157.2 (C-5), 153.2 (C-q), 146.3 (C-q), 138.4 (C-10), 137.0 (C-q), 128.7 (C-8), 127.2 (C-1), 120.1 (C-q), 117.0 (C-q), 115.6 (C-11), 114.9 (C-2), 102.8 (C-4), 88.4 (C-9); IR *v*<sub>max</sub>/cm<sup>-1</sup>: 3092, 1638, 1626, 1574, 1560, 1508, 1479, 1453, 1420, 1382, 1329, 1314, 1283, 1263,

1210, 1200, 1170, 1117, 1103, 997, 964, 925, 863, 836, 805, 764, 753, 700, 694, 652, 641, 623; HRMS (ESI<sup>-</sup>) m/z: calcd for [C<sub>15</sub>H<sub>7</sub>IO<sub>4</sub> – H]<sup>-</sup>: 376.9311, found 376.9310; HPLC-MS (ESI) m/z; (λ = 235 nm): Rt = 12.58 min; 376.9304 [M – H]<sup>-</sup>.

**3-Hydroxy-8-iodo-5a,10a-dihydro-11H-benzofuro[3,2-b]chromen-11-one (1j):** The general procedure B was followed using 8-iodo-3-methoxy-5a,10a-dihydro-11H-benzofuro[3,2-b]chromen-11-one **1g** (0.100 g, 0.255 mmol, 1 eq) and 1 M BBr<sub>3</sub> in CH<sub>2</sub>Cl<sub>2</sub> (10 mL). The crude was purified by flash column chromatography (Cyclohexane/EtOAc, 8:2) to get **1j** as a pink solid (0.009 g, 0.024 mmol) in 9% yield. R<sub>f</sub> = 0.45 (Cyclohexane/EtOAc 7:3); <sup>1</sup>H NMR (500 MHz, DMSO-*d*<sub>6</sub>) δ: 10.97 (s, 1H, OH), 8.37 (s, 1H, H-11), 8.12 (d, *J*<sub>H-1,H-2</sub> = 8.5 Hz, 1H, H-1), 7.91–7.83 (m, 2H, H-8, H-9), 7.09 (brs, 1H, H-4), 7.02 (d, *J*<sub>H-2,H-1</sub> = 8.5 Hz, 1H, H-2); <sup>13</sup>C NMR (126 MHz, DMSO-*d*<sub>6</sub>) δ: 165.8 (C-14), 162.8 (C-q), 157.2 (C-q), 154.1 (C-q), 147.5 (C-q), 136.5 (C-q), 133.3 (C-9), 127.2 (C-1), 122.1 (C-11), 121.9 (C-8), 117.2 (C-q), 117.1 (C-q), 114.9 (C-2), 102.9 (C-4), 96.0 (C-10). IR ν<sub>max</sub>/cm<sup>-1</sup>: 3017, 2922, 2851, 1738, 1651, 1621, 1605, 1589, 1480, 1446, 1365, 1353, 1253, 1246, 1229, 1217, 1206, 1175, 1115, 1103, 991, 968, 919, 858, 848, 799, 768, 719; HRMS (ESI<sup>-</sup>) m/z: calcd for [C<sub>15</sub>H<sub>7</sub>IO<sub>4</sub> – H]<sup>-</sup>: 376.9311, found 376.9304; HPLC-MS (ESI) m/z; (λ = 235 nm): Rt = 12.52 min; 376.9301 [M – H]<sup>-</sup>.

**1-(4-Hydroxyphenyl)-2-(4-iodophenoxy)ethan-1-one (2a):** The general procedure D was followed using sodium methylate (0.075 g, 1.359 mmol), THF (8 mL), 4-iodophenol (0.205 g, 0.93 mmol) and 2-bromo-1-(4-hydroxyphenyl)ethan-1-one (0.200 g, 0.93 mmol). Compound **2a** was obtained as a white solid (0.059 g, 0.166 mmol) in 18% yield. R<sub>f</sub> = 0.19 (Cyclohexane/EtOAc, 8:2); <sup>1</sup>H NMR (500 MHz, DMSO-*d*<sub>6</sub>) δ: 10.45 (s, 1H, OH), 7.88 (d, *J*<sub>H-10,H-11</sub> = *J*<sub>H-14,H-13</sub> = 8.5 Hz, 2H, H-10, H-14), 7.57 (d, *J*<sub>H-3,H-2</sub> = *J*<sub>H-5,H-6</sub> = 9.0 Hz, 2H, H-3, H-5), 6.88 (d, *J*<sub>H-11,H-10</sub> = *J*<sub>H-13,H-14</sub> = 8.5 Hz, 2H, H-11, H-13), 6.79 (d, *J*<sub>H-2,H-3</sub> = *J*<sub>H-6,H-5</sub> = 9.0 Hz, 2H, H-2, H-6), 5.45 (s, 2H, H-7); <sup>13</sup>C NMR (126 MHz, DMSO-*d*<sub>6</sub>) δ: 192.2 (C-8), 162.6 (C-12), 158.0 (C-1), 137.8 (C-3, C-5), 130.4 (C-10, C-14), 125.8 (C-9), 117.4 (C-2, C-6), 115.4 (C-11, C-13), 83.3 (C-4), 69.7 (C-7); IR ν<sub>max</sub>/cm<sup>-1</sup>: 3674, 3134, 2970, 2920, 1664, 1605, 1572, 1515, 1484, 1438, 1401, 1377, 1362, 1343, 1293, 1261, 1240, 1218, 1166, 1110, 1078, 1057, 1003, 988, 865, 838, 820, 797, 781, 721;

HRMS (ESI<sup>-</sup>) m/z: calcd for [C<sub>14</sub>H<sub>11</sub>O<sub>3</sub> – H]<sup>-</sup>: 352.9675, found 352.9684; HPLC-MS (ESI) m/z; (λ = 235 nm): Rt = 12.65 min; 352.9668 [M – H]<sup>-</sup>.

**1-(4-Hydroxyphenyl)-2-(4-(trifluoromethyl)phenoxy)ethan-1-one (2b)**: The general procedure D was followed using sodium methylate (0.075 g, 1.359 mmol), THF (8 mL), 4-(trifluoromethyl)phenol (0.150 g, 0.93 mmol) and 2-bromo-1-(4-hydroxyphenyl)ethan-1-one (0.200 g, 0.93 mmol). Product **2b** was obtained as a white solid (0.054 g, 0.182 mmol) in 19% yield. R<sub>f</sub> = 0.33 (Cyclohexane/EtOAc, 7:3); <sup>1</sup>H NMR (500 MHz, DMSO-*d*<sub>6</sub>) δ: 10.48 (s, 1H, OH), 7.90 (d, *J*<sub>H-10,H-11</sub> = *J*<sub>H-14,H-13</sub> = 8.5 Hz, 2H, H-10, H-14), 7.63 (d, *J*<sub>H-3,H-2</sub> = *J*<sub>H-5,H-6</sub> = 8.5 Hz, 2H, H-3, H-5), 7.12 (d, *J*<sub>H-2,H-3</sub> = *J*<sub>H-6,H-5</sub> = 8.5 Hz, 2H, H-2, H-6), 6.89 (d, *J*<sub>H-11,H-10</sub> = *J*<sub>H-13,H-14</sub> = 8.5 Hz, 2H, H-11, H-13), 5.59 (s, 2H, H-7); <sup>13</sup>C NMR (126 MHz, DMSO-*d*<sub>6</sub>) δ: 191.8 (C-8), 162.6 (C-12), 161.0 (C-1), 130.4 (C-10, C-14), 126.8 (d, <sup>4</sup>*J*<sub>C-F</sub> = 3.6 Hz, C-3, C-5), 125.7 (C-9), 124.5 (q, <sup>1</sup>*J*<sub>C-F</sub> = 272 Hz, CF<sub>3</sub>), 121.2 (d, <sup>2</sup>*J*<sub>C-F</sub> = 32.4 Hz, C-4), 115.4 (C-11, C-13), 115.1 (C-2, C-6), 69.8 (C-7); <sup>19</sup>F<sub>cpd</sub> NMR (470 MHz, DMSO-*d*<sub>6</sub>) δ: –59.8; IR ν<sub>max</sub>/cm<sup>-1</sup>: 3147, 2931, 1670, 1607, 1573, 1518, 1439, 1423, 1378, 1331, 1310, 1293, 1217, 1168, 1107, 1063, 1011, 988, 836, 809, 774, 720; HRMS (ESI<sup>-</sup>) m/z: calcd for [C<sub>15</sub>H<sub>11</sub>F<sub>3</sub>O<sub>4</sub> – H]<sup>-</sup>: 295.0582, found 295.0589; HPLC-MS (ESI) m/z; (λ = 235 nm): Rt = 12.66 min; 295.0573 [M – H]<sup>-</sup>.

**1-(4-Hydroxyphenyl)-2-(4-nitrophenoxy)ethan-1-one (2c)**: The general procedure F was followed using **7c** (0.211 g, 0.669 mmol) in EtOH (7 mL) and NaOAc (0.549 g, 6.69 mmol) in water (1 mL). The crude residue was purified by column chromatography on silica gel (Cyclohexane/EtOAc, 7:3) to yield **2c** as a white solid (0.088 g, 0.322 mmol) in 48% yield. R<sub>f</sub> = 0.30 (Cyclohexane/EtOAc, 6:4); <sup>1</sup>H NMR (500 MHz, DMSO-*d*<sub>6</sub>) δ: 10.50 (s, 1H, OH), 8.19 (d, *J*<sub>H-3,H-2</sub> = *J*<sub>H-5,H-6</sub> = 9.0 Hz, 2H, H-3, H-5), 7.90 (d, *J*<sub>H-10,H-11</sub> = *J*<sub>H-14,H-13</sub> = 9.0 Hz, 2H, H-10, H-14), 7.15 (d, *J*<sub>H-2,H-3</sub> = *J*<sub>H-6,H-5</sub> = 9.0 Hz, 2H, H-2, H-6), 6.90 (d, *J*<sub>H-11,H-10</sub> = *J*<sub>H-13,H-14</sub> = 9.0 Hz, 2H, H-11, H-13), 5.70 (s, 2H, H-7); <sup>13</sup>C NMR (126 MHz, DMSO-*d*<sub>6</sub>) δ: 191.4 (C-8), 163.5 (C-1), 162.7 (C-12), 140.9 (C-4), 130.5 (C-10, C-14), 125.7 (C-3, C-5), 125.6 (C-9), 115.4, 115.2 (C-2, C-6, C-11, C-13), 70.3 (C-7). IR ν<sub>max</sub>/cm<sup>-1</sup>: 3371, 1675, 1596, 1507, 1446, 1428, 1380, 1331, 1299, 1275, 1250, 1237, 1175, 1108, 1072, 986, 879, 843, 752; HRMS (ESI<sup>-</sup>) m/z: calcd for [C<sub>14</sub>H<sub>11</sub>NO<sub>5</sub> – H]<sup>-</sup>: 272.0559, found 272.0561; HPLC-MS (ESI) m/z; (λ = 235 nm): Rt = 10.88 min; 272.0554 [M – H]<sup>-</sup>.



**4-(2-(4-Hydroxyphenyl)-2-oxoethoxy)benzotrile (2d):** The general procedure F was followed using **7d** (0.224 g, 0.758 mmol) in EtOH (8 mL) and NaOAc (0.622 g, 7.58 mmol) in water (1 mL). The crude residue was purified by column chromatography on silica gel (Cyclohexane/EtOAc, 7:3) to yield **2d** as a white solid (0.126 g, 0.497 mmol) in 66% yield.  $R_f = 0.32$  (Cyclohexane/EtOAc, 6:4);  $^1\text{H NMR}$  (500 MHz, DMSO- $d_6$ )  $\delta$ : 10.49 (s, 1H, OH), 7.89 (d,  $J_{\text{H-3,H-2}} = J_{\text{H-5,H-6}} = 9.0$  Hz, 2H, H-10, H-14), 7.75 (d,  $J_{\text{H-10,H-11}} = J_{\text{H-14,H-13}} = 9.0$  Hz, 2H, H-3, H-5), 7.11 (d,  $J_{\text{H-2,H-3}} = J_{\text{H-6,H-5}} = 9.0$  Hz, 2H, H-2, H-6), 6.89 (d,  $J_{\text{H-11,H-10}} = J_{\text{H-13,H-14}} = 9.0$  Hz, 2H, H-11, H-13), 5.62 (s, 2H, H-7);  $^{13}\text{C NMR}$  (126 MHz, DMSO- $d_6$ )  $\delta$ : 191.6 (C-8), 162.7 (C-12), 161.6 (C-1), 134.0 (C-3, C-5), 130.5 (C-10, C-14), 125.7 (C-9), 119.1 (C $\equiv$ N), 115.7, 115.4 (C-2, C-6, C-11, C-13), 103.0 (C-4), 69.9 (C-7); IR  $\nu_{\text{max}}/\text{cm}^{-1}$ : 3275, 2923, 2230, 1692, 1604, 1584, 1507, 1439, 1420, 1386, 1366, 1304, 1288, 1269, 1223, 1169, 1116, 1082, 983, 873, 852, 823, 810; HRMS (ESI $^-$ )  $m/z$ : calcd for  $[\text{C}_{15}\text{H}_{11}\text{NO}_3 - \text{H}]^-$ : 252.0661, found 252.0641; HPLC-MS (ESI)  $m/z$ ; ( $\lambda = 235$  nm):  $R_t = 10.15$  min; 252.0651  $[\text{M} - \text{H}]^-$ .

**1-(4-Hydroxyphenyl)-2-(4-iodo-3-methylphenoxy)ethan-1-one (2e):** The general procedure F was followed using **7e** (0.157 g, 0.38 mmol) in EtOH (6 mL) and NaOAc (0.314 g, 3.83 mmol) in water (1 mL). The crude residue was purified by column chromatography (Cyclohexane/EtOAc, 9:1) on silica gel to yield **2e** as a white solid (0.100 g, 0.271 mmol) in 71% yield.  $R_f = 0.33$  (Cyclohexane/EtOAc, 7:3);  $^1\text{H NMR}$  (500 MHz, DMSO- $d_6$ )  $\delta$ : 10.45 (s, 1H, OH), 7.88 (d,  $J_{\text{H-10,H-11}} = J_{\text{H-14,H-13}} = 7.5$  Hz, 2H, H-10, H-14), 7.64 (d,  $J_{\text{H-5,H-6}} = 9.0$  Hz, 1H, H-5), 6.99 (s, 1H, H-2), 6.88 (d,  $J_{\text{H-11,H-10}} = J_{\text{H-13,H-14}} = 7.5$  Hz, 2H, H-11, H-13), 6.58 (dd,  $J_{\text{H-6,H-5}} = 9.0$  Hz,  $J = 3.0$  Hz, 1H, H-6), 5.43 (s, 2H, H-7), 2.31 (s, 3H, CH $_3$ );  $^{13}\text{C NMR}$  (126 MHz, DMSO- $d_6$ )  $\delta$ : 192.2 (C-8), 162.6 (C-12), 158.4 (C-1), 141.7 (C-3), 138.9 (C-5), 130.4 (C-10, C-14), 125.9 (C-9), 116.7 (C-2), 115.3 (C-11, C-13), 114.5 (C-6), 90.0 (C-4), 69.7 (C-7), 27.5 (CH $_3$ ); IR  $\nu_{\text{max}}/\text{cm}^{-1}$ : 3160, 1664, 1604, 1571, 1515, 1471, 1437, 1405, 1376, 1291, 1241, 1221, 1165, 1140, 1091, 1013, 988, 933, 878, 836, 818, 787; HRMS (ESI $^-$ )  $m/z$ : calcd for  $[\text{C}_{15}\text{H}_{13}\text{IO}_3 - \text{H}]^-$ : 366.9831, found 366.9836; HPLC-MS (ESI)  $m/z$ ; ( $\lambda = 235$  nm):  $R_t = 13.26$  min; 366.9804  $[\text{M} - \text{H}]^-$ .

**1-(4-Hydroxyphenyl)-2-(4-iodo-2-methylphenoxy)ethan-1-one (2f):** The general procedure F was followed using **7f** (0.259 g, 0.631 mmol) in EtOH (8 mL) and NaOAc (0.517 g, 6.31 mmol) in water (1

mL). The crude residue was purified by column chromatography on silica gel (Cyclohexane/EtOAc, 7:3) to yield **2f** as a white solid (0.078 g, 0.211 mmol) in 34% yield;  $R_f = 0.54$  (Cyclohexane/EtOAc, 6:4);  $^1\text{H}$  NMR (500 MHz,  $\text{DMSO-}d_6$ )  $\delta$ : 10.45 (s, 1H, OH), 7.88 (d,  $J_{\text{H-10,H-11}} = J_{\text{H-14,H-13}} = 8.5$  Hz, 2H, H-10, H-14), 7.49 (d,  $J = 1.5$  Hz, 1H, H-3), 7.40 (dd,  $J_{\text{H-5,H-6}} = 8.5$  Hz,  $J_{\text{H-5,H-3}} = 1.5$  Hz, 1H, H-5), 6.88 (d,  $J_{\text{H-11,H-10}} = J_{\text{H-13,H-14}} = 8.5$  Hz, 2H, H-11, H-13), 6.67 (d,  $J_{\text{H-6,H-5}} = 8.5$  Hz, 1H, H-6), 5.46 (s, 2H, H-7), 2.18 (s, 3H,  $\text{CH}_3$ );  $^{13}\text{C}$  NMR (126 MHz,  $\text{DMSO-}d_6$ )  $\delta$ : 192.4 (C-8), 162.5 (C-12), 156.2 (C-1), 138.4 (C-3), 135.1 (C-5), 130.4 (C-10, C-14), 129.1 (C-2), 125.9 (C-9), 115.3 (C-11, C-13), 114.2 (C-6), 83.2 (C-4), 70.0 (C-7), 15.6 ( $\text{CH}_3$ ); IR  $\nu_{\text{max}}/\text{cm}^{-1}$ : 3202, 1665, 1602, 1574, 1518, 1488, 1438, 1369, 1305, 1286, 1248, 1222, 1191, 1172, 1152, 1137, 979, 877, 842, 816, 802, 742, 718; HRMS ( $\text{ESI}^-$ )  $m/z$ : calcd for  $[\text{C}_{15}\text{H}_{13}\text{IO}_3 - \text{H}]^-$ : 366.9831, found 366.9837; HPLC-MS ( $\text{ESI}^-$ )  $m/z$ ; ( $\lambda = 235$  nm):  $R_t = 13.62$  min; 366.9813  $[\text{M} - \text{H}]^-$ .

**2-(2,4-Dichlorophenoxy)-1-(4-hydroxyphenyl)ethan-1-one (2g)**: The general procedure F was followed using the acetate **7g** (0.236 g, 0.696 mmol) in EtOH (8 mL) and NaOAc (0.570 g, 6.958 mmol) in water (1 mL). The crude residue was purified by column chromatography on silica gel (Cyclohexane/EtOAc, 7:3) to yield **2g** as a white solid (0.127 g, 0.427 mmol) in 62% yield.  $R_f = 0.24$  (Cyclohexane/EtOAc, 7:3);  $^1\text{H}$  NMR (500 MHz,  $\text{DMSO-}d_6$ )  $\delta$ : 10.48 (s, 1H, OH), 7.88 (d,  $J_{\text{H-10,H-11}} = J_{\text{H-14,H-13}} = 8.5$  Hz, 2H, H-10, H-14), 7.58 (d,  $J_{\text{H-3,H-5}} = 2.5$  Hz, 1H, H-3), 7.30 (dd,  $J_{\text{H-5,H-6}} = 9.0$  Hz,  $J_{\text{H-5,H-3}} = 2.5$  Hz, 1H, H-5), 7.03 (d,  $J_{\text{H-6,H-5}} = 9.0$  Hz, 1H, H-6), 6.89 (d,  $J_{\text{H-11,H-10}} = J_{\text{H-13,H-14}} = 8.5$  Hz, 2H, H-11, H-13), 5.63 (s, 2H, H-7);  $^{13}\text{C}$  NMR (126 MHz,  $\text{DMSO-}d_6$ )  $\delta$ : 191.6 (C-8), 162.7 (C-12), 152.6 (C-1), 130.4 (C-10, C-14), 129.2 (C-3), 127.8 (C-5), 125.6 (C-9), 124.5, 122.1 (C-2, C-4), 115.3 (C-11, C-13), 115.2 (C-6), 70.5 (C-7). IR  $\nu_{\text{max}}/\text{cm}^{-1}$ : 3265, 2920, 1675, 1602, 1576, 1516, 1484, 1436, 1391, 1365, 1287, 1248, 1217, 1174, 1103, 1087, 1056, 989, 857, 833, 808, 793, 741, 721; HRMS ( $\text{ESI}^-$ )  $m/z$ : calcd for  $[\text{C}_{14}\text{H}_{10}\text{Cl}_2\text{O}_3 - \text{H}]^-$ : 294.9929, found 294.9934; HPLC-MS ( $\text{ESI}^-$ )  $m/z$ ; ( $\lambda = 235$  nm):  $R_t = 13.02$  min; 294.9921  $[\text{M} - \text{H}]^-$ .

**1-(4-Hydroxyphenyl)-2-(*p*-tolylloxy)ethan-1-one (2h)**: The general procedure C was followed using *p*-cresol (0.085 g, 0.781 mmol) and  $\text{K}_2\text{CO}_3$  (0.119 g, 0.879 mmol) in acetone (5 mL) and acetate **6** (0.200 g, 0.781 mmol). The crude residue was purified by column chromatography on silica gel (Cyclohexane/EtOAc, 7:3) to yield **2h** as a white solid (0.060 g, 0.247 mmol) in 27% yield.  $R_f = 0.25$

(Cyclohexane/EtOAc, 7:3);  $^1\text{H}$  NMR (500 MHz,  $\text{DMSO-}d_6$ )  $\delta$ : 10.43 (s, 1H, OH), 7.89 (d,  $J_{\text{H-10,H-11}} = J_{\text{H-14,H-13}} = 9.0$  Hz, 2H, H-10, H-14), 7.06 (d,  $J_{\text{H-3,H-2}} = J_{\text{H-5,H-6}} = 9.0$  Hz, 2H, H-3, H-5), 6.88 (d,  $J_{\text{H-11,H-10}} = J_{\text{H-13,H-14}} = 9.0$  Hz, 2H, H-11, H-13), 6.81 (d,  $J_{\text{H-2,H-3}} = J_{\text{H-6,H-5}} = 9.0$  Hz, 2H, H-2, H-6), 5.36 (s, 2H, H-7), 2.22 (s, 3H,  $\text{CH}_3$ );  $^{13}\text{C}$  NMR (126 MHz,  $\text{DMSO-}d_6$ )  $\delta$ : 192.7 (C-8), 162.4 (C-12), 155.9 (C-1), 130.4 (C-10, C-14), 129.6 (C-3, C-5), 129.4 (C-9), 126.0 (C-4), 115.3 (C-11, C-13), 114.4 (C-2, C-6), 69.7 (C-7), 20.0 ( $\text{CH}_3$ ); IR  $\nu_{\text{max}}/\text{cm}^{-1}$ : 3287, 2922, 1705, 1673, 1605, 1578, 1512, 1434, 1378, 1296, 1229, 1169, 1109, 1089, 989, 877, 839, 824, 814, 801; HRMS ( $\text{ESI}^-$ )  $m/z$ : calcd for  $[\text{C}_{15}\text{H}_{14}\text{O}_3 - \text{H}]^-$ : 241.0865, found 241.0867; HPLC-MS ( $\text{ESI}^-$ )  $m/z$ ; ( $\lambda = 235$  nm):  $R_t = 11.45$  min; 241.0850  $[\text{M} - \text{H}]^-$ .

**1-(4-Hydroxyphenyl)-2-(4-methoxyphenoxy)ethan-1-one (2i)**: The general procedure F was followed using acetate **7i** (0.095 g, 0.316 mmol) in EtOH (5 mL) and NaOAc (0.259 g, 3.16 mmol) in water (1 mL). The crude residue was purified by column chromatography on silica gel (Cyclohexane/EtOAc, 7:3) to yield **2i** as a white solid (0.047 g, 0.181 mmol) in 58% yield.  $R_f = 0.22$  (Cyclohexane/EtOAc, 7:3);  $^1\text{H}$  NMR (500 MHz,  $\text{DMSO-}d_6$ )  $\delta$ : 10.43 (s, 1H, OH), 7.89 (d,  $J_{\text{H-10,H-11}} = J_{\text{H-14,H-13}} = 9.0$  Hz, 2H, H-10, H-14), 6.88–6.82 (m, 6H, H-11, H-13, H-2, H-6, H-3, H-5), 5.34 (s, 2H, H-7), 3.69 (s, 3H,  $\text{CH}_3$ );  $^{13}\text{C}$  NMR (126 MHz,  $\text{DMSO-}d_6$ )  $\delta$ : 192.8 (C-8), 162.4 (C-12), 153.5 (C-1), 152.0 (C-4), 130.4 (C-10, C-14), 126.0 (C-9), 115.5 (C-11, C-13), 115.3 (C-3, C-5), 114.5 (C-2, C-6), 70.3 (C-7), 55.3 ( $\text{CH}_3$ ). IR  $\nu_{\text{max}}/\text{cm}^{-1}$ : 3172, 1672, 1604, 1577, 1508, 1466, 1445, 1383, 1362, 1288, 1250, 1226, 1171, 1109, 1087, 1039, 1007, 990, 872, 842, 812, 773, 722; HRMS ( $\text{ESI}^-$ )  $m/z$ : calcd for  $[\text{C}_{15}\text{H}_{14}\text{O}_4 - \text{H}]^-$ : 257.0814, found 257.0818; HPLC-MS ( $\text{ESI}^-$ )  $m/z$ ; ( $\lambda = 235$  nm):  $R_t = 10.46$  min; 257.0805  $[\text{M} - \text{H}]^-$ .

**2-(3,4-Dimethoxyphenoxy)-1-(4-hydroxyphenyl)ethan-1-one (2j)**: The general procedure F was followed using acetate **7j** (0.253 g, 0.877 mmol) in EtOH (7 mL) and NaOAc (0.719 g, 8.77 mmol) in water (1 mL). The crude residue was purified by column chromatography on silica gel (Cyclohexane/EtOAc, 7:3) to yield **2j** as a white solid (0.103 g, 0.357 mmol) in 37% yield.  $R_f = 0.5$  (Cyclohexane/EtOAc, 6:4);  $^1\text{H}$  NMR (500 MHz,  $\text{DMSO-}d_6$ )  $\delta$ : 10.43 (s, 1H, OH), 7.90 (d,  $J_{\text{H-10,H-11}} = J_{\text{H-14,H-13}} = 8.0$  Hz, 2H, H-10, H-14), 6.88 (d,  $J_{\text{H-11,H-10}} = J_{\text{H-13,H-14}} = 7.5$  Hz, 2H, H-11, H-13), 6.82 (d,  $J_{\text{H-5,H-6}} = 9.0$  Hz, 1H, H-5), 6.63 (d,  $J_{\text{H-2,H-6}} = 1.5$  Hz, 1H, H-2), 6.41 (dd,  $J_{\text{H-6,H-5}} = 9.0$  Hz,  $J_{\text{H-6,H-2}} = 1.5$  Hz, 1H, H-6), 5.33 (s,

2H, H-7), 3.73 (s, 3H, CH<sub>3</sub>O-C3), 3.68 (s, 3H, CH<sub>3</sub>O-C4); <sup>13</sup>C NMR (126 MHz, DMSO-*d*<sub>6</sub>) δ: 192.7 (C-8), 162.4 (C-12), 152.6 (C-1), 149.6 (C-9), 143.3 (C-4), 130.4 (C-10, C-14), 126.1 (C-3), 115.3 (C-11, C-13), 112.7 (C-5), 104.4 (C-2), 101.2 (C-6), 70.3 (C-7), 56.1 (CH<sub>3</sub>O-C3), 55.5 (CH<sub>3</sub>O-C4); IR ν<sub>max</sub>/cm<sup>-1</sup>: 3219, 1671, 1600, 1512, 1448, 1285, 1265, 1229, 1204, 1145, 1095, 1026, 994, 834, 788, 754; HRMS (ESI<sup>-</sup>) m/z: calcd for [C<sub>16</sub>H<sub>16</sub>O<sub>5</sub> – H]<sup>-</sup>: 287.0919, found 287.0928; HPLC-MS (ESI) m/z; (λ = 235 nm): Rt = 9.87 min; 287.0905 [M – H]<sup>-</sup>.

**2-(4-Bromophenoxy)-1-(4-hydroxyphenyl)ethan-1-one (2k)**: The general procedure F was followed using acetate **7k** (0.118 g, 0.384 mmol) in EtOH (5 mL) and NaOAc (0.315 g, 3.84 mmol) in water (0.5 mL). The crude residue was purified by column chromatography on silica gel (Cyclohexane/EtOAc, 7:3) to yield **2k** as a white solid (0.053 g, 0.172 mmol) in 45% yield. R<sub>f</sub> = 0.46 (Cyclohexane/EtOAc, 7:3); <sup>1</sup>H NMR (500 MHz, DMSO-*d*<sub>6</sub>) δ: 10.46 (s, 1H, OH), 7.89 (d, *J*<sub>H-10,H-11</sub> = *J*<sub>H-14,H-13</sub> = 9.0 Hz, 2H, H-10, H-14), 7.43 (d, *J*<sub>H-11,H-10</sub> = *J*<sub>H-13,H-14</sub> = 9.0 Hz, 2H, H-11, H-13), 6.91 (d, *J*<sub>H-3,H-2</sub> = *J*<sub>H-5,H-6</sub> = 9.0 Hz, 2H, H-3, H-5), 6.88 (d, *J*<sub>H-2,H-3</sub> = *J*<sub>H-6,H-5</sub> = 9.0 Hz, 2H, H-2, H-6), 5.47 (s, 2H, H-7); <sup>13</sup>C NMR (126 MHz, DMSO-*d*<sub>6</sub>) δ: 192.1 (C-8), 162.5 (C-12), 157.4 (C-1), 131.9 (C-11, C-13), 130.4 (C-10, C-14), 125.8 (C-9), 116.9 (C-3, C-5), 115.3 (C-2, C-6), 112.0 (C-4), 69.8 (C-7); IR ν<sub>max</sub>/cm<sup>-1</sup>: 3136, 2972, 1665, 1606, 1573, 1515, 1488, 1438, 1379, 1293, 1261, 1241, 1220, 1166, 1069, 1005, 990, 867, 837, 795; HRMS (ESI<sup>+</sup>) m/z: calcd for [C<sub>14</sub>H<sub>11</sub>BrO<sub>3</sub> + H]<sup>+</sup>: 306.9970, found 306.9968; HRMS (ESI<sup>-</sup>) m/z: calcd for [C<sub>14</sub>H<sub>11</sub>BrO<sub>3</sub> – H]<sup>-</sup>: 304.9813, found 304.9819; HPLC-MS (ESI) m/z; (λ = 235 nm): Rt = 12.17 min; 304.9807 [M – H]<sup>-</sup>.

**2-(4-Chlorophenoxy)-1-(4-hydroxyphenyl)ethan-1-one (2l)**: The general procedure F was followed using **7l** (0.057 g, 0.187 mmol) in EtOH (5 mL) and NaOAc (0.153 g, 1.87 mmol) in water (0.5 mL). The crude residue was purified by column chromatography on silica gel (Cyclohexane/EtOAc, 8:2) to yield **2l** as a white solid (0.030 g, 0.114 mmol) in 61% yield. R<sub>f</sub> = 0.42 (Cyclohexane/EtOAc, 7:3); <sup>1</sup>H NMR (500 MHz, DMSO-*d*<sub>6</sub>) δ: 10.46 (s, 1H, OH), 7.89 (d, *J*<sub>H-10,H-11</sub> = *J*<sub>H-14,H-13</sub> = 8.5 Hz, 2H, H-10, H-14), 7.31 (d, *J*<sub>H-3,H-2</sub> = *J*<sub>H-5,H-6</sub> = 9.0 Hz, 2H, H-3, H-5), 6.96 (d, *J*<sub>H-2,H-3</sub> = *J*<sub>H-6,H-5</sub> = 9.0 Hz, 2H, H-2, H-6), 6.88 (d, *J*<sub>H-13,H-14</sub> = *J*<sub>H-11,H-10</sub> = 8.5 Hz, 2H, H-11, H-13), 5.47 (s, 2H, H-7); <sup>13</sup>C NMR (126 MHz, DMSO-*d*<sub>6</sub>) δ: 192.2 (C-8), 162.5 (C-12), 156.9 (C-1), 130.4 (C-10, C-14), 129.1 (C-3, C-5), 125.8 (C-9), 124.4 (C-4), 116.4 (C-2, C-6), 115.3 (C-11,

C-13), 69.9 (C-7). IR  $\nu_{\max}/\text{cm}^{-1}$ : 3119, 1667, 1601, 1574, 1515, 1492, 1438, 1378, 1362, 1292, 1240, 1220, 1165, 1093, 1076, 1009, 990, 836, 819, 792, 720; HRMS (ESI<sup>+</sup>) m/z: calcd for [C<sub>14</sub>H<sub>11</sub>ClO<sub>3</sub> + H]<sup>+</sup>: 263.0475, found 263.0472; HRMS (ESI<sup>-</sup>) m/z: calcd for [C<sub>14</sub>H<sub>11</sub>ClO<sub>3</sub> - H]<sup>-</sup>: 261.0318, found 261.0320; HPLC-MS (ESI) m/z; ( $\lambda$  = 235 nm): Rt = 11.91 min; 261.0305 [M - H]<sup>-</sup>.

**2-(2,4-Dibromophenoxy)-1-(4-hydroxyphenyl)ethan-1-one (2m)**: The general procedure F was followed using **7m** (0.217 g, 0.507 mmol) in EtOH (7 mL) and NaOAc (0.416 g, 5.07 mmol) in water (1 mL). The crude residue was purified by column chromatography on silica gel (Cyclohexane/EtOAc, 8:2) to get **2m** as a white solid (0.144 g, 0.373 mmol) in 74% yield. Rf = 0.44 (Cyclohexane/EtOAc, 7:3); <sup>1</sup>H NMR (500 MHz, DMSO-*d*<sub>6</sub>)  $\delta$ : 10.47 (s, 1H, OH), 7.88 (d,  $J_{\text{H-10,H-11}} = J_{\text{H-14,H-13}} = 8.5$  Hz, 2H, H-10, H-14), 7.79 (d,  $J_{\text{H-3,H-5}} = 2.5$  Hz, 1H, H-3), 7.45 (dd,  $J_{\text{H-5,H-6}} = 8.5$  Hz,  $J_{\text{H-5,H-3}} = 2.5$  Hz 1H, H-5), 6.94 (d,  $J_{\text{H-6,H-5}} = 8.5$  Hz, 1H, H-6), 6.88 (d,  $J_{\text{H-11,H-10}} = J_{\text{H-13,H-14}} = 8.5$  Hz, 2H, H-11, H-13), 5.62 (s, 2H, H-7); <sup>13</sup>C NMR (126 MHz, DMSO-*d*<sub>6</sub>)  $\delta$ : 191.6 (C-8), 162.7 (C-12), 154.0 (C-1), 134.6 (C-5), 131.3 (C-3), 130.5 (C-10, C-14), 125.7 (C-9), 115.5 (C-2), 115.4 (C-11, C-13), 112.2 (C-4), 111.9 (C-6), 70.7 (C-7). IR  $\nu_{\max}/\text{cm}^{-1}$ : 3363, 2924, 1674, 1603, 1576, 1515, 1473, 1430, 1360, 1300, 1245, 1215, 1171, 1110, 1082, 1038, 969, 872, 837, 816, 795, 730; HRMS (ESI<sup>-</sup>) m/z: calcd for [C<sub>14</sub>H<sub>10</sub>Br<sub>2</sub>O<sub>3</sub> - H]<sup>-</sup>: 382.8918, found 382.8918; HPLC-MS (ESI) m/z; ( $\lambda$  = 235 nm): Rt = 13.43 min; 384.8876 [M + H]<sup>+</sup>.

**2-(4-Bromo-2-chlorophenoxy)-1-(4-hydroxyphenyl)ethan-1-one (2n)**: The general procedure F was followed using **7n** (0.401 g, 1.045 mmol) in EtOH (8 mL) and NaOAc (0.857 g, 10.45 mmol) in water (1 mL). The crude residue was purified by column chromatography on silica gel (Cyclohexane/EtOAc, 8:2) to furnish **2n** as a white solid (0.158 g, 0.462 mmol) in 44% yield. Rf = 0.50 (Cyclohexane/EtOAc, 7:3); <sup>1</sup>H NMR (500 MHz, DMSO-*d*<sub>6</sub>)  $\delta$ : 10.48 (s, 1H, OH), 7.88 (d,  $J_{\text{H-10,H-11}} = J_{\text{H-14,H-13}} = 8.5$  Hz, 2H, H-10, H-14), 7.68 (d,  $J_{\text{H-3,H-5}} = 2.0$  Hz, 1H, H-3), 7.42 (d,  $J_{\text{H-5,H-6}} = 8.5$  Hz,  $J_{\text{H-5,H-3}} = 2.0$  Hz, 1H, H-5), 6.98 (d,  $J_{\text{H-6,H-5}} = 8.5$  Hz, 1H, H-6), 6.89 (d,  $J_{\text{H-11,H-10}} = J_{\text{H-13,H-14}} = 8.5$  Hz, 2H, H-11, H-13), 5.63 (s, 2H, H-7); <sup>13</sup>C NMR (126 MHz, DMSO-*d*<sub>6</sub>)  $\delta$ : 191.6 (C-8), 162.7 (C-12), 153.1 (C-1), 131.9 (C-5), 130.7 (C-3), 130.5 (C-10, C-14), 125.7 (C-9), 122.5 (C-4), 115.7 (C-2), 115.4 (C-11, C-13), 111.8 (C-6), 70.5 (C-7); IR  $\nu_{\max}/\text{cm}^{-1}$ : 3268, 1675, 1602, 1576, 1517, 1485, 1436, 1288, 1256, 1244, 1215, 1175, 1090, 989, 858, 834, 793, 744, 712; HRMS (ESI<sup>+</sup>)

m/z: calcd for  $[C_{14}H_{10}Br_2ClO_3 + H]^+$ : 340.9580, found 340.9579; HPLC-MS (ESI) m/z; ( $\lambda = 235$  nm): Rt = 13.22 min; 340.9390  $[M - H]^-$ .

**2-Fluoro-4-(2-(4-hydroxyphenyl)-2-oxoethoxy)benzaldehyde (2o)**: The general procedure F was followed using 2-fluoro-4-(2-(4-hydroxyphenyl)-2-oxoethoxy)benzaldehyde **7o** (0.115 g, 0.363 mmol) in EtOH (6 mL) and NaOAc (0.298 g, 3.63 mmol) in water (1 mL). The crude residue was purified by column chromatography on silica gel (Cyclohexane/EtOAc, 7:3) to yield **2o** as a white solid (0.087 g, 0.317 mmol) in 87% yield. Rf = 0.36 (Cyclohexane/EtOAc, 6:4);  $^1H$  NMR (500 MHz, DMSO- $d_6$ )  $\delta$ : 10.49 (s, 1H, OH), 10.07 (s, 1H, CHO), 7.90 (d,  $J_{H-10,H-11} = J_{H-14,H-13} = 9.0$  Hz, 2H, H-10, H-14), 7.77 (t,  $J_{H-5,H-6} = J_{H-5,F} = 8.5$  Hz, 1H, H-5), 7.05 (dd,  $J_{H-2,F} = 13.0$  Hz,  $J_{H-2,H-6} = 2.0$  Hz, 1H, H-2), 6.97 (dd,  $J_{H-6,H-5} = 8.5$  Hz,  $J_{H-6,H-2} = 2.0$  Hz, 1H, H-6), 6.90 (d,  $J_{H-11,H-10} = J_{H-13,H-14} = 9.0$  Hz, 2H, H-11, H-13), 5.67 (s, 2H, H-7);  $^{13}C$  NMR (126 MHz, DMSO- $d_6$ )  $\delta$ : 191.2 (C-8), 186.1 (d,  $J_{CHO,F} = 4.5$  Hz, CHO), 171.9 (d,  $J_{C-3,F} = 253.4$  Hz, C-3), 170.9 (C-1), 162.7 (C-12), 130.6 (C-5), 130.5 (C-10, C-14), 125.6 (C-9), 118.2 (d,  $J_{C-4,F} = 3.1$  Hz, C-4), 115.3 (C-11, C-13), 112.2 (C-6), 102.5 (d,  $J_{C-2,F} = 24.2$  Hz, C-2), 70.3 (C-7);  $^{19}F$  NMR (470 MHz, DMSO- $d_6$ )  $\delta$ : -118.4; IR  $\nu_{max}/cm^{-1}$ : 3160, 2964, 2921, 1692, 1666, 1615, 1575, 1501, 1434, 1379, 1344, 1291, 1249, 1223, 1162, 1101, 1067, 994, 839, 809; HRMS (ESI $^-$ ) m/z: calcd for  $[C_{15}H_{11}FO_4 - H]^-$ : 273.0563, found 273.0564; HPLC-MS (ESI) m/z; ( $\lambda = 235$  nm): Rt = 10.15 min; 273.0564  $[M - H]^-$ .

**2-(3,4-Dinitrophenoxy)-1-(4-hydroxyphenyl)ethan-1-one (2p)**: The general procedure F was followed using acetate **7p** (0.370 g, 1.027 mmol) in EtOH (8 mL) and NaOAc (0.842 g, 10.27 mmol) in water (1 mL). The crude residue was purified by column chromatography on silica gel (Cyclohexane/EtOAc, 7:3) to yield **2p** as a yellow solid (0.124 g, 0.389 mmol) in 34% yield. Rf = 0.36 (Cyclohexane/EtOAc, 6:4);  $^1H$  NMR (500 MHz, DMSO- $d_6$ )  $\delta$ : 10.52 (s, 1H, OH), 8.24 (d,  $J_{H-5,H-6} = 9.0$  Hz, 1H, H-5), 7.88 (d,  $J_{H-10,H-11} = J_{H-14,H-13} = 9.0$  Hz, 2H, H-10, H-14), 7.86 (d,  $J_{H-2,H-6} = 3.0$  Hz, 1H, H-2), 7.43 (dd,  $J_{H-6,H-5} = 9.0$  Hz,  $J_{H-6,H-2} = 3.0$  Hz, 1H, H-6), 6.90 (d,  $J_{H-11,H-10} = J_{H-13,H-14} = 9.0$  Hz, 2H, H-11, H-13), 5.81 (s, 2H, H-7);  $^{13}C$  NMR (126 MHz, DMSO- $d_6$ )  $\delta$ : 190.7 (C-8), 163.0, 162.8 (C-1, C-12), 145.0 (C-5), 133.2 (C-10, C-14), 130.5 (C-9), 127.9 (C-3), 125.4 (C-4), 118.3 (C-6), 115.4 (C-11, C-13), 111.1 (C-2), 71.0 (C-7); IR  $\nu_{max}/cm^{-1}$ : 3171, 2923, 2853, 1729, 1663, 1603, 1573, 1551, 1539, 1514, 1491, 1465, 1439, 1365, 1348, 1322, 1290, 1252,

1240, 1215, 1171, 1084, 992, 931, 903, 838, 823, 775, 748, 723; HRMS (ESI<sup>-</sup>) m/z: calcd for [C<sub>14</sub>H<sub>10</sub>N<sub>2</sub>O<sub>7</sub> – H]<sup>-</sup>: 317.0410, found 317.0407; HPLC-MS (ESI) m/z; (λ = 235 nm): Rt = 11.76 min; 317.0407 [M – H]<sup>-</sup>.

**2,6-Difluoro-4-(2-(4-hydroxyphenyl)-2-oxoethoxy)benzonitrile (2q):** The general procedure F was followed using acetate **7q** (0.365 g, 1.102 mmol) in EtOH (8 mL) and NaOAc (0.904 g, 11.02 mmol) in water (1 mL). The crude residue was recrystallized from methanol to obtain **2q** as a white pink solid (0.278 g, 0.961 mmol) in 87% yield. R<sub>f</sub> = 0.30 (Cyclohexane/EtOAc, 6:4); <sup>1</sup>H NMR (500 MHz, DMSO-*d*<sub>6</sub>) δ: 10.50 (s, 1H, OH), 7.88 (d, *J*<sub>H-10,H-11</sub> = *J*<sub>H-14,H-13</sub> = 9.0 Hz, 2H, H-10, H-14), 7.17 (d, *J*<sub>H-2,F</sub> = *J*<sub>H-6,F</sub> = 10.5 Hz, 2H, H-2, H-6), 6.90 (d, *J*<sub>H-11,H-10</sub> = *J*<sub>H-13,H-14</sub> = 9.0 Hz, 2H, H-11, H-13), 5.71 (s, 2H, H-7). <sup>13</sup>C NMR (126 MHz, DMSO-*d*<sub>6</sub>) δ: 190.6 (C-8), 164.7 (t, *J*<sub>C-1,F</sub> = 14.5 Hz, C-1), 163.4 (dd, *J*<sub>C-3,F-3</sub> = *J*<sub>C-5,F-5</sub> = 254.3 Hz, *J*<sub>C-3,F-5</sub> = *J*<sub>C-5,F-3</sub> = 7.8 Hz, C-3, C-5), 162.7 (C-12), 130.5 (C-10, C-14), 125.4 (C-9), 115.3 (C-11, C-13), 109.9 (C≡N), 100.3 (d, *J*<sub>C-2,F-3</sub> = *J*<sub>C-6,F-5</sub> = 22.8 Hz, C-2, C-6), 83.0 (C-4), 71.0 (C-7); <sup>19</sup>F<sub>cpd</sub> NMR (470 MHz, DMSO-*d*<sub>6</sub>) δ: –105.6; IR ν<sub>max</sub>/cm<sup>-1</sup>: 3113, 2239, 1668, 1635, 1604, 1577, 1513, 1495, 1456, 1437, 1392, 1374, 1360, 1284, 1256, 1228, 1200, 1194, 1179, 1064, 1043, 1010, 968, 867, 851, 823, 805, 719; HRMS (ESI<sup>-</sup>) m/z: calcd for [C<sub>15</sub>H<sub>9</sub>F<sub>2</sub>NO<sub>3</sub> – H]<sup>-</sup>: 288.0472, found 288.0480; HPLC-MS (ESI) m/z; (λ = 235 nm): Rt = 11.59 min; 288.0472 [M – H]<sup>-</sup>.

**2-(4-Bromo-2,6-difluorophenoxy)-1-(4-hydroxyphenyl)ethan-1-one (2r):** The general procedure F was followed using **7r** (0.260 g, 0.675 mmol) in EtOH (8 mL) and NaOAc (0.553 g, 6.750 mmol) in water (1 mL). The crude residue was crystallized in cyclohexane to obtain **2r** as a white solid (0.106 g, 0.309 mmol) in 46% yield. R<sub>f</sub> = 0.30 (Cyclohexane/EtOAc, 6:4); <sup>1</sup>H NMR (500 MHz, DMSO-*d*<sub>6</sub>) δ: 10.47 (s, 1H, OH), 7.82 (d, *J*<sub>H-10,H-11</sub> = *J*<sub>H-14,H-13</sub> = 8.5 Hz, 2H, H-10, H-14), 7.48 (d, *J*<sub>H-3,F-2</sub> = *J*<sub>H-5,F-6</sub> = 8.5 Hz, 2H, H-3, H-5), 6.86 (d, *J*<sub>H-11,H-10</sub> = *J*<sub>H-13,H-14</sub> = 8.5 Hz, 2H, H-11, H-13), 5.58 (s, 2H, H-7); <sup>13</sup>C NMR (126 MHz, DMSO-*d*<sub>6</sub>) δ: 191.7 (C-8), 162.6 (C-12), 154.3 (dd, *J*<sub>C-2,F-2</sub> = *J*<sub>C-6,F-6</sub> = 250.1 Hz, *J*<sub>C-2,F-6</sub> = *J*<sub>C-6,F-2</sub> = 6.8 Hz, C-2, C-6), 134.4 (C-1), 130.3 (C-10, C-14), 125.3 (C-9), 116.2 (dd, *J*<sub>C-3,F-2</sub> = *J*<sub>C-5,F-6</sub> = 19.5 Hz, *J*<sub>C-3,F-6</sub> = *J*<sub>C-5,F-2</sub> = 7.3 Hz, C-3, C-5), 115.4 (C-11, C-13), 112.5 (d, *J*<sub>C-4,F</sub> = 11.8 Hz, C-4), 74.1 (C-7); <sup>19</sup>F<sub>cpd</sub> NMR (470 MHz, DMSO-*d*<sub>6</sub>) δ: –127.3; IR ν<sub>max</sub>/cm<sup>-1</sup>: 3228, 2925, 1666, 1602, 1575, 1516, 1496, 1423, 1372, 1320, 1283, 1255, 1217,

1173, 1090, 1068, 1037, 1003, 977, 877, 861, 853, 813, 726; HRMS (ESI<sup>-</sup>) m/z: calcd for [C<sub>14</sub>H<sub>9</sub>BrF<sub>2</sub>O<sub>3</sub> – H]<sup>-</sup>: 340.9625, found 340.9611; HPLC-MS (ESI) m/z; (λ = 235 nm): Rt = 12.69 min; 340.9622 [M – H]<sup>-</sup>.

**1-(4-Hydroxyphenyl)-2-(3-iodophenoxy)ethan-1-one (2s):** The general procedure F was followed using the acetate **7s** (0.140 g, 0.353 mmol) in EtOH (5 mL) and NaOAc (0.290 g, 3.530 mmol) in water (1 mL). The crude residue was crystallized in cyclohexane to obtain **2s** as a white solid (0.063 g, 0.177 mmol) in 50% yield. R<sub>f</sub> = 0.24 (Cyclohexane/EtOAc, 7:3); <sup>1</sup>H NMR (500 MHz, DMSO-*d*<sub>6</sub>) δ: 10.46 (s, 1H, OH), 7.89 (d, *J*<sub>H-10,H-11</sub> = *J*<sub>H-14,H-13</sub> = 9.0 Hz, 2H, H-10, H-14), 7.33 (dd, *J*<sub>H-2,H-6</sub> = 2.5 Hz, *J*<sub>H-2,H-4</sub> = 1.5 Hz, 1H, H-2), 7.30 (dt, *J*<sub>H-4,H-5</sub> = 8.0 Hz, *J*<sub>H-4,H-2</sub> = *J*<sub>H-4,H-6</sub> = 1.5 Hz, 1H, H-4), 7.06 (t, *J*<sub>H-5,H-4</sub> = *J*<sub>H-5,H-6</sub> = 8.0 Hz, 1H, H-5), 6.96 (ddd, *J*<sub>H-6,H-5</sub> = 8.0 Hz, *J*<sub>H-6,H-2</sub> = 2.5 Hz, *J*<sub>H-6,H-4</sub> = 1.5 Hz, 1H, H-6), 6.88 (d, *J*<sub>H-11,H-10</sub> = *J*<sub>H-13,H-14</sub> = 9.0 Hz, 2H, H-11, H-13), 5.48 (s, 2H, H-7); <sup>13</sup>C NMR (126 MHz, DMSO-*d*<sub>6</sub>) δ: 192.1 (C-8), 162.6 (C-12), 158.8 (C-1), 131.2 (C-5), 130.4 (C-10, C-14), 129.6 (C-4), 125.8 (C-9), 123.0 (C-2), 115.3 (C-11, C-13), 114.6 (C-6), 94.8 (C-3), 69.7 (C-7); IR ν<sub>max</sub>/cm<sup>-1</sup>: 3673, 3203, 2988, 2901, 1667, 1603, 1574, 1517, 1478, 1437, 1421, 1380, 1287, 1271, 1241, 1217, 1173, 1080, 1066, 988, 886, 833, 812, 772, 721; HRMS (ESI<sup>-</sup>) m/z: calcd for [C<sub>14</sub>H<sub>11</sub>IO<sub>3</sub> – H]<sup>-</sup>: 352.9675, found 352.9660; HPLC-MS (ESI) m/z; (λ = 235 nm): Rt = 12.57 min; 352.9666 [M – H]<sup>-</sup>.

**2-(2,4-Difluorophenoxy)-1-(4-hydroxyphenyl)ethan-1-one (2t):** The general procedure F was followed using the acetate **7t** (0.143 g, 0.492 mmol) in EtOH (5 mL) and NaOAc (0.404 g, 4.920 mmol) in water (1 mL). The crude residue was crystallized in cyclohexane to obtain **2t** as a white solid (0.060 g, 0.227 mmol) in 46% yield. R<sub>f</sub> = 0.23 (Cyclohexane/EtOAc, 7:3); <sup>1</sup>H NMR (500 MHz, DMSO-*d*<sub>6</sub>) δ: 10.47 (s, 1H, OH), 7.89 (d, *J*<sub>H-10,H-11</sub> = *J*<sub>H-14,H-13</sub> = 8.5 Hz, 2H, H-10, H-14), 6.89 (d, *J*<sub>H-13,H-14</sub> = *J*<sub>H-11,H-10</sub> = 8.5 Hz, 2H, H-11, H-13), 6.81–6.73 (m, 3H, H-3, H-5, H-6), 5.54 (s, 2H, H-7); <sup>13</sup>C NMR (126 MHz, DMSO-*d*<sub>6</sub>) δ: 191.5 (C-8), 163.0, 162.9 (2d, *J*<sub>C-2,F-2</sub> = *J*<sub>C-4,F-4</sub> = 243.4 Hz, C-2, C-4), 162.6 (C-12), 160.4 (d, *J*<sub>C-1,F-2</sub> = 14.6 Hz, C-1), 130.4 (C-10, C-14), 125.7 (C-9), 115.3 (C-11, C-13), 98.9 (2d, *J*<sub>C-5,F-4</sub> = 28.6 Hz, *J*<sub>C-6,F</sub> = 14.5 Hz, C-5, C-6), 96.2 (t, *J*<sub>C-3,F-2</sub> = *J*<sub>C-3,F-4</sub> = 26.5 Hz, C-3), 70.3 (C-7); IR ν<sub>max</sub>/cm<sup>-1</sup>: 3241, 1669, 1627, 1600, 1578, 1519, 1479, 1436, 1388, 1365, 1349, 1312, 1295, 1258, 1250, 1213, 1160, 1111, 1083, 1018, 1000, 992, 965, 859, 840,



823, 807, 734, 715; HRMS (ESI<sup>-</sup>) m/z: calcd for [C<sub>14</sub>H<sub>10</sub>F<sub>2</sub>O<sub>3</sub> – H]<sup>-</sup>: 263.0520, found 263.0511; HPLC-MS (ESI) m/z; (λ = 235 nm): Rt = 11.71 min; 263.0516 [M – H]<sup>-</sup>.

**4-(2-(4-Hydroxyphenyl)-2-oxoethoxy)benzenesulfonamide (2u):** The general procedure F was followed using 4-(2-(4-hydroxyphenyl)-2-oxoethoxy) benzenesulfonamide **7u** (0.068 g, 0.221 mmol) in EtOH (4 mL) and NaOAc (0.181 g, 2.221 mmol) in water (0,5 mL). The crude residue was purified by column chromatography on silica gel (DCM/MeOH, 9.9:0.1) to yield **2u** as a white solid (0.022 g, 0.071 mmol) in 33% yield. Rf = 0.10 (CH<sub>2</sub>Cl<sub>2</sub>/MeOH, 99:1); <sup>1</sup>H NMR (500 MHz, DMSO-*d*<sub>6</sub>) δ: 10.47 (s, 1H, OH), 7.90 (d, *J*<sub>H-10,H-11</sub> = *J*<sub>H-14,H-13</sub> = 9.0 Hz, 2H, H-10, H-14), 7.72 (d, *J*<sub>H-3,H-2</sub> = *J*<sub>H-5,H-6</sub> = 9.0 Hz, 2H, H-3, H-5), 7.18 (s, 2H, NH<sub>2</sub>), 7.08 (d, *J*<sub>H-2,H-3</sub> = *J*<sub>H-6,H-5</sub> = 9.0 Hz, 2H, H-2, H-6), 6.89 (d, *J*<sub>H-2,H-3</sub> = *J*<sub>H-6,H-5</sub> = 9.0 Hz, 2H, H-11, H-13), 5.58 (s, 2H, H-7); <sup>13</sup>C NMR (126 MHz, DMSO-*d*<sub>6</sub>) δ: 191.8 (C-8), 162.6 (C-12), 160.5 (C-1), 136.3 (C-4), 130.4 (C-10, C-14), 127.5 (C-3, C-5), 125.7 (C-9), 115.3 (C-2, C-6), 114.6 (C-11, C-13), 69.8 (C-7). IR ν<sub>max</sub>/cm<sup>-1</sup>: 3380, 3269, 3109, 2924, 1672, 1598, 1578, 1519, 1503, 1426, 1412, 1396, 1372, 1333, 1306, 1250, 1232, 1180, 1158, 1097, 1076, 994, 900, 824, 780; HRMS (ESI<sup>-</sup>) m/z: calcd for [C<sub>14</sub>H<sub>13</sub>NO<sub>5</sub>S – H]<sup>-</sup>: 306.0436, found 306.0428.

**2-(4-Bromo-2,6-dichlorophenoxy)-1-(4-hydroxyphenyl)ethan-1-one (2v):** The general procedure F was followed using the acetate **7v** (0.147 g, 0.351 mmol) in EtOH (6 mL) and NaOAc (0.287 g, 3.510 mmol) in water (1 mL). The crude residue was purified by column chromatography on silica gel (Cyclohexane/EtOAc, 7:3) to yield **2v** as a white solid (0.066 g, 0.175 mmol) in 50% yield. Rf = 0.45 (Cyclohexane/EtOAc, 7:3); <sup>1</sup>H NMR (500 MHz, DMSO-*d*<sub>6</sub>) δ: 10.47 (s, 1H, OH), 7.86 (d, *J*<sub>H-10,H-11</sub> = *J*<sub>H-14,H-13</sub> = 8.5 Hz, 2H, H-10, H-14), 7.82 (s, 2H, H-3, H-5), 6.86 (d, *J*<sub>H-11,H-10</sub> = *J*<sub>H-13,H-14</sub> = 8.5 Hz, 2H, H-11, H-13), 5.33 (s, 2H, H-7); <sup>13</sup>C NMR (126 MHz, DMSO-*d*<sub>6</sub>) δ: 190.7 (C-8), 162.6 (C-12), 150.1 (C-1), 131.6 (C-10, C-14), 130.5 (C-3, C-5), 129.4 (C-2, C-6), 125.5 (C-9), 116.5 (C-4), 115.4 (C-11, C-13), 74.3 (C-7); IR ν<sub>max</sub>/cm<sup>-1</sup>: 3169, 2971, 2901, 1667, 1601, 1573, 1556, 1518, 1455, 1429, 1416, 1394, 1381, 1294, 1248, 1219, 1172, 1065, 982, 879, 852, 840, 821, 800, 743; MS (ESI<sup>+</sup>) m/z: 374.90 [M + H]<sup>+</sup>; HRMS (ESI<sup>-</sup>) m/z: calcd for [C<sub>14</sub>H<sub>9</sub>BrCl<sub>2</sub>O<sub>3</sub> – H]<sup>-</sup>: 372.9034, found 372.9027; HPLC-MS (ESI) m/z; (λ = 235 nm): Rt = 13.54 min; 374.8999 [M + H]<sup>+</sup>.

**2-(4-Bromo-2-fluorophenoxy)-1-(4-hydroxyphenyl)ethan-1-one (2w):** The general procedure F was followed using 4-(2-(4-bromo-2-chlorophenoxy)acetyl)phenyl acetate **7w** (0.401 g, 1.045 mmol) in EtOH (8 mL) and NaOAc (0.857 g, 10.45 mmol) in water (1 mL). The crude residue was purified by column chromatography on silica gel (Cyclohexane/EtOAc, 7:3) to yield **2w** as a white solid (0.067 g, 0.206 mmol) in 35% yield.  $R_f = 0.31$  (Cyclohexane/EtOAc, 7:3);  $^1\text{H NMR}$  (500 MHz,  $\text{DMSO-}d_6$ )  $\delta$ : 10.48 (s, 1H, OH), 7.88 (d,  $J_{\text{H-10,H-11}} = J_{\text{H-14,H-13}} = 8.5$  Hz, 2H, H-10, H-14), 7.54 (dd,  $J_{\text{H-3,F}} = 11.0$  Hz,  $J_{\text{H-3,H-5}} = 1.0$  Hz, 1H, H-3), 7.27 (dd,  $J_{\text{H-5,H-6}} = 9.0$  Hz,  $J_{\text{H-5,H-3}} = 1.0$  Hz, 1H, H-5), 7.05 (t,  $J_{\text{H-6,H-5}} = J_{\text{H-6,F}} = 9.0$  Hz, 1H, H-6), 6.89 (d,  $J_{\text{H-11,H-10}} = J_{\text{H-13,H-14}} = 8.5$  Hz, 2H, H-11, H-13), 5.59 (s, 2H, H-7);  $^{13}\text{C NMR}$  (126 MHz,  $\text{DMSO-}d_6$ )  $\delta$ : 191.7 (C-8), 162.6 (C-12), 151.5 (d,  $J_{\text{C-2,F}} = 248.9$  Hz, C-2), 145.6 (d,  $J_{\text{C-1,F}} = 10.1$  Hz, C-1), 130.4 (C-10, C-14), 127.3 (d,  $J_{\text{C-5,F}} = 3.6$  Hz, C-5), 125.7 (C-9), 119.2 (d,  $J_{\text{C-3,F}} = 21.4$  Hz, C-3), 116.7 (C-6), 115.3 (C-11, C-13), 111.1 (d,  $J_{\text{C-4,F}} = 8.6$  Hz, C-4), 70.4 (C-7);  $^{19}\text{F}_{\text{cpd}}$  NMR (470 MHz,  $\text{DMSO-}d_6$ )  $\delta$ :  $-131.2$ ; IR  $\nu_{\text{max}}/\text{cm}^{-1}$ : 3304, 2988, 2971, 2922, 1681, 1603, 1579, 1506, 1438, 1409, 1391, 1307, 1278, 1268, 1253, 1246, 1222, 1203, 1182, 1136, 1110, 1084, 1066, 1056, 989, 879, 851, 834, 811, 804, 791, 708; HRMS (ESI $^-$ )  $m/z$ : calcd for  $[\text{C}_{14}\text{H}_{10}\text{BrFO}_3 - \text{H}]^-$ : 322.9719, found 322.9718; HPLC-MS (ESI)  $m/z$ ; ( $\lambda = 235$  nm):  $R_t = 12.54$  min; 322.9718  $[\text{M} - \text{H}]^-$ .

**2-(3-Hydroxyphenoxy)-1-(4-hydroxyphenyl)ethan-1-one (2x):** The general procedure F was followed using **7x** (0.469 g) in EtOH (7 mL) and NaOAc (0.600 g, 7.31 mmol) in water (1 mL). The crude residue was purified by column chromatography on silica gel (Cyclohexane/EtOAc, 6:4) to yield **2x** as a white solid (0.068 g, 0.278 mmol) in 25% yield.  $R_f = 0.25$  (Cyclohexane/EtOAc, 6:4);  $^1\text{H NMR}$  (500 MHz,  $\text{DMSO-}d_6$ )  $\delta$ : 10.44 (s, 1H, OH), 9.34 (s, 1H, OH), 7.90 (d,  $J_{\text{H-10,H-11}} = J_{\text{H-14,H-13}} = 9.0$  Hz, 2H, H-10, H-14), 7.02 (t,  $J_{\text{H-5,H-4}} = J_{\text{H-5,H-6}} = 8.0$  Hz, 1H, H-5), 6.88 (d,  $J_{\text{H-11,H-10}} = J_{\text{H-13,H-14}} = 9.0$  Hz, 2H, H-11, H-13), 6.35 (dd,  $J_{\text{H-6,H-5}} = 8.0$  Hz,  $J_{\text{H-6,H-2}} = 2.5$  Hz, 1H, H-6), 6.34 (dd,  $J_{\text{H-4,H-5}} = 8.0$  Hz,  $J_{\text{H-4,H-2}} = 2.5$  Hz, 1H, H-4), 6.30 (t,  $J_{\text{H-2,H-4}} = J_{\text{H-2,H-6}} = 2.5$  Hz, 1H, H-2), 5.34 (s, 2H, H-7);  $^{13}\text{C NMR}$  (126 MHz,  $\text{DMSO-}d_6$ )  $\delta$ : 192.6 (C-8), 162.5 (C-12), 159.2 (C-1), 158.4 (C-3), 130.4 (C-10, C-14), 129.7 (C-5), 125.9 (C-9), 115.3 (C-11, C-13), 108.0, 105.3 (C-4, C-6), 101.9 (C-2), 69.6 (C-7); IR  $\nu_{\text{max}}/\text{cm}^{-1}$ : 3660, 3324, 2988, 2901, 1682, 1601, 1593, 1510, 1493, 1450, 1434, 1383, 1332, 1284, 1241, 1183, 1159, 1100, 1109, 1078, 1066, 1057, 1002, 993, 876, 827,

762; HRMS (ESI<sup>-</sup>) m/z: calcd for [C<sub>14</sub>H<sub>12</sub>O<sub>4</sub> – H]<sup>-</sup>: 243.0657, found 243.0649; HPLC-MS (ESI) m/z; (λ = 235 nm): Rt = 8.16 min; 243.0648 [M – H]<sup>-</sup>.

**2-(3-Hydroxyphenoxy)-1-(4-hydroxyphenyl)ethan-1-one (2y):** The general procedure F was followed using **7y** (0.251 g) in EtOH (5 mL) and NaOAc (0.400 g, 4.87 mmol) in water (1 mL). The crude residue was purified by column chromatography on silica gel (Cyclohexane/EtOAc, 6:4) to yield **2y** as a white solid (0.021 g, 0.08 mmol) in 7% yield. R<sub>f</sub> = 0.125 (Cyclohexane/EtOAc, 7:3); <sup>1</sup>H NMR (500 MHz, DMSO-*d*<sub>6</sub>) δ: 10.50 (s, 1H, OH), 8.96 (s, 1H, OH), 7.88 (d, *J*<sub>H-10,H-11</sub> = *J*<sub>H-14,H-13</sub> = 9.0 Hz, 2H, H-10, H-14), 6.87 (d, *J*<sub>H-11,H-10</sub> = *J*<sub>H-13,H-14</sub> = 9.0 Hz, 2H, H-11, H-13), 6.75 (d, *J*<sub>H-3,H-2</sub> = *J*<sub>H-5,H-6</sub> = 8.5 Hz, 2H, H-3, H-5), 6.64 (d, *J*<sub>H-2,H-3</sub> = *J*<sub>H-6,H-5</sub> = 8.5 Hz, 2H, H-2, H-6), 5.26 (s, 2H, H-7); <sup>13</sup>C NMR (126 MHz, DMSO-*d*<sub>6</sub>) δ: 193.3 (C-8), 162.5 (C-12), 151.5, 151.0 (C-1, C-4), 130.5 (C-10, C-14), 126.2 (C-9), 115.7, 115.6, 115.5 (C-11, C-13, C-2, C-6, C-3, C-5), 70.5 (C-7); IR ν<sub>max</sub>/cm<sup>-1</sup>: 3430, 2918, 2850, 1654, 1600, 1589, 1514, 1506, 1446, 1433, 1360, 1291, 1263, 1236, 1212, 1169, 1121, 1108, 1085, 998, 987, 879, 835, 741; HRMS (ESI<sup>-</sup>) m/z: calcd for [C<sub>14</sub>H<sub>12</sub>O<sub>4</sub> – H]<sup>-</sup>: 243.0657, found 243.0649; HPLC-MS (ESI) m/z; (λ = 235 nm): Rt = 7.46 min; 243.0656 [M – H]<sup>-</sup>.

**4-(2-(4-Hydroxyphenyl)-2-oxoethoxy)benzoic acid (2z):** The general procedure F was followed using **7z** (0.305 g) in EtOH (5 mL) and NaOAc (0.500 g, 6.09 mmol) in water (1 mL). The crude residue was purified by column chromatography on silica gel (Cyclohexane/EtOAc/CH<sub>3</sub>COOH, 6:4:0.1) to yield **2z** as a white solid (0.029 g, 0.11 mmol) in 9% yield. R<sub>f</sub> = 0.16 (Cyclohexane/EtOAc, 6:4); <sup>1</sup>H NMR (500 MHz, DMSO-*d*<sub>6</sub>) δ: 10.47, 10.37 (2s, 2H, OH), 7.87 (d, *J*<sub>H-3,H-2</sub> = *J*<sub>H-5,H-6</sub> = *J*<sub>H-10,H-11</sub> = *J*<sub>H-14,H-13</sub> = 9.0 Hz, 4H, H-3, H-5, H-10, H-14), 6.89, 6.88 (2d, *J*<sub>H-2,H-3</sub> = *J*<sub>H-6,H-5</sub> = *J*<sub>H-11,H-10</sub> = *J*<sub>H-13,H-14</sub> = 9.0 Hz, 4H, H-2, H-6, H-11, H-13), 5.55 (s, 2H, H-7); <sup>13</sup>C NMR (126 MHz, DMSO-*d*<sub>6</sub>) δ: 190.9 (C-8), 165.1 (C-1), 162.6, 162.2 (C-12, CO<sub>2</sub>H), 131.7 (C-3, C-5), 130.3 (C-10, C-14), 125.6 (C-9), 119.9 (C-4), 115.4, 115.3 (C-2, C-6, C-11, C-13), 66.2 (C-7); IR ν<sub>max</sub>/cm<sup>-1</sup>: 3027, 2970, 2926, 1738, 1728, 1673, 1598, 1508, 1442, 1424, 1366, 1284, 1229, 1217, 1168, 1135, 1116, 973, 843, 764; HRMS (ESI<sup>-</sup>) m/z: calcd for [C<sub>15</sub>H<sub>12</sub>O<sub>5</sub> – H]<sup>-</sup>: 271.0606, found 271.0610; HPLC-MS (ESI) m/z; (λ = 235 nm): Rt = 9.31 min; 271.0606 [M – H]<sup>-</sup>.

**2-(4-Bromo-2-fluorophenoxy)-1-(3,4-dihydroxyphenyl)ethan-1-one (3):** The general procedure F was followed using compound **10** (0.221 g, 0.519 mmol) in EtOH (7 mL) and NaOAc (0.426 g, 82.03 mmol) in water (1 mL). The crude residue was purified by column chromatography on silica gel (Cyclohexane/EtOAc, 6:4) to yield **3** as a white solid (0.075 g, 0.219 mmol) in 42% yield.  $R_f = 0.08$  (Cyclohexane/EtOAc, 7:3);  $^1\text{H NMR}$  (500 MHz, DMSO- $d_6$ )  $\delta$ : 9.70 (s, 2H, OH), 7.54 (dd,  $J_{\text{H-3,F}} = 11.0$  Hz,  $J_{\text{H-3,H-5}} = 2.0$  Hz, 1H, H-3), 7.41 (d,  $J_{\text{H-10,H-11}} = 8.0$  Hz,  $J_{\text{H-10,H-14}} = 2.0$  Hz, 1H, H-10), 7.35 (d,  $J_{\text{H-14,H-10}} = 2.0$  Hz, 1H, H-14), 7.26 (dt,  $J_{\text{H-5,H-6}} = 9.0$  Hz,  $J_{\text{H-5,H-3}} = J_{\text{H-5,F}} = 2.0$  Hz, 1H, H-5), 7.02 (t,  $J_{\text{H-6,H-5}} = J_{\text{H-6,F}} = 9.0$  Hz, 1H, H-6), 6.84 (d,  $J_{\text{H-11,H-10}} = 8.0$  Hz, 1H, H-11), 5.56 (s, 2H, H-7);  $^{13}\text{C NMR}$  (126 MHz, DMSO- $d_6$ )  $\delta$ : 191.7 (C-8), 151.4 (d,  $J_{\text{C-2,F}} = 249.3$  Hz, C-2), 151.4 (C-12), 145.7 (d,  $J_{\text{C-1,F}} = 10.0$  Hz, C-1), 145.4 (C-13), 127.3 (C-5), 125.9 (C-9), 121.2 (C-10), 119.2 (d,  $J_{\text{C-3,F}} = 21.8$  Hz, C-3), 116.7 (C-6), 115.1 (C-11), 114.6 (C-14), 111.1 (d,  $J_{\text{C-4,F}} = 8.2$  Hz, C-4), 70.3 (C-7);  $^{19}\text{F}_{\text{cpd}}$  NMR (470 MHz, DMSO- $d_6$ )  $\delta$ : -131.3; IR  $\nu_{\text{max}}/\text{cm}^{-1}$ : 3479, 3277, 1692, 1602, 1521, 1506, 1474, 1437, 1387, 1337, 1287, 1276, 1265, 1211, 1188, 1129, 1082, 1015, 948, 909, 882, 846, 819, 794; HRMS (ESI $^-$ )  $m/z$ : calcd for  $[\text{C}_{14}\text{H}_{10}\text{BrFO}_4 - \text{H}]^-$ : 338.9668, found 338.9669; HPLC-MS (ESI)  $m/z$ ; ( $\lambda = 235$  nm):  $R_t = 11.69$  min; 340.9645  $[\text{M} - \text{H}]^-$ .

**2-(4-Bromo-2-fluorophenoxy)-1-(3-fluoro-4-hydroxyphenyl)ethan-1-one (4a):** The general procedure F was followed using **13a** (0.381 g, 0.0989 mmol) in EtOH (6 mL) and NaOAc (0.811 g, 9.89 mmol) in water (1 mL). The crude residue was purified by column chromatography on silica gel (Cyclohexane/EtOAc, 8:2) to yield **4a** as a white solid (0.059 g, 0.171 mmol) in 17% yield over two steps.  $R_f = 0.28$  (Cyclohexane/EtOAc, 7:3);  $^1\text{H NMR}$  (500 MHz, DMSO- $d_6$ )  $\delta$ : 11.01 (s, 1H, OH), 7.79 (dd,  $J_{\text{H-14,F-13}} = 11.5$  Hz,  $J_{\text{H-14,H-10}} = 1.5$  Hz, 1H, H-14), 7.71 (dd,  $J_{\text{H-10,H-11}} = 8.5$  Hz,  $J_{\text{H-10,H-14}} = 1.5$  Hz, 1H, H-10), 7.55 (dd,  $J_{\text{H-3,F-2}} = 11.0$  Hz,  $J_{\text{H-3,H-5}} = 2.0$  Hz, 1H, H-3), 7.28 (dd,  $J_{\text{H-5,H-6}} = 9.0$  Hz,  $J_{\text{H-5,H-3}} = 2.0$  Hz, 1H, H-5), 7.08 (t,  $J_{\text{H-6,H-5}} = J_{\text{H-11,H-10}} = 9.0$  Hz, 2H, H-6, H-11), 5.61 (s, 2H, H-7);  $^{13}\text{C NMR}$  (126 MHz, DMSO- $d_6$ )  $\delta$ : 191.3 (C-8), 151.4 (d,  $J_{\text{C-2,F}} = 248.9$  Hz, C-2), 150.6 (d,  $J_{\text{C-13,F}} = 242.9$  Hz, C-13), 150.5 (C-12), 145.5 (d,  $J_{\text{C-1,F-1}} = 10.1$  Hz, C-1), 127.3 (d,  $J = 3.6$  Hz, C-5), 125.8 (C-9), 125.6 (C-10), 119.2 (d,  $J_{\text{C-3,F}} = 21.4$  Hz, C-3), 117.5, 116.7 (C-6, C-11), 115.9 (d,  $J_{\text{C-14,F}} = 19.2$  Hz, C-14), 111.2 (d,  $J_{\text{C-4,F}} = 8.2$  Hz, C-4), 70.5 (C-7);  $^{19}\text{F NMR}$  (470 MHz, DMSO- $d_6$ )  $\delta$ : -131.3 (t,  $J = 9.4$  Hz), -135.8 (dd,  $J = 11.3$  Hz,  $J = 9.4$  Hz);  $^{19}\text{F}_{\text{cpd}}$  NMR (470 MHz, DMSO- $d_6$ )  $\delta$ :

–131.3, –135.8; IR  $\nu_{\max}/\text{cm}^{-1}$ : 3026, 2970, 2946, 1728, 1669, 1587, 1527, 1491, 1455, 1448, 1434, 1366, 1314, 1277, 1260, 1229, 1217, 1205, 1177, 1135, 1063, 1013, 891, 828, 818, 785; HRMS (ESI<sup>-</sup>) m/z: calcd for [C<sub>14</sub>H<sub>9</sub>BrF<sub>2</sub>O<sub>3</sub> – H]<sup>-</sup>: 340.9625, found 340.9621; HPLC-MS (ESI) m/z; ( $\lambda$  = 235 nm): Rt = 12.87 min; 340.9621 [M – H]<sup>-</sup>.

**2-(4-Bromo-2-fluorophenoxy)-1-(3,5-difluoro-4-hydroxyphenyl)ethan-1-one: (4b):** The general procedure F was followed using **13b** (0.236 g) in EtOH (5 mL) and NaOAc (0.480 g, 5.85 mmol) in water (0.5 mL). The crude residue was purified by column chromatography on silica gel (Cyclohexane/EtOAc, 8:2) and triturated in pentane to yield **4b** (0.013 g, 0.036 mmol) in 20% yield over two steps. Rf = 0.25 (Cyclohexane/EtOAc, 7:3); <sup>1</sup>H NMR (500 MHz, DMSO-*d*<sub>6</sub>)  $\delta$ : 11.44 (s, 1H, OH), 7.71 (d,  $J_{\text{H-10, F-11}} = J_{\text{H-14, F}} = 7.5$  Hz, 2H, H-10, H-14), 7.55 (dd,  $J_{\text{H-3, F}} = 10.5$  Hz,  $J_{\text{H-3, H-5}} = 1.5$  Hz, 1H, H-3), 7.29 (brd,  $J_{\text{H-5, H-6}} = 8.5$  Hz, 1H, H-5), 7.10 (t,  $J_{\text{H-6, H-5}} = J_{\text{H-6, F}} = 8.5$  Hz, 1H, H-6), 5.62 (s, 2H, H-7); <sup>13</sup>C NMR (126 MHz, DMSO-*d*<sub>6</sub>)  $\delta$ : 190.9 (C-8), 151.8 (dd,  $J_{\text{C-11, F-11}} = J_{\text{C-13, F-13}} = 244.3$  Hz,  $J_{\text{C-11, F-13}} = J_{\text{C-13, F-11}} = 7.3$  Hz, C-11, C-13), 151.4 (d,  $J_{\text{C-2, F}} = 248.8$  Hz, C-2), 145.4 (d,  $J_{\text{C-1, F}} = 10.5$  Hz, C-1), 139.4 (C-12), 127.4 (C-5), 127.3 (C-9), 119.3 (d,  $J_{\text{C-3, F}} = 20.9$  Hz, C-3), 116.8 (C-6), 112.0 (d,  $J = 22.3$  Hz, C-10, C-14), 112.0 (d,  $J_{\text{C-4, F}} = 8.8$  Hz, C-4), 70.6 (C-7); <sup>19</sup>F NMR (470 MHz, DMSO-*d*<sub>6</sub>)  $\delta$ : –131.2 (t,  $J = 9.4$  Hz), –131.4 (s); <sup>19</sup>F<sub>cpd</sub> NMR (470 MHz, DMSO-*d*<sub>6</sub>)  $\delta$ : –131.2, –131.4; IR  $\nu_{\max}/\text{cm}^{-1}$ : 3178, 2921, 1685, 1619, 1591, 1530, 1493, 1440, 1409, 1388, 1334, 1276, 1254, 1199, 1174, 1120, 1072, 1063, 1030, 1012, 914, 891, 858, 836, 813, 785, 747, 719; HRMS (ESI<sup>-</sup>) m/z: calcd for [C<sub>14</sub>H<sub>8</sub>BrF<sub>3</sub>O<sub>3</sub> – H]<sup>-</sup>: 358.9531, found 358.9524; HPLC-MS (ESI) m/z; ( $\lambda$  = 235 nm): Rt = 13.42 min; 358.9537 [M – H]<sup>-</sup>.

Synthesis of compounds **5-13** and spectra of all final compounds are found in the Supporting Information.

## Pharmacology

### *Cell Culture and Transfection.*

HEK293 cells were transiently transfected with rat mGlu receptors encoding plasmids by electroporation and cultured in Dulbecco's modified Eagle's medium (Life Technologies, Cergy

Pontoise, France) supplemented with 10% of fetal bovine serum. Cells were seeded in polyornithine-coated 96-well plates at a density of 150 000 cells/well.

*IP-One Functional Assay.* To monitor receptor signalling activity through inositol monophosphate (IP1) production, group II and group III mGlu receptors were cotransfected with the chimeric Gq $\alpha$ 9 protein to allow their coupling to the phospholipase C pathway. Experiments were conducted 24h after transfection and IP1 production was measured using the IP-One HTRF kit (Revvity, Codolet, France) according to the manufacturer's recommendations. Experiments were performed in triplicates, and data were analysed using Prism software (GraphPad, La Jolla, CA, USA).

#### *Mutations.*

For the generation of rat mGlu7 mutants, the Snap-tagged reference receptor was subjected to site-directed mutagenesis following QuickChange™ mutagenesis protocol from Agilent Technologies.

#### *Binding experiments.*

[<sup>3</sup>H]-LY341495 binding experiments. Culture of CHO cells expressing mGlu receptors and preparation of membranes were done as described by Mitsukawa et al. (2005)<sup>13</sup> and by references therein. [<sup>3</sup>H]-LY341495 binding was conducted essentially as previously described by Johnson et al. (1999)<sup>38</sup> and Wright et al. (2000).<sup>39</sup>

## **Molecular modeling**

All the molecular modeling methods were performed within Discovery Studio 2019.<sup>28</sup>

#### *Homology models.*

All starting structures went through the "Prepare Protein" protocol, which allows standardizing the atom names, inserting missing atoms and removing the alternate conformations. It also inserts missing loops smaller than 20 residues, and performs a quick minimization on them. Additionally, after the insertion of the larger missing loops (above 5 residues), we performed further optimization on them using MODELER<sup>40</sup> functionalities ("Build Homology Models" and "Loop Refinement") as

implemented in Discovery Studio. We systematically asked for a 100 models and selected the model with the best *PDF Total energy*. For the  $\alpha 2$ - $\beta 6$  loop, we first refined the cryo-EM structure loop of the mGlu5 receptor 6N52<sup>41</sup> (for the Roo model) and 6N51<sup>41</sup> (for the Acc model). Because in the mGlu7 receptor this loop is three residues shorter, we built a homology model from the mGlu5 receptor refined loop (from the  $\alpha 2$  helix to the  $\beta 6$  sheet) (**Table S3 & S5**). For the  $\beta 10$ - $\alpha 7$  loop, we built a homology model based upon the mGlu8 receptor crystal structure 6BSZ and selected the model with the best *PDF Total energy* out of 100 loop models (**Table S4**).

For every region that were modeled, we carried out a short minimization cascade reducing progressively the constraints (from 15 to 0 kcal / mol, with 5 kcal / mol steps). During those minimizations, the backbone of the other regions was heavily constraint (50 kcal / mol) and the side-chain were left free. All force-field based simulations were carried out in CHARMM 42.2.<sup>42</sup>

#### *Docking experiments.*

The docking experiments were carried out using GOLD<sup>31</sup> as implemented within Discovery Studio. With this protocol, we were able to perform the docking with flexible side chains as well as specify some interaction sites that could act as constraints for the docking (similar to a pharmacophoric feature).

Seven sites were defined for the docking of L-AP4 and LSP4-2022, based on the mutagenesis data and the known binding mode of the glutamate like moieties:

- H-bond donor sites on R78 side chain primary amines / on S159 side chain alcohol and backbone amine / on K319 and K407 side chain amine.
- H-bond acceptor on T182 side chain alcohol

Ligand poses were scored using the CHEMPLP scoring function<sup>34</sup>, and chose the Automatic Very Flexible pre-defined Generic Algorithm (GA) setting.

#### *Molecular dynamics simulations.*

The systems were typed using the charmm36 forcefield<sup>43</sup> for the protein and the MATCH algorithm<sup>44</sup> for the ligands. Then, we solvated our system in an orthorhombic cell around the protein with TIP3P

water molecules, sodium cation and chloride anions. The distance of the protein from the boundaries was set at 7 Å. All the following simulations were carried in periodic boundary condition with a NPT ensemble (constant pressure and temperature) at 300K, with a pair list distance of 14 Å and a local interaction cutoff at 12 Å. Moreover SHAKE was applied to constrain all covalent bonds involving hydrogens. After solvation we carried out a “Standard Dynamics Cascade” protocol which consist in two minimization steps, one heating step (10 ps) and one equilibration step (40 ps). This protocol uses CHARMM. Then the production phase was carried out with NAMD 2.13<sup>45</sup> GPU version in the same conditions.

## ASSOCIATED CONTENT

The Supporting Information is available: Synthesis of compounds **5-13**. <sup>1</sup>H NMR and <sup>13</sup>C NMR and HPLC traces of compounds. Figures S1-S7. Tables S1-S5 (PDF).

3D-model of **XAP044** docked at mGlu7 VFT (PDB).

Molecular formula strings (CSV).

## AUTHOR INFORMATION

### Corresponding author

**Francine C. Acher** - Saints-Pères Paris Institute for the Neurosciences, Université Paris Cité, CNRS UMR 8003, 75006 Paris, France ; Laboratoire de Chimie et Biochimie Pharmacologiques et Toxicologiques, Université Paris Cité, CNRS UMR 8601, 75006 Paris, France ; [orcid.org/0000-0002-5413-4181](https://orcid.org/0000-0002-5413-4181) ; E-mail : [francine.acher@parisdescartes.fr](mailto:francine.acher@parisdescartes.fr)

### Authors

**Nunzia Cristiano** - *Laboratoire de Chimie et Biochimie Pharmacologiques et Toxicologiques, Université Paris Cité, CNRS UMR 8601, 75006 Paris, France* ; Present Address : French National Agency for the Safety of Medicines and Health Products, 93200 Saint-Denis, France



**Alexandre Cabayé** - *Laboratoire de Chimie et Biochimie Pharmacologiques et Toxicologiques, Université Paris Cité, CNRS UMR 8601, 75006 Paris, France ; BIOVIA Dassault Systèmes, F-78140, Vélizy-Villacoublay Cedex, France ; Present Address : BIOVIA Dassault Systèmes, F-78140, Vélizy-Villacoublay Cedex, France*

**Isabelle Brabet** - *Institute of Functional Genomics, University of Montpellier, CNRS, Inserm, 34094 Montpellier, France*

**Ralf Glatthar** - *Novartis Biomedical Research, CH-4002 Basel, Switzerland*

**Amélie Tora** - *Institute of Functional Genomics, University of Montpellier, CNRS, Inserm, 34094 Montpellier, France*

**Cyril Goudet** - *Institute of Functional Genomics, University of Montpellier, CNRS, Inserm, 34094 Montpellier, France; orcid.org/0000-0002-8255-3535*

**Hugues-Olivier Bertrand** - *BIOVIA Dassault Systèmes, F-78140, Vélizy-Villacoublay Cedex, France*

**Anne Goupil-Lamy** – *BIOVIA Dassault Systèmes, F-78140, Vélizy-Villacoublay Cedex, France; orcid.org/0009-0002-2828-2639*

**Peter J. Flor** - *Laboratory of Molecular and Cellular Neurobiology, Faculty of Biology and Preclinical Medicine, University of Regensburg, 93053 Regensburg, Germany*

**Jean-Philippe Pin** - *Institute of Functional Genomics, University of Montpellier, CNRS, Inserm, 34094 Montpellier, France; orcid.org/0000-0002-1423-345X*

**Isabelle McCort-Tranchepain** - *Laboratoire de Chimie et Biochimie Pharmacologiques et Toxicologiques, Université Paris Cité, CNRS UMR 8601, 75006 Paris, France; orcid.org/0000-0001-7447-8806*

### **Author Contributions**

NC and AC are equally contributing first authors. NC performed the synthetic chemistry supervised by IMcC and FA. AC performed the modeling experiments supervised by HOB, AGL and FA. IB and AT performed the pharmacological assays supervised by CG and JPP. RG and PF initiated the project with

an input in the drug design. FA wrote the paper with contributions from the other authors. All authors have given approval to the final version of the manuscript.

## Notes

The authors declare no competing financial interest.

## ACKNOWLEDGMENTS

NC and AT have been the recipient of a scholarship from the Ministère de l'Éducation Nationale de la Recherche et de la Technologie. AT was also funded by the Fondation pour la Recherche Médicale (FDT20140931071). AC was supported by the Association Nationale de la Recherche et de la Technologie (ANRT) and Dassault Systèmes BIOVIA (CIFRE PhD scholarship no. 2018/0027). This work was funded by the French National Agency for Research (ANR-13-BSV1-0006). The Science Ambassador Program from Dassault Systèmes BIOVIA is acknowledged for the support of FA. The Pharmacological assays on recombinant mGlu receptors were performed at the ARPEGE (Pharmacology Screening-Interactome) platform facility at the Institute of Functional Genomics (Montpellier, France) which is acknowledged.

## ABBREVIATIONS

AC, adenylyl cyclase; Acc, active closed-closed state; AMN082, N,N'-dibenzhydrylethane-1,2-diamine; ADX71743, 6-(2,4-dimethylphenyl)-2-ethyl-6,7-dihydrobenzo[d]oxazol-4(5H)-one; CNS, Central nervous system; CRD, Cysteine rich domain; CVN636, (S)-2-(4-fluorophenyl)-N-((3S,4S)-4-(methylsulfonyl)chroman-3-yl)propanamide; 3,5-DHPG, 3,5-dihydroxyphenylglycine; EC<sub>50</sub>, half maximal effective concentration; GABA, Gamma-AminoButyric Acid; GPCR, G-protein coupled receptor; IC<sub>50</sub>, half maximal inhibitory concentration; iGlu receptor, ionotropic glutamate receptor; L-AP4, L-2-amino-4-phosphonobutyric acid; LSP, Laboratoire des Saints-Pères; LSP4-2022, (2S)-2-amino-4-(((4-(carboxymethoxy)phenyl)(hydroxy)methyl)(hydroxy)phosphoryl)butanoic acid; LSP2-9166, (2S)-2-amino-4-(((4-(carboxymethoxy)-3-(trifluoromethyl)phenyl)(hydroxy)methyl)(hydroxy)phosphoryl)butanoic acid; LY354740,

(1*S*,2*S*,5*R*,6*S*)-2-aminobicyclo[3.1.0]hexane-2,6-dicarboxylic acid; LY341495, (2*S*)-2-amino-2-[(1*S*,2*S*)-2-carboxycycloprop-1-yl]-3-(xanth-9-yl)propanoic acid;  $\mu$ M, micro molar; MD, molecular dynamics; mGlu receptor, metabotropic glutamate receptor; MMPIP, 6-(4-methoxyphenyl)-5-methyl-3-pyridin-4-ylisoxazolo[4,5-*c*]pyridin-4(5*H*)-one; NAM, negative allosteric modulators; PAM, positive allosteric modulators; PDB, protein data bank; SAR, structure activity relationship; PLC, phospholipase C; Roo, resting open-open state; SEM standard error of the mean; 7TM, 7 transmembrane domain; VFT, venus flytrap domain; VU6027459, 8-( $\lambda^4$ -oxidaneyl-*d*3)-6-fluoro-4-(4-(2-fluorophenyl)piperazin-1-yl)quinoline-3-carbonitrile; VU6046980, (*S*)-6-fluoro-4-(10-fluoro-1,2,4*a*,5-tetrahydrobenzo[*b*]pyrazino[1,2-*d*][1,4]oxazin-3(4*H*)-yl)-8-methoxycinnoline-3-carbonitrile; WT, wild type; XAP044, 7-hydroxy-3-(4-iodophenoxy)-4*H*-chromen-4-one; XAP044, 7-hydroxy-3-(4-iodophenoxy)-4*H*-chromen-4-one.

## REFERENCES and NOTES

- (a) Neves, D.; Salazar, I. L.; Almeida, R. D.; Silva, R. M., Molecular mechanisms of ischemia and glutamate excitotoxicity. *Life Sci* **2023**, 121814; (b) Chen, T. S.; Huang, T. H.; Lai, M. C.; Huang, C. W., The Role of Glutamate Receptors in Epilepsy. *Biomedicines* **2023**, *11* (3); (c) Zhang, Z.; Zhang, S.; Fu, P.; Lin, K.; Ko, J. K.; Yung, K. K., Roles of Glutamate Receptors in Parkinson's Disease. *Int J Mol Sci* **2019**, *20* (18); (d) Girgis, R. R.; Zoghbi, A. W.; Javitt, D. C.; Lieberman, J. A., The past and future of novel, non-dopamine-2 receptor therapeutics for schizophrenia: A critical and comprehensive review. *J Psychiatr Res* **2019**, *108*, 57-83; (e) Wolf, M. E., Synaptic mechanisms underlying persistent cocaine craving. *Nat Rev Neurosci* **2016**, *17* (6), 351-65; (f) Fries, G. R.; Saldana, V. A.; Finnstein, J.; Rein, T., Molecular pathways of major depressive disorder converge on the synapse. *Mol Psychiatry* **2023**, *28* (1), 284-297; (g) Temmermand, R.; Barrett, J. E.; Fontana, A. C. K., Glutamatergic systems in neuropathic pain and emerging non-opioid therapies. *Pharmacol Res* **2022**, *185*, 106492.
- Lv, S.; Yao, K.; Zhang, Y.; Zhu, S., NMDA receptors as therapeutic targets for depression treatment: Evidence from clinical to basic research. *Neuropharmacology* **2023**, *225*, 109378.
- Crupi, R.; Impellizzeri, D.; Cuzzocrea, S., Role of Metabotropic Glutamate Receptors in Neurological Disorders. *Front Mol Neurosci* **2019**, *12*, 20.
- (a) Kinon, B. J.; Millen, B. A.; Zhang, L.; McKinzie, D. L., Exploratory analysis for a targeted patient population responsive to the metabotropic glutamate 2/3 receptor agonist pomaglumetad methionil in schizophrenia. *Biol Psychiatry* **2015**, *78* (11), 754-62; (b) Rascol, O.; Medori, R.; Baayen, C.; Such, P.; Meulien, D., A Randomized, Double-Blind, Controlled Phase II Study of Foliclurax in Parkinson's Disease. *Mov Disord* **2022**, *37* (5), 1088-1093.
- Watanabe, M.; Marcy, B.; Kinoshita, K.; Fukasawa, M.; Hikichi, H.; Chaki, S.; Okuyama, S.; Gevorkyan, H.; Yoshida, S., Safety and pharmacokinetic profiles of MGS0274 besylate (TS-134), a novel metabotropic glutamate 2/3 receptor agonist prodrug, in healthy subjects. *Br J Clin Pharmacol* **2020**, *86* (11), 2286-2301.
- Acher, F.; Battaglia, G.; Bräuner-Osborne, H.; Conn, P. J.; Duvoisin, R.; Ferraguti, F.; Flor, P. J.; Goudet, C.; Gregory, K. J.; Hampson, D.; Johnson, M. P.; Kubo, Y.; Monn, J.; Nakanishi, S.; Nicoletti, F.; Niswender, C.; Pin, J. P.; Rondard, P.; Schoepp, D. D.; Shigemoto, R.; Tateyama, M., Metabotropic glutamate receptors in GtoPdb v.2023.1. *IUPHAR/BPS Guide to Pharmacology CITE*. **2023**, Available from: <https://doi.org/10.2218/gtopdb/F40/2023.1>.
- (a) Sansig, G.; Bushell, T. J.; Clarke, V. R.; Rozov, A.; Burnashev, N.; Portet, C.; Gasparini, F.; Schmutz, M.; Klebs, K.; Shigemoto, R.; Flor, P. J.; Kuhn, R.; Knoepfel, T.; Schroeder, M.; Hampson, D. R.; Collett, V. J.; Zhang, C.; Duvoisin, R. M.; Collingridge, G. L.; van Der Putten, H., Increased seizure susceptibility in mice lacking metabotropic glutamate receptor 7. *J Neurosci* **2001**, *21* (22), 8734-45; (b) Fisher, N. M.; Gould, R. W.; Gogliotti, R. G.; McDonald, A. J.; Badivuku, H.; Chennareddy, S.; Buch, A. B.; Moore, A. M.; Jenkins, M. T.; Robb, W. H.; Lindsley, C. W.; Jones, C. K.; Conn, P. J.; Niswender, C. M., Phenotypic profiling of mGlu(7) knockout mice reveals new implications for neurodevelopmental disorders. *Genes Brain Behav* **2020**, *19* (7), e12654.
- Fisher, N. M.; AlHashim, A.; Buch, A. B.; Badivuku, H.; Samman, M. M.; Weiss, K. M.; Cestero, G. I.; Does, M. D.; Rook, J. M.; Lindsley, C. W.; Conn, P. J.; Gogliotti, R. G.; Niswender, C. M., A GRM7 mutation associated with developmental delay reduces mGlu7 expression and produces neurological phenotypes. *JCI Insight* **2021**, *6* (4).
- Fisher, N. M.; Seto, M.; Lindsley, C. W.; Niswender, C. M., Metabotropic Glutamate Receptor 7: A New Therapeutic Target in Neurodevelopmental Disorders. *Front Mol Neurosci* **2018**, *11*, 387.
- Acher, F. C.; Cabaye, A.; Eshak, F.; Goupil-Lamy, A.; Pin, J. P., Metabotropic glutamate receptor orthosteric ligands and their binding sites. *Neuropharmacology* **2022**, *204*, 108886.

11. Reed, C. W.; Kalbfleisch, J. J.; Wong, M. J.; Washecheck, J. P.; Hunter, A.; Rodriguez, A. L.; Blobaum, A. L.; Conn, P. J.; Niswender, C. M.; Lindsley, C. W., Discovery of VU6027459: A First-in-Class Selective and CNS Penetrant mGlu(7) Positive Allosteric Modulator Tool Compound. *ACS Med Chem Lett* **2020**, *11* (9), 1773-1779.
12. Kalbfleisch, J. J.; Rodriguez, A. L.; Lei, X.; Weiss, K.; Blobaum, A. L.; Boutaud, O.; Niswender, C. M.; Lindsley, C. W., Persistent challenges in the development of an mGlu(7) PAM in vivo tool compound: The discovery of VU6046980. *Bioorg Med Chem Lett* **2023**, *80*, 129106.
13. Mitsukawa, K.; Yamamoto, R.; Ofner, S.; Nozulak, J.; Pescott, O.; Lukic, S.; Stoehr, N.; Mombereau, C.; Kuhn, R.; McAllister, K. H.; van der Putten, H.; Cryan, J. F.; Flor, P. J., A selective metabotropic glutamate receptor 7 agonist: activation of receptor signaling via an allosteric site modulates stress parameters in vivo. *Proc Natl Acad Sci U S A* **2005**, *102* (51), 18712-7.
14. Dickson, L.; Teall, M.; Chevalier, E.; Cheung, T.; Liwicki, G. M.; Mack, S.; Stephenson, A.; White, K.; Fosbeary, R.; Harrison, D. C.; Brice, N. L.; Doyle, K.; Ciccocioppo, R.; Wu, C.; Almond, S.; Patel, T. R.; Mitchell, P.; Barnes, M.; Ayscough, A. P.; Dawson, L. A.; Carlton, M.; Burli, R. W., Discovery of CVN636: A Highly Potent, Selective, and CNS Penetrant mGluR(7) Allosteric Agonist. *ACS Med Chem Lett* **2023**, *14* (4), 442-449.
15. Suzuki, G.; Tsukamoto, N.; Fushiki, H.; Kawagishi, A.; Nakamura, M.; Kurihara, H.; Mitsuya, M.; Ohkubo, M.; Ohta, H., In vitro pharmacological characterization of novel isoxazolopyridone derivatives as allosteric metabotropic glutamate receptor 7 antagonists. *J Pharmacol Exp Ther* **2007**, *323* (1), 147-56.
16. Kalinichev, M.; Rouillier, M.; Girard, F.; Royer-Urios, I.; Bournique, B.; Finn, T.; Charvin, D.; Campo, B.; Le Poul, E.; Mutel, V.; Poli, S.; Neale, S. A.; Salt, T. E.; Lutjens, R., ADX71743, a potent and selective negative allosteric modulator of metabotropic glutamate receptor 7: in vitro and in vivo characterization. *J Pharmacol Exp Ther* **2013**, *344* (3), 624-36.
17. Gee, C. E.; Peterlik, D.; Neuhauser, C.; Bouhelal, R.; Kaupmann, K.; Laue, G.; Uschold-Schmidt, N.; Feuerbach, D.; Zimmermann, K.; Ofner, S.; Cryan, J. F.; van der Putten, H.; Fendt, M.; Vranesic, I.; Glatthar, R.; Flor, P. J., Blocking metabotropic glutamate receptor subtype 7 (mGlu7) via the Venus flytrap domain (VFTD) inhibits amygdala plasticity, stress, and anxiety-related behavior. *The Journal of biological chemistry* **2014**, *289* (16), 10975-10987.
18. (a) Sukoff Rizzo, S. J.; Leonard, S. K.; Gilbert, A.; Dollings, P.; Smith, D. L.; Zhang, M. Y.; Di, L.; Platt, B. J.; Neal, S.; Dwyer, J. M.; Bender, C. N.; Zhang, J.; Lock, T.; Kowal, D.; Kramer, A.; Randall, A.; Huselton, C.; Vishwanathan, K.; Tse, S. Y.; Butera, J.; Ring, R. H.; Rosenzweig-Lipson, S.; Hughes, Z. A.; Dunlop, J., The metabotropic glutamate receptor 7 allosteric modulator AMN082: a monoaminergic agent in disguise? *J Pharmacol Exp Ther* **2011**, *338* (1), 345-52; (b) Ahnaou, A.; Raeyemaekers, L.; Huysmans, H.; Drinkenburg, W., Off-target potential of AMN082 on sleep EEG and related physiological variables: Evidence from mGluR7 (-/-) mice. *Behav Brain Res* **2016**, *311*, 287-297.
19. Miller, C. P.; Collini, M. D.; Harris, H. A., Constrained phytoestrogens and analogues as ERbeta selective ligands. *Bioorg Med Chem Lett* **2003**, *13* (14), 2399-403.
20. Chemicalize, Chemaxon. <https://chemicalize.com/> **2023**.
21. Perrin, C. L.; Nielson, J. B., "Strong" hydrogen bonds in chemistry and biology. *Annu Rev Phys Chem* **1997**, *48*, 511-44.
22. Moller, T. C.; Moreno-Delgado, D.; Pin, J. P.; Kniazeff, J., Class C G protein-coupled receptors: reviving old couples with new partners. *Biophys Rep* **2017**, *3* (4), 57-63.
23. Liu, L.; Lin, L.; Shen, C.; Rondard, P.; Pin, J. P.; Xu, C.; Liu, J., Asymmetric activation of dimeric GABA(B) and metabotropic glutamate receptors. *Am J Physiol Cell Physiol* **2023**, *325* (1), C79-C89.
24. (a) Grushevskiy, E. O.; Kukaj, T.; Schmauder, R.; Bock, A.; Zabel, U.; Schwabe, T.; Benndorf, K.; Lohse, M. J., Stepwise activation of a class C GPCR begins with millisecond dimer rearrangement. *Proc Natl Acad Sci U S A* **2019**, *116* (20), 10150-10155; (b) Du, J.; Wang, D.; Fan, H.; Xu, C.; Tai, L.; Lin, S.; Han, S.; Tan, Q.; Wang, X.; Xu, T.; Zhang, H.; Chu, X.; Yi, C.; Liu, P.;

- Zhou, Y.; Pin, J. P.; Rondard, P.; Liu, H.; Liu, J.; Sun, F.; Wu, B.; Zhao, Q., Structures of human mGlu2 and mGlu7 homo- and heterodimers. *Nature* **2021**, *594* (7864), 589-593.
25. Muto, T.; Tsuchiya, D.; Morikawa, K.; Jingami, H., Structures of the extracellular regions of the group II/III metabotropic glutamate receptors. *Proc Natl Acad Sci U S A* **2007**, *104* (10), 3759-64.
  26. Dobrovetsky, E.; Khutoreskaya, G.; Seitova, A.; He, H.; Edwards, A. M.; Arrowsmith, C. H.; Bountra, C.; Weigelt, J.; Cossar, D.; Bochkarev, A.; Structural Genomics Consortium, S., Metabotropic Glutamate Receptor mGluR7 Complexed with LY341495 Antagonist. **2010**, <https://doi.org/10.2210/pdb3MQ4/pdb>.
  27. Dong, A.; Dobrovetsky, E.; Hutchinson, A.; Tempel, W.; Edwards, A. M.; Bountra, C.; Arrowsmith, C. H.; Structural Genomics Consortium, S., Human metabotropic glutamate receptor 7, extracellular ligand binding domain. **2015**, <https://doi.org/10.2210/pdb5C5C/pdb>.
  28. DassaultSystèmesBIOVIA, "Discovery Studio Modeling Environment ", Release 2019, San Diego CA USA: Dassault Systèmes, 2019.
  29. Schkeryantz, J. M.; Chen, Q.; Ho, J. D.; Atwell, S.; Zhang, A.; Vargas, M. C.; Wang, J.; Monn, J. A.; Hao, J., Determination of L-AP4-bound human mGlu8 receptor amino terminal domain structure and the molecular basis for L-AP4's group III mGlu receptor functional potency and selectivity. *Bioorg Med Chem Lett* **2018**, *28* (4), 612-617.
  30. Selvam, C.; Lemasson, I. A.; Brabet, I.; Oueslati, N.; Karaman, B.; Cabaye, A.; Tora, A. S.; Commare, B.; Courtiol, T.; Cesarini, S.; McCort-Tranchepain, I.; Rigault, D.; Mony, L.; Bessiron, T.; McLean, H.; Leroux, F. R.; Colobert, F.; Daniel, H.; Goupil-Lamy, A.; Bertrand, H. O.; Goudet, C.; Pin, J. P.; Acher, F. C., Increased Potency and Selectivity for Group III Metabotropic Glutamate Receptor Agonists Binding at Dual sites. *J Med Chem* **2018**, *61* (5), 1969-1989.
  31. Jones, G.; Willett, P.; Glen, R. C.; Leach, A. R.; Taylor, R., Development and validation of a genetic algorithm for flexible docking. *J Mol Biol* **1997**, *267* (3), 727-48.
  32. Tora, A. S.; Rovira, X.; Dione, I.; Bertrand, H. O.; Brabet, I.; De Koninck, Y.; Doyon, N.; Pin, J. P.; Acher, F.; Goudet, C., Allosteric modulation of metabotropic glutamate receptors by chloride ions. *Faseb J* **2015**, *29* (10), 4174-88.
  33. Rosemond, E.; Wang, M.; Yao, Y.; Storjohann, L.; Stormann, T.; Johnson, E. C.; Hampson, D. R., Molecular basis for the differential agonist affinities of group III metabotropic glutamate receptors. *Mol Pharmacol* **2004**, *66* (4), 834-42.
  34. Korb, O.; Stutzle, T.; Exner, T. E., Empirical scoring functions for advanced protein-ligand docking with PLANTS. *J Chem Inf Model* **2009**, *49* (1), 84-96.
  35. Shinada, N. K.; de Brevern, A. G.; Schmidtke, P., Halogens in Protein-Ligand Binding Mechanism: A Structural Perspective. *J Med Chem* **2019**, *62* (21), 9341-9356.
  36. (a) Fisher, N. M.; Seto, M.; Lindsley, C. W.; Niswender, C. M., Corrigendum: Metabotropic Glutamate Receptor 7: A New Therapeutic Target in Neurodevelopmental Disorders. *Front Mol Neurosci* **2018**, *11*, 444; (b) Estrela, K. A. R.; Senninger, L.; Arndt, J.; Kabas, M.; Schmid, F.; Dillmann, L.; Auer, S.; Stepfer, T.; Flor, P. J.; Uschold-Schmidt, N., Blocking Metabotropic Glutamate Receptor Subtype 7 via the Venus Flytrap Domain Promotes a Chronic Stress-Resilient Phenotype in Mice. *Cells* **2022**, *11* (11).
  37. Vazquez-Villa, H.; Trabanco, A. A., Progress toward allosteric ligands of metabotropic glutamate 7 (mGlu7) receptor: 2008-present. *Medchemcomm* **2019**, *10* (2), 193-199.
  38. Johnson, B. G.; Wright, R. A.; Arnold, M. B.; Wheeler, W. J.; Ornstein, P. L.; Schoepp, D. D., [3H]-LY341495 as a novel antagonist radioligand for group II metabotropic glutamate (mGlu) receptors: characterization of binding to membranes of mGlu receptor subtype expressing cells. *Neuropharmacology* **1999**, *38* (10), 1519-29.
  39. Wright, R. A.; Arnold, M. B.; Wheeler, W. J.; Ornstein, P. L.; Schoepp, D. D., Binding of [3H](2S,1'S,2'S)-2-(9-xanthylmethyl)-2-(2'-carboxycyclopropyl) glycine ([3H]LY341495) to cell membranes expressing recombinant human group III metabotropic glutamate receptor subtypes. *Naunyn Schmiedebergs Arch Pharmacol* **2000**, *362* (6), 546-54.

40. Sali, A.; Blundell, T. L., Comparative protein modelling by satisfaction of spatial restraints. *J Mol Biol* **1993**, *234* (3), 779-815.
41. Koehl, A.; Hu, H.; Feng, D.; Sun, B.; Zhang, Y.; Robertson, M. J.; Chu, M.; Kobilka, T. S.; Laeremans, T.; Steyaert, J.; Tarrasch, J.; Dutta, S.; Fonseca, R.; Weis, W. I.; Mathiesen, J. M.; Skiniotis, G.; Kobilka, B. K., Structural insights into the activation of metabotropic glutamate receptors. *Nature* **2019**, *566* (7742), 79-84.
42. Brooks, B. R.; Brooks, C. L., 3rd; Mackerell, A. D., Jr.; Nilsson, L.; Petrella, R. J.; Roux, B.; Won, Y.; Archontis, G.; Bartels, C.; Boresch, S.; Caflisch, A.; Caves, L.; Cui, Q.; Dinner, A. R.; Feig, M.; Fischer, S.; Gao, J.; Hodoscek, M.; Im, W.; Kuczera, K.; Lazaridis, T.; Ma, J.; Ovchinnikov, V.; Paci, E.; Pastor, R. W.; Post, C. B.; Pu, J. Z.; Schaefer, M.; Tidor, B.; Venable, R. M.; Woodcock, H. L.; Wu, X.; Yang, W.; York, D. M.; Karplus, M., CHARMM: the biomolecular simulation program. *J Comput Chem* **2009**, *30* (10), 1545-614.
43. Huang, J.; Mackerell, A. D., Jr., CHARMM36 all-atom additive protein force field: validation based on comparison to NMR data. *J Comput Chem* **2013**, *34* (25), 2135-45.
44. Yesselman, J. D.; Price, D. J.; Knight, J. L.; Brooks, C. L., 3rd, MATCH: an atom-typing toolset for molecular mechanics force fields. *J Comput Chem* **2012**, *33* (2), 189-202.
45. Stone, J. E.; Gullingsrud, J.; Schulten, K., A system for interactive molecular dynamics simulation. In *13D '01: Proceedings of the 2001 symposium on Interactive 3D graphics*, Hughes, J. F.; Séquin, C. H., Eds. New York, New York, USA: ACM Press: 2001; Vol. March 2001, pp 191-194.

## TOC

